Preservation of Missouri Transportation Infrastructures: Life Expectancy Modeling for FRP Strengthened Concrete Bridges

by

J.J. Myers and A.V. Sawant

UTC R95

Disclaimer

The contents of this report reflect the views of the author(s), who are responsible for the facts and the accuracy of information presented herein. This document is disseminated under the sponsorship of the Department of Transportation, University Transportation Centers Program and the Center for Infrastructure Engineering Studies UTC program at the Missouri University of Science & Technology, in the interest of information exchange. The U.S. Government and Center for Infrastructure Engineering Studies assumes no liability for the contents or use thereof.

1. Report No. UTC R95	2. Government Accession No.	3. Recipient's Catalog No.
4. Title and Subtitle Preservation of Missouri Transportation Infrastructures: Life Expectancy Modeling for FRP Strengthened Concrete Bridges	5. Report Date July 2008	
	6. Performing Organization Code	
7. Author/s J.J. Myers and A.V. Sawant	8. Performing Organization Report No. RG001232	
9. Performing Organization Name and Address Center for Infrastructure Engineering Studies/UTC program Missouri University of Science & Technology 220 Engineering Research Lab Rolla, MO 65409	10. Work Unit No. (TRAIS)	
	11. Contract or Grant No. DTRS98-G-0021	
12. Sponsoring Organization Name and Address U.S. Department of Transportation Research and Special Programs Administration 400 7th Street, SW Washington, DC 20590-0001	13. Type of Report and Period Covered Final	
	14. Sponsoring Agency Code MoDOT	

15. Supplementary Notes

16. Abstract

The use of fiber reinforced polymers (FRP) in repairing and strengthening bridges has been an active area of research and implementation in recent years. In particular, adhering FRP to the tension face of reinforced concrete (RC) beams has provided an increase in load carrying capacity and extended the service life of structures. However, the life expectancy of this technology has not yet been fully investigated or documented due to insufficient data. In this report, the authors present one possible strength degradation approach using analytical modeling to determine the life expectancy of FRP strengthened bridges. An actual Carbon FRP field strengthened bridge in Dallas County, Missouri, USA, was utilized to demonstrate the life expectancy approach. The Dallas County Bridge P-0962 was constructed in 1955 and strengthened in 2003. To predict the life expectancy behavior of the bridge structure, a theoretical model was derived using basic concepts, past research, and the properties of specimens tested for critical chloride concentration. An interaction model for life expectancy estimation is based on the reduction of moment capacity due to corrosion of reinforcement before and after strengthening, bond degradation of FRP and substrate concrete, and degradation of FRP material itself based on fatigue analysis. This model is the first possible approach to determine the life expectancy of FRP strengthened structures based on the statistical data available in literature.

17. Key Words Life expectancy of FRP Strengthened Bridges, FRP durability, FRP bond retention, steel corrosion	18. Distribution Statement No restrictions. This document is available to the public through the National Technical Information Service, Springfield, Virginia 22161.		
19. Security Classification (of this report) unclassified	20. Security Classification (of this page) unclassified	21. No. Of Pages 132	22. Price

Form DOT F 1700.7 (8-72)

PRESERVATION OF MISSOURI

TRANSPORATION INFRASTRUCTURES:

Life Expectancy Modeling for FRP Strengthened Concrete Bridges

VALIDATION OF FRP COMPOSITE TECHNOLOGY

THROUGH FIELD TESTING

Prepared for:

Missouri Department of Transportation

Missouri University of Science & Technology

The mission of CIES is to provide leadership in research and education for solving society's problems affecting the nation's infrastructure systems. CIES is the primary conduit for communication among those on the Missouri S&T campus interested in infrastructure studies and provides coordination for collaborative efforts. CIES activities include interdisciplinary research and development with projects tailored to address needs of federal agencies, state agencies, and private industry as well as technology transfer and continuing/distance education to the engineering community and industry.

Center for Infrastructure Engineering Studies (CIES)
Missouri University of Science and Technology
223 Engineering Research Laboratory
1870 Miner Circle
Rolla, MO 65409-0710
Tel: (573) 341-4497; fax -6215
E-mail: cies@mst.edu
http://utc.mst.edu/

Research Investigation R119

LIFE EXPECTANCY MODELING FOR
FRP STRENGTHENED CONCRETE BRIDGES

Prepared for the
Missouri Department of Transportation

In Cooperation with the
National University Transportation Center

Written By:

John J. Myers, Ph.D., P.E., Associate Professor at Missouri S&T
Amol Sawant Graduate Research Assistant at Missouri S&T

CENTER FOR INFRASTRUCTURE ENGINEERING STUDIES
MISSOURI UNIVERSITY OF SCIENCE AND TECHNOLOGY

Submitted

July 2008

LIFE EXPECTANCY MODELING FOR
FRP STRENGTHENED CONCRETE BRIDGES

EXECUTIVE SUMMARY

The use of fiber reinforced polymers (FRP) in repairing and strengthening bridges has been an active area of research and implementation in recent years. In particular, adhering FRP to the tension face of reinforced concrete (RC) beams has provided an increase in load carrying capacity and extended the service life of structures. However, the life expectancy of this technology has not yet been fully investigated or documented due to insufficient data.

In this report, the authors present one possible strength degradation approach using analytical modeling to determine the life expectancy of FRP strengthened bridges. An actual Carbon FRP field strengthened bridge in Dallas County, Missouri, USA, was utilized to demonstrate the life expectancy approach. The Dallas County Bridge P-0962 was constructed in 1955 and strengthened in 2003. To predict the life expectancy behavior of the bridge structure, a theoretical model was derived using basic concepts, past research, and the properties of specimens tested for critical chloride concentration.

An interaction model for life expectancy estimation is based on the reduction of moment capacity due to corrosion of reinforcement before and after strengthening, bond degradation of FRP and substrate concrete, and degradation of FRP material itself based on fatigue analysis. This model is the first possible approach to determine the life expectancy of FRP strengthened structures based on the statistical data available in literature.

ACKNOWLEDGMENTS

TABLE OF CONTENTS

APPENDICES

LIST OF ILLUSTRATIONS

LIST OF TABLES

NOTATIONS

Symbol	Description
A	c/s area of beam, m^2 (in.^{2})
A_f	area of FRP external reinforcement, mm^2 (in.^{2})
A_{st}	total area of longitudinal reinforcement, mm^2 (in.^{2})
a	depth of compression block, mm (in.)
b_{eff}	effective width of flange, mm (in.)
b_w	width of web, mm (in.)
C_E	environmental-reduction factor
c	distance from extreme compression fiber to the neutral axis, mm (in.)
D_L	dead load, kN/m (kip/ft)
d	distance from extreme compression fiber to the neutral axis, mm (in.)
E_c	modulus of elasticity of concrete, MPa (psi)
E_s	modulus of elasticity of steel, MPa (psi)
E_f	modulus of elasticity of FRP, MPa (psi)
F_{fe}	effective stress in FRP, MPa (psi)
F_s	effective stress in steel, MPa (psi)
f'_c	specified compressive strength of concrete, MPa (psi)
f_{fe}	effective stress in the FRP; stress level attained atsection failure, MPa (psi)
f_{fu}	design ultimate tensile strength of FRP, MPa (psi)
f_{fum}	ultimate tensile strength of the FRP material as reported by the manufacturer, MPa (psi)
f_y	specified yield strength of nonprestressed steel reinforcement, MPa (psi)

h	total depth of girder, mm (in.)
h_f	height of flange, mm (in.)
I	inpact factor, kN/m (kip/ft)
I_{cr}	moment of inertia of cracked section transformed to concrete, mm^4 ($in.^4$)
K_m	bond dependent coefficient
k	depth of neutral axis of cracked transformed section, mm (in.)
L	length of span m (ft)
L_L	live load, kN/m (kip/ft)
M_{DL}	moment strength du to dead load, N-mm (in.-lb)
M_{LL}	moment strength du to live load, N-mm (in.-lb)
M_n	nominal moment strength, N-mm (in-lb)
n	number of plies
n_e	ratio of elastic modulus of steel to that of concrete
t_f	nominal thickness of one ply of the FRP reinforcement, mm (in.)
w_f	width of the FRP reinforcing plies, mm (in.)
w_u	factored total load as per AASHTO, kN/m (kip/ft)
X_i	year at which moment capacity is to be determined
X_s	year at which bridge strengthened
β_1	ratio of the depth of the equivalent rectangular stress block to the depth of the neutral axis
β_d	dead load coefficient as per AASHTO
ε_{bi}	strain level in the concrete substrate at the time of the FRP installation (tension is positive), mm/mm (in./in.)

ε_{fe} effective strain level in FRP reinforcement; strain level attained at section failure, mm/mm (in./in.)

ε_{fu} mean rupture stain of FRP reinforcement based on a population of 20 or more tensile tests per ASTM D 3039, mm/mm (in./in.)

ε_{fum} ultimate rupture strain of the FRP reinforcement, mm/mm (in./in.)

ε_{s} strain level in the nonprestessed steel reinforcement, mm/mm (in./in.)

Φ strength reduction factor for concrete

ρ_{f} FRP reinforcement ratio

ρ_{s} ratio of nonprestressed reinforcement

γ multiplier on f'_c to determine the intensity of an equivalent rectangular stress distribution for concrete

ψ additional FRP strength-reduction factor as per ACI 440.2R

ψ_{b} bond degradation factor

ψ_{cor} strength reduction factor for steel loss

ψ_{f} FRP material degradation factor

1. INTRODUCTION

1.1. BACKGROUND

The number of deficient bridges nationwide has become a major problem for civil engineers in the past few decades. Recently, bridge designers have been faced with the challenge of remedying the increasing number of deteriorating bridge decks. According to an article from American Concrete International (ACI'S), "Concrete bridge decks deteriorate faster than any other bridge components because of direct exposure to the environment, de-icing chemicals, and ever increasing traffic loads" (Benmokrane et al., 2004). In the United States, 100 billion dollars per year is wasted due to corrosion alone (Chong, 1998). Figures 1.1 and 1.2 illustrate structural and functional deficiencies of bridges in the state of Missouri and in the United States, respectively. Table 1.1 presents rural and urban bridge deficiencies in the United States.
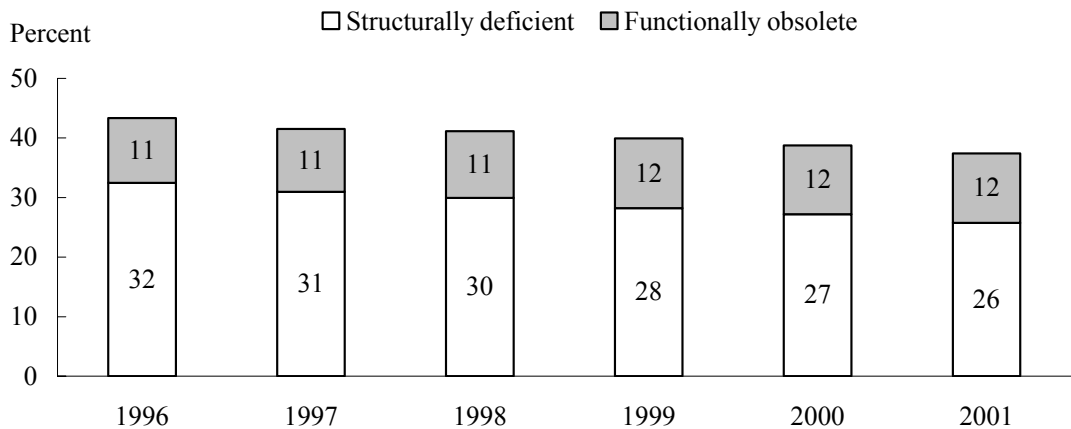
Figure 1.1 Deficiencies of bridges in Missouri, (FHWA, 2002)
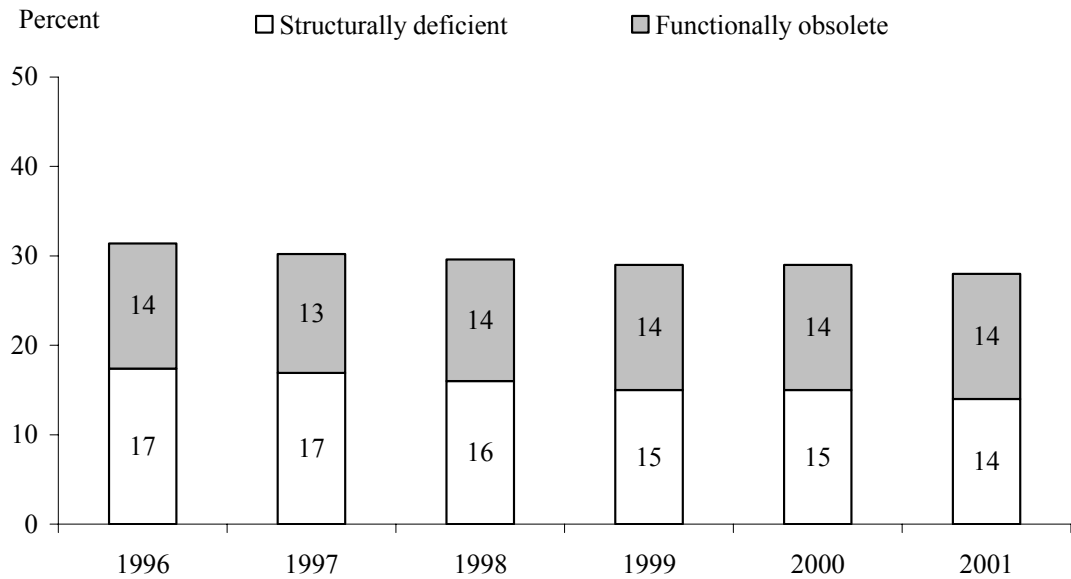
Figure 1.2. Deficiencies for all bridges in the United States, (FHWA, 2002)

According to the "National Bridge Inventory" (NBI) and as illustrated in Figure 1.2., over 28 percent bridges in the United States are classified as either structurally deficient or functionally obsolete (FHWA, 2002). Figure 1.3 illustrates the increase in structural deficiency in bridge structure due to corrosion. To address this problem, previous technologies for repair and strengthening of bridge girders included bonding steel plates to the deficient concrete members. This procedure has been used in Europe for many years and is becoming widely accepted in the United States (Norris and Saadatmanesh, 1994). However, bonding steel plates to concrete presents some disadvantages, including corrosion of the steel/adhesive joint and the heavy weight of the material. These problems increase installation and maintenance costs. Bonding of fiber reinforced polymers (FRP) to structures provides an attractive alternative to steel plates.

This material is corrosion resistant, lightweight, has a high strength-to-weight ratio, and possesses nonconductive properties.

Table 1.1. Rural and urban bridge deficiencies in the United States, 1994–2000

	1994		1996		1998		2000	
	Number	%	Number	%	Number	%	Number	%
Rural Bridges	455,319		456,913		454,664		455,365	
Deficient Bridges	144,799	31.80%	139,545	30.50%	130,911	28.80%	125,523	27.60%
Structurally Deficient	91,991	20.20%	86,424	18.90%	78,999	17.40%	73,599	16.20%
Functionally Obsolete	52,808	11.60%	53,121	11.60%	51,912	11.40%	51,924	11.40%
Urban Bridges	121,141		124,949		128,312		131,781	
Deficient Bridges	42,716	35.30%	43,181	34.60%	41,661	32.50%	42,031	31.90%
Structurally Deficient	15,692	13.00%	15,094	12.10%	14,073	11.00%	13,079	9.90%
Functionally Obsolete	27,024	22.30%	28,087	22.50%	27,558	21.50%	28,952	22.00%
Total Bridges	576,460		581,862		582,976		587,146	
Deficient Bridges	187,515	32.50%	182,726	31.40%	172,572	29.60%	167,554	28.50%
Structurally Deficient	107,683	18.70%	101,518	17.40%	93,072	16.00%	86,678	14.80%
Functionally Obsolete	79,832	13.80%	81,208	14.00%	79,500	13.60%	80,876	13.80%
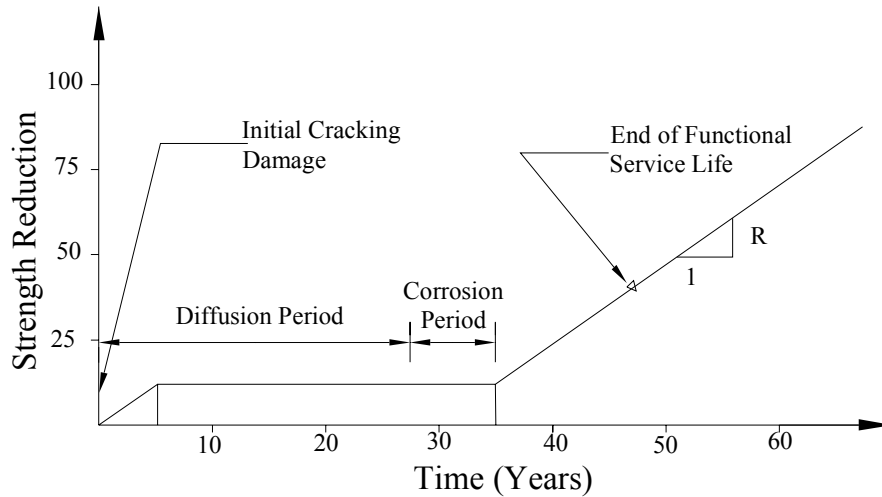
Figure 1.3. Increase in structural deficiency due to corrosion

1.2. SCOPE OF RESEARCH

The use of FRP in repairing and strengthening bridges has been researched in recent years. In particular, attaching FRP to the tension face of reinforced concrete beams has provided an increase in stiffness and load capacity of the structure (Meier et al., 1991). One of the most important criteria in the design of all FRP strengthening system is the required life expectancy of the system. Significant data from field cases does not yet exist due to the short period since the first Carbon FRP (CFRP) application to a concrete bridge was carried out in 1991. Limited research in this area has been conducted to date. However, some mathematical models are available to predict the long-term characteristics of fibers, resin, existing concrete and bond between FRP and concrete. Consequently, for the safety of the structure it is important to provide and/or develop guidelines for the life expectancy of FRP strengthened reinforced concrete bridges.

4

The primary object of this research study was to evaluate the life expectancy of repairing/strengthening reinforced concrete bridge girders with CFRP sheets. The main components of this investigation included a literature review, development of models to account for steel corrosion, bond degradation at the FRP-concrete substrate and combined strength degradation approach. A final approach, which involves limiting stress values of the material, is not considered in this report.

1.3. BRIDGE P-0962

As a part of this investigation, a case study bridge P-0962 was used to illustrate how a strength degradation model could be applied. Bridge P-0962, located in Dallas County, Missouri, consists of 3 equal spans each 12.9 m (42.5 ft) long and simply supported. Each span is made up of 3 reinforced concrete girders monolithically cast with a 150 mm (6 in) slab as illustrated in Figure 1.4. Each of the spans contains 1 diaphragm beam located at midspan. The total width of the structure is 7.25 m (23.75 ft). Bridge P-0962 was originally constructed in 1955 and was strengthened in 2003 with an external FRP strengthening system.

Figure 1.4. Superstructure of bridge P-0962

Bridge P-0962 was selected because it is very typical of numerous bridges in Missouri that are either structurally deficient or functionally obsolete. Bridge P-0962 is classified as a non-continuous concrete bridge, of which type over 40 percent are either structurally deficient or functionally obsolete in Missouri. Over 1,300 bridges in this classification no longer meet the current design codes (National Bridge Inventory, 2003). The bridge is located on a farm-to-market (FM) road, a type of road which connects rural and municipal areas and which are a major part of Missouri's highway system. These roads are a crucial element of Missouri's rural society and economy. Figure 1.5 illustrates the exact location of the bridge P-0962 in Dallas County.
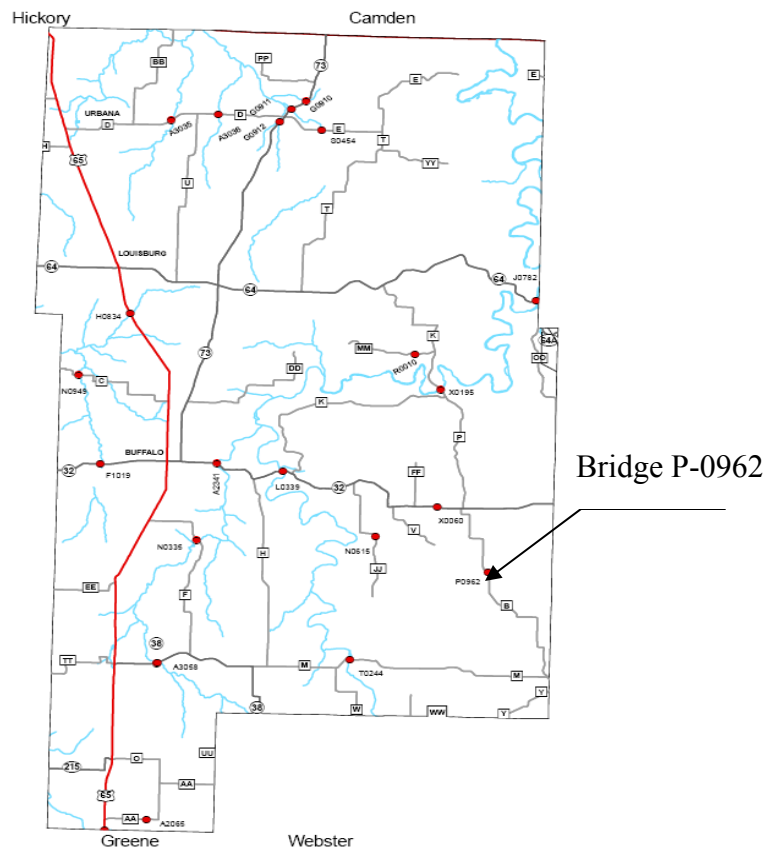
Figure 1.5. Location of bridge P-0962

2. LITERATURE REVIEW

2.1. MATERIAL

2.1.1. Introduction. The method of strengthening concrete structures externally with FRP composites is becoming increasingly popular among researchers and design engineers. When compared with more traditional techniques (e.g., bonding of steel plates, Post-tensioning), it offers advantages of rapid installation and the use of non-corrosive materials. Extensive research has shown that externally bonded CFRP laminates improve both the short-term (Ritchie et al., 1991; Saadatmanesh and Ehsani, 1991; Jones and Swamy, 1992; Triantafillou and Pelvris, 1992; Arduini and Nanni, 1997) and long-term behavior (Shahawy and Beitelman, 1999) of concrete girders. Based on research conducted so far, ACI committee 440 has developed design guidelines for external strengthening of concrete structures using fiber reinforced polymer systems [ACI 440, 2R-02 (2002)]. With the exception of a few studies, most of the research conducted on Carbon FRP-strengthened reinforced concrete structures has been done in a deterministic manner, and the statistical variations associated with the main design variables have been largely ignored.

FRP has been in use since the 1940s. Due to the incurring of very heavy financial costs, however, the application of FRP was limited to the aerospace and defense industries. To meet the higher performance challenges of space exploration and air travel in the 1960s and 1970s, fiber materials with higher strength, higher stiffness and lower density (such as boron, aramid, and carbon) were commercialized. During the 1970s, research was channeled to develop ways to improve the cost of high performance FRP. By the late 1980s and early 1990s, the defense industry waned, and emphasis was now

placed on cost reduction and the continued growth of the FRP industry (Bakis et al., 2002).

Although FRP has had a long history, only in recent times has it won the attention of civil engineers as a potential alternative to more conventional structural materials. Throughout the 1990s, various industries financed demonstration projects and sponsored research programs on this burgeoning field. As research continues and costs become more competitive, FRP materials are now finding wider acceptance in the construction industry.

2.1.2. State-of-the-Art Review. Prior to the 1970s, pultruded FRP structural shapes were developed but limited to small sized commodity products for non-structural applications. In the 1970s and 1980s, larger pultruded shapes for structural purposes and load-bearing elements were produced largely as a result of the advancement in pultrusion technology. Pultrusion companies in the United States began to produce "standard" I-shaped beams for construction purposes. A customized building system of pultruded components for the construction of industrial cooling towers was developed in the late 1980s and 1990s. Small pultruded FRP structural shapes for the construction of walkways and short-span pedestrian bridges have increased in use since the early 1990s (Bakis et al., 2002). Several bridges have been constructed in various parts of the world using FRP. These include both pedestrian and vehicular bridges. One example is the Aberfeldy Footbridge, which crosses the River Tay in Scotland; erected in 1992, it is the world's first and longest advanced composite footbridge. Another example is the Bonds Mill lift bridge (completed in 1994), which is an electrically operated lift bridge and the first bridge in England to be constructed from polymers. Some of the first applications of

FRP for complete bridge structures were in China. A number of pedestrian bridges have been built, but the first all-composite bridge deck was the Miyun Bridge, completed in September of 1982 near Beijing, which carries full highway traffic. Ulenbergstrasse Bridge in Germany was the world's first in the use of high tensile strength glass fiber prestressing tendons.

2.1.3. Properties of FRP Sheets. Although FRP composites are a relatively new class of material in the field of civil engineering, the last decade has seen rapid growth in the use of composites for civil engineering applications. This section explains properties of FRP composites related to structural and civil applications.

2.1.3.1 General characteristics. FRP materials consist of two parts—fibers and resin. The load-carrying component is the fibers. These fibers may be made of aramid, carbon, glass, or, more recently, a natural material.. Generally, the type of fiber used dictates the strength and stiffness properties of the FRP. The polymer component of FRP consists of a resin into which the fibers are embedded. The primary function of the resin is to allow stresses to be transferred between individual fibers. Epoxy, vinylester, and polyester are the most common resins used.

FRP materials can be found in the form of bars, plates, and sheets. The application dictates which form of FRP material is the most practical to be used in a structure. Bars are generally used in new construction where they may be a suitable substitute for the steel in a reinforced or prestressed concrete member. Plates and sheets are more commonly used for strengthening or rehabilitation, where the application requires that they be bonded to the surface of a structure. Plates, sometimes referred to as strips, are often used for flexural reinforcement since they have a relatively high

9

thickness-to-width ratio and there is generally a limited surface area on the soffit of a beam for bonding to take place. Sheets are most commonly used for shear reinforcement, confinement of concrete columns, or flexural strengthening of thin slabs or decks. Sheets have a low thickness-to-width ratio, and therefore require a large bonded area over which to transmit bond stresses. The flexibility of the sheets, when applied in a wet lay-up process, also allows them to follow irregular surface geometry, such as curved surfaces or rounded corners.

The primary advantages of FRP materials are their high strength-to-weight ratios, typically good fatigue behavior, and corrosion resistance to aggressive chemicals. High strength to weight is important in the strengthening and rehabilitation of structures for two reasons: first, materials are light enough that strengthening can be accomplished without adding dead weight to the structure, which would negate the strengthening added and second, the light weight eases handling by construction workers and reduces the need for staging and schemes for temporary support of the strengthening material. These factors significantly reduce labor costs compared to other types of strengthening schemes. High fatigue resistance is particularly important for bridge structures. Carbon fibers offer very good fatigue resistance. Much of the infrastructure problems in concrete structures are directly attributable to corrosion of the steel reinforcement. Corrosion causes cracking and peeling of concrete and leads to further ingress of water and chlorides, which exacerbates the corrosion problem. Ultimately corrosion, if left unabated, leads to significant loss in the cross-sectional area of the steel reinforcement, potentially leading to an unsafe condition. FRP materials do not suffer from this problem since they do not corrode with exposure to chlorides.

2.1.3.2 Material properties. FRP composites are defined as a polymer (plastic) matrix, either thermoset or thermoplastic, that is reinforced (combined) with a fiber or other reinforcing material with a sufficient aspect ratio (length to thickness) to provide a discernable reinforcing function in one or more directions. FRP composites are different from traditional construction materials such as steel or aluminum. FRP composites are anisotropic (properties only apparent in the direction of the applied load), whereas steel and aluminum are isotropic (uniform properties in all directions, independent of applied load). Therefore, FRP composite properties are directional, meaning that the best mechanical properties are in the direction of the fiber placement. Composites are similar to reinforced concrete where the rebar is embedded in an isotropic matrix called concrete.

The behavior of FRP materials is linear elastic to failure. Ultimate elongation strains are considerably higher than steel yielding strains. This factor results in ultimate tensile strengths that are typically between four and nine times the yield stress of steel. Failure in FRP is sudden and brittle, with no load carrying capacity after failure. Unlike steel or concrete, the properties of FRP materials may differ from one manufacturer to another, since the materials may be unique to that manufacturer. For this reason, the necessary material properties are obtained from the manufacturer. Mechanical properties of composites vary to a high degree depending on the orientation of load with respect to the fiber orientation and the fiber-to-resin volume ratio (Volnyy and Pantelides, 1999). FRP materials exhibit the highest strength when loaded in the direction of the fibers and have only the strength of the resin when loaded perpendicular to the fibers. Using FRP sheets with the fibers woven orthogonally to produce a fabric that has the same properties

in two directions can offset this effect. Sheets with three fiber directions are also available.

Many terms have been used to define FRP composites. Modifiers have been used to identify a specific fiber such as Glass Fiber Reinforced Polymer (GFRP), Carbon Fiber Reinforced Polymer (CFRP), and Aramid Fiber Reinforced Polymer (AFRP). Another familiar term used is Fiber Reinforced Polymers. In addition, other acronyms were developed over the years, and the use depended on geographical location or market use. For example, Fiber Reinforced Composites (FRC), Glass Reinforced Polymers (GRP), and Polymer Matrix Composites (PMC) can be found in many references. Although different, each of the aforementioned terms means the same thing—FRP composites.

2.1.3.2.1 <u>Resins</u>. The primary functions of the resin are to transfer stress between the reinforcing fibers, act as a glue to hold the fibers together, and protect the fibers from mechanical and environmental damage. Resins are divided into two major groups known as thermoset and thermoplastic. Thermoplastic resins become soft when heated and may be shaped or molded while in a heated semi-fluid state, but become rigid when cooled. Thermoset resins, on the other hand, are usually liquids or low melting point solids in their initial form. When used to produce finished goods, these thermosetting resins are "cured" by the use of a catalyst, heat, or a combination of the two. Once cured, solid thermoset resins cannot be converted back to their original liquid form. Unlike thermoplastic resins, cured thermosets will not melt and flow but will soften when heated (and lose hardness); once formed they cannot be reshaped. Heat Distortion Temperature (HDT) and Glass Transition Temperature (T_g) are used to measure the softening of a

cured resin. Both test methods (HDT and T_g) measure the approximate temperature at which the cured resin will soften significantly to yield (bend or sag) under load.

2.1.3.2.2 <u>Polyester.</u> Unsaturated polyester resins (UPR) are the workhorse of the composites industry and represent approximately 75 percent of total resins used. To avoid any confusion in terms, readers should be aware that there is a family of thermoplastic polyesters that are best known for their use as fibers for textiles and clothing. Thermoset polyesters are produced by the condensation polymerization of dicarboxylic acids and difunctional alcohols (glycols). In addition, unsaturated polyesters contain an unsaturated material, such as maleic anhydride or fumaric acid, as part of the dicarboxylic acid component. The finished polymer is dissolved in a reactive monomer, such as styrene, to give a low viscosity liquid. When this resin is cured, the monomer reacts with the unsaturated sites on the polymer, converting it to a solid thermoset structure.

A range of raw materials and processing techniques are available to achieve the desired properties in the formulated or processed polyester resin. Polyesters are versatile because of their capacity to be modified or tailored during building of the polymer chains. They have been found to have almost unlimited usefulness in all segments of the composites industry. The principal advantages of these resins are a balance of properties (including mechanical, chemical, and electrical), dimensional stability, cost, and ease of handling or processing.

2.1.3.2.3 <u>Epoxy.</u> Epoxy resins have a well-established record in a wide range of composite parts, structures, and concrete repair. The structure of the resin can be engineered to yield a number of different products with varying levels of performance. A

major benefit of epoxy resins over unsaturated polyester resins is lower shrinkage. Epoxy resins can also be formulated with different materials or blended with other epoxy resins to achieve specific performance features. Cure rates can be controlled to match process requirements through the proper selection of hardeners and/or catalyst systems. Generally, epoxies are cured by the addition of an anhydride or an amine hardener as a 2-part system. Different hardeners, as well as the quantity of a hardener, produce a different cure profile and give different properties to the finished composite.

Epoxies are used primarily for fabricating high performance composites with superior mechanical properties, resistance to corrosive liquids and environments, superior electrical properties, good performance at elevated temperatures, good adhesion to a substrate, or a combination of these benefits. Epoxy resins do not, however, have particularly good UV resistance. Since the viscosity of epoxy is much higher than most polyester resins, it requires a post-cure (elevated heat) to obtain ultimate mechanical properties, making epoxies more difficult to use. However, compared to polyesters, epoxies emit little odor.

Epoxy resins are used with a number of fibrous reinforcing materials, including glass, carbon, and aramid. This latter group is small in volume, has comparatively high costs, and is usually used to meet high strength and/or high stiffness requirements. Epoxies are compatible with most composite manufacturing processes, particularly vacuum-bag molding, autoclave molding, pressure-bag molding, compression molding, filament winding, and hand lay-up.

2.1.3.2.4 Vinyl esters. Vinyl esters were developed to combine the advantages of epoxy resins with the better handling and faster cure typical of unsaturated polyester

resins. These resins are produced by reacting epoxy resin with acrylic or methacrylic acid. This provides unsaturated polyester, much like that produced in polyester resins when maleic anhydride is used. The resulting material is dissolved in styrene to yield a liquid that is similar to polyester resin. Vinyl esters are also cured with the conventional organic peroxides used with polyester resins. Vinyl esters offer mechanical toughness and excellent corrosion resistance. These enhanced properties are obtained without complex processing, handling, or special shop fabricating practices typical to epoxy resins.

2.1.3.2.5 Phenolic. Phenolics are a class of resins commonly based on phenol (carbolic acid) and formaldehyde. Phenolics are thermosetting resins that cure through a condensation reaction producing water that should be removed during processing. Pigmented applications are limited to red, brown, or black. Phenolic composites have many desirable performance qualities including high temperature resistance, creep resistance, excellent thermal insulation and sound damping properties, corrosion resistance, and excellent fire/smoke/smoke toxicity properties. Phenolics are applied as adhesives or matrix binders in engineered woods (plywood), brake linings, clutch plates, and circuit boards, to name a few.

2.1.3.2.6 Polyurethane. Polyurethane is a family of polymers with widely ranging properties and uses, all based on the exothermic reaction of an organic polyisocyanate with a polyol (an alcohol containing more than one hydroxl group). A few basic constituents of different molecular weights and functionalities are used to produce the whole spectrum of polyurethane materials. The versatility of polyurethane

chemistry enables the polyurethane chemist to engineer polyurethane resin to achieve the desired properties.

Polyurethanes appear in an amazing variety of forms. These materials are all around us, playing important roles in more facets of our daily lives than perhaps any other single polymer. They are used as a coating, elastomer, foam, or adhesive. When used as a coating in exterior or interior finishes, polyurethanes are tough, flexible, chemical resistant, and fast curing. Polyurethanes as an elastomer have superior toughness and abrasion resistance in such applications as solid tires, wheels, bumper components or insulation. There are many formulations of polyurethane foam to optimize density for insulation, structural sandwich panels, and architectural components. Polyurethanes are often used to bond composite structures together. Benefits of polyurethane adhesive bonds are that they have good impact resistance, the resin cures rapidly and the resin bonds well to a variety of different surfaces (e.g., concrete).

2.1.3.3 Development of fiber reinforcement. Early in the development of composites, the only reinforcements available were derived from traditional textiles and fabrics. Particularly in the case of glass fibers, experience showed that the chemical surface treatments, or "sizings," required to process these materials into fabrics and other sheet goods were detrimental to the adhesion of composite polymers to the fiber surface. Techniques to remove these materials were developed, primarily continuous or batch heat cleaning. It was then necessary to apply new "coupling agents" (also known as finishes or surface treatments), an important ingredient in sizing systems, to facilitate adhesion of polymers to fibers, particularly under wet conditions and fiber processing.

Most reinforcements for either thermosetting or thermoplastic resins receive some form of surface treatments, either during fiber manufacture or as a subsequent treatment. Other materials applied to fibers as they are produced include resinous binders, to hold fibers together in bundles, and lubricants, to protect fibers from degradation caused by process abrasion.

2.1.3.3.1 <u>Aramid fibers.</u> Aramid fiber is an aromatic polyimid that is a human-made organic fiber for composite reinforcement. Aramid fibers offer good mechanical properties at a low density with the added advantage of toughness, or damage/impact resistance. Table 2.1 indicates the properties of different types of aramid fibers. The tensile strength of aramid fibers is higher than glass fibers, and the modulus is about 50 percent higher than glass. These fibers increase the impact resistance of composites and provide products with higher tensile strengths. Aramid fibers are insulators of both electricity and heat. They are resistant to organic solvents, fuels, and lubricants. Aramid composites are not as good in compressive strength as glass or carbon composites. Dry aramid fibers are tough and have been used as cables or ropes and are frequently used in ballistic applications.

Table 2.1. Properties of aramid fibers (Berenberg B. -www.composites.about.com)

Kevlar #	29	49	149
Tensile Modulus (MPa)	83	131	186
Tensile Strength (MPa)	3.6	3.6	3.4
Elongation (%)	4	2.8	2
Density (g/cc)	1.44	1.44	1.47

Conversion units: 1 MPa = 145.04 psi, 1 g/cc = 0.58 oz/in^3

2.1.3.3.2 <u>Glass fibers.</u> Based on an alumina-lime-borosilicate composition, "E" glass produced fibers are considered the predominant reinforcement for polymer matrix composites due to their high electrical insulating properties, low susceptibility to moisture, and high mechanical properties. Table 2.2 indicates the properties of different types of glass fibers. Other commercial compositions include "S" glass, with higher strength, heat resistance, and modulus, as well as some specialized glass reinforcements with improved chemical resistance, such as AR glass (alkali resistant).

Glass fibers used for reinforcing composites generally range in diameter from 9 to 23 microns (0.00035 in. to 0.00090 in.). Fibers are drawn at high speeds, approaching 320 kilometers per hours (200 miles per hour), through small holes in electrically heated bushings.

These bushings form the individual filaments. The filaments are gathered into groups or bundles called "strands." The filaments are attenuated from the bushing, water and air cooled, and then coated with a proprietary chemical binder or sizing to protect them and enhance the composite laminate properties. The sizing also determines the processing characteristics of the glass fiber and the conditions at the fiber-matrix interface in the composite.

Glass is generally a good impact-resistant fiber but weighs more than carbon or aramid. Glass fibers have excellent characteristics, equal to or better than steel in certain forms. The lower modulus requires special design treatment where stiffness is critical. Composites made from this material exhibit very good electrical and thermal insulation properties. Glass fibers are also transparent to radio frequency radiation and are used in radar antenna applications.

Table 2.2. Properties of glass fibers (Berenberg B. -www.composites.about.com)

Property	Type of glass		
	C	E	S
Density(g/cc)	2.49-2.50	2.54-2.62	2.48-2.50
Tensile Strength (MPa)			
@22 C	3034-3309	3447	4585
@371 C	-	380	545-645
@538 C	-	250	350
Tensile Modulus			
@22 C	10	10.5	12.4
@538 C	-	11.8	12.9
Coefficient of thermal expansion			
(mm/mm/C)	7.2	5.05	5.58
Specific Heat, @22 C	0.188-0.212	0.193-0.197	0.176
Softening Point, (C)	749-750	840-846	970
Dielectric Strength, kV/cm	-	103-196	130
Dielectric Constant			
@ 60 H2	-	0.003-0.005	0.003-0.013
@ 10^6 H2	0.008	0.002-0.0025	0.003-0.0034
Index of Reflection	1.532	1.547-1.562	1.523-1.525
Chemical resistance			
(%of weight gain after 24hr. Expose)			
In H_2O	1.1	0.7	0.7
In 10% HCL	4.1	4.2	3.8
In 10% H_2SO_4	2.2	3.9	4.1
In 1% Na_2CO_3	2.4	2.1	2

Conversion units: 1 MPa = 145.04 psi, 1 g/cc = 0.58 oz/in^3, 1 kV/cm = 2.54 V/mil

2.1.3.3.3 <u>Carbon fibers.</u> Carbon fiber is created using polyacrylonitrile (PAN), pitch, or rayon fiber precursors. PAN-based fibers offer good strength and modulus values up to 6×10^6 to 6.5×10^6 KN/m^2 (0.85 to 1.0 msi). They also offer excellent compression strength for structural applications up to 6.5×10^6 KN/m^2 (1000 ksi). Pitch fibers are made from petroleum or coal tar pitch. Pitch fibers have extremely high modulus values, and the favorable coefficient of thermal expansion make them the choice material used in space/satellite applications. Table 2.3 indicates the properties of carbon fibers. Carbon fibers are more expensive than glass fibers; however, carbon fibers offer an excellent combination of strength, low weight, and high modulus. The tensile strength of fiber is equal to glass, while its modulus is about three to four times higher than glass. Carbon fibers are supplied in a number of different forms, from continuous filament tows to chopped fibers and mats. The highest strength and modulus are obtained by using unidirectional continuous reinforcement. Twist-free rows of continuous filament carbon contain 1,000 to 75,000 individual filaments, which can be woven or knitted into woven roving and hybrid fabrics with glass fibers and aramid fibers. Carbon fiber composites are more brittle (less strain at break) than glass or aramid. Carbon fibers can cause galvanic corrosion when used next to metals. A barrier material, such as glass and resin, is used to prevent this occurrence.

2.1.4. Durability of Composites. The earliest FRP materials used glass fibers embedded in polymeric resins that were made available by a burgeoning petrochemical industry following World War II. The combination of high-strength, high-stiffness structural fibers with low cost, light-weight, environmentally resistant polymers resulted in composite materials with mechanical properties and durability better than either of the

constituents alone. Fiber material with higher strength, higher stiffness, and lower

density, such as carbon, aramid, and boron, were commercialized to meet higher

performance challenges of space exploration and air travel in the 1960's and 1970's.

This section has a literature review on durability of composites.

Table 2.3. Properties of carbon fibers (Berenberg B. -www.composites.about.com)

Fiber	Typical diameter (micro m)	Specific Gravity	Tensile Modulus (GPa)	Tensile Strength (GPa)	Strain to Failure (%)	Coefficient Of Themal Exp.(micro m/C) (0-100)	Poisson's Ratio
Pan-carbon							
T-300c	7	1.76	228	3.2	1.4	-0.1 to -0.5	0.2
ASd	7	1.77	220	3.1	1.2	-0.5 to -1.2	
T-40c	6	1.81	276	5.65	2		
HMSd	7	1.85	344.5	2.34	0.58		
GY-70e	8.4	1.96	483	1.52	0.38		
Pitch-carbon							
P-55c	10	2	380	1.9	0.5	-0.9	
P-100c	10	2.15	690	2.2	0.31	-1.6	

Conversion units: 1 GPa = 145.04 ksi, 1 μm = 39.37 μin

2.1.4.1 General. Polymer and polymer composites are increasingly being used in

a wide range of applications where long-term service in hostile environments is required.

As a consequence, there is growing demand for manufacturers to guarantee the life

expectancy of their products, particularly where inspection can be difficult or failure

catastrophic. Examples of such applications include strengthening of existing bridge structures, gas pipelines, chemical storage tanks, underground cabling, aerospace components, personnel safety equipment, and medical implants. Stringent product guarantees are also increasingly being demanded for engineering components in products such as cars and domestic appliances, where consumers often view extended lifetime warranties as a sign of product quality. While the life expectancy of products in non-demanding applications has traditionally been predicted from past experience, the use of polymers in long-term or critical applications requires a far better understanding of the failure mechanisms to enable lifetime predictions to be made.

2.1.4.2 Aging mechanism in polymers. As FRP matrices find greater use in markets such as civil infrastructure and ground transportation, the expectations placed on these materials are ever increasing. High performance materials have led to the disappearance of resins such as bismaleimides (BMI), cyanate esters, and other high performance polyimides and epoxys. In their place polymers, such as polyester and vinylester, have arisen. This section will review the aging mechanism of polymers.

2.1.4.2.1 <u>Thermal aging</u>. Thermal degradation refers to the chemical and physical processes in polymers that occur at elevated temperatures. Increased temperature accelerates most of the degradation processes that occur in polymers such as oxidation, chemical attack and mechanical creep. The influence of temperature on the oxidation processes will depend on the chemical structure of the polymer. Thermo oxidation is initiated by the reaction of free radicals P^O with oxygen to form peroxide radicals (see Equation 2.1).

$$P^O + O_2 \rightarrow POO^O \qquad\qquad (2.1)$$

All polymers contain these free radicals due to their polymerization and processing history. However, the concentration of free radicals can be significantly increased by interaction with light, ionizing radiation, or the presence of transition metals. Once formed, the peroxide radicals undergo slower propagation reactions that break down the polymer chains. The overall degradation process will normally involve a relatively long induction period during which little degradation is observed. At the end of this period, there is a rapid increase in degradation leading to a significant reduction in the mechanical properties of the polymer. This induction period is temperature sensitive and is reduced significantly at elevated temperatures. The induction period of the degradation process can normally be regarded as the serviceable lifetime of the polymer.

Other physical changes can occur in a polymer at elevated temperatures, one of the most common being thermal expansion. Thermal expansion is reversible and in general does not significantly affect the life expectancy of a polymer. However, in polymer composites, the mismatch between the thermal expansion of the polymer matrix and the fibers may cause thermo-mechanical degradation during thermal cycling. Similar mechanisms may also occur in adhesive joints. A sudden brief exposure to high temperatures can result in a phenomenon known as thermal spiking.

2.1.4.2.2 <u>Weathering</u>. Weathering, or more specifically photo-oxidation of polymers, refers to the chemical and physical changes that occur when radiation is absorbed by a polymer. Photo degradation is initiated by solar radiation, which results in the absorption of UV radiation by chromospheres and in the activation of excited states in macromolecules. However, other climatic quantities such as heat, moisture, and air-

23

bourn pollution, all influence the mechanisms of degradation and the subsequent results of aging.

When a polymer is exposed to solar radiation the energy absorbed by the polymer results in the formation of free radicals within the polymer by the dissociation of the C-H bonds in the polymer chains.

$$PH \rightarrow P^O + H^O \qquad (2.2)$$

The extent of this chemical reaction depends upon the radiation exposure that is the quantity of ultraviolet light (<350 nanometers) to which it is exposed. Once free radicals have been produced, reaction with oxygen generates hydro peroxides (POOH).

$$P^O + O_2 \rightarrow POO^O \qquad (2.3)$$

$$POO^O + PH \rightarrow POOH + P^O \qquad (2.4)$$
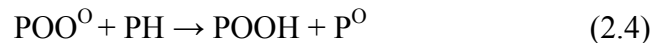
These hydro peroxides can dissociate further to produce a series of decomposition products including aldehydes and ketones. The presence of these carbonyl groups in a degraded polymer can be used as a chemical index for degradation. Once formed, free radicals can continue to react via propagation reactions long after the initial UV exposure has ended. Termination of free radical reactions is normally achieved through the reaction of pairs of free radicals.

$$P^O + P^O \rightarrow P\text{-}P \qquad (2.5)$$

The formation and propagation of free radicals in itself does not seriously affect the mechanical properties of the polymer, as they do not significantly alter the long-chain nature of the polymer molecules. Degradation of the mechanical properties occurs because the free radicals produced are highly unstable and readily undergo chain scission reactions resulting in the formation of two smaller polymer chains, one of which is a free radical and capable of further reactions.

The intensity of the UV radiation decreases with increasing depth in the material, so the reaction tends to be a near-surface process. Since oxygen is involved in the reaction process, there is an important balance between UV radiation, oxygen diffusion, and temperature, which determines the kinetics of reaction and the transport of the reactive species. Under natural exposure conditions, there will be wetting and drying cycles and dark periods. The significance of the latter is that some recovery of the oxygen concentration in the material can occur, which otherwise is confined to the very near surface due to consumption by reaction with the polymer radicals. Since the concentration of these radicals diminishes by a termination reaction during the dark period, oxygen ingress can extend to greater depth.

2.1.4.2.3 <u>Chemical degradation.</u> Chemical attack of thermoplastics involves a specific chemical reaction of the polymer with the fluid; the most common mode of failure is hydrolysis by water, acids, and alkalis. Esters, amides, imides, and carbonate groups are particularly susceptible. Where these groups are located in the backbone chain rather than the side chain, chain scission ensues. A general hydrolysis scheme can be summarized as follows:

The reduction in molecular weight consequent upon chain scission can lead to a reduction of toughness and fracture strain. Stress is known to accelerate the chain scission process and also to enhance the rate of fluid uptake.

2.1.4.2.4 <u>Environmental stress cracking</u>. Environmental stress cracking (ESC) remains one of the most common causes of failure in polymers. The main reason for this failure is the complexity of the phenomenon, with aspects such as chemical compatibility, liquid diffusion, craze formation, and crack development all playing their parts. While crystalline and amorphous polymers are both susceptible to ESC, amorphous polymers are particularly susceptible due to their relatively open structure which leads to easy fluid penetration. Once the fluid has penetrated the polymer, it becomes locally dissolved, promoting cracking and crazing in the polymer. Cracking is normally preceded by the formation of crazes initiated at sites of stress concentration or at regions of local microstructural homogeneity.

Crazes are voids that are held together by highly drawn fibrils, which bridge the void allowing the craze to transmit stress and prevent the craze from propagating. The mechanism of crazing in chemical environments is generally considered to be identical to that in air. In general terms, craze initiation is considered to evolve from micro deformation processes in localized regions about 30 mm (1.2 in.) in diameter.

As the deformation region develops, further localized deformation is induced. The growth and coalescence of such deformed nuclei create a narrow plastic zone. In the presence of dilatational stress, voids develop. This voided structure is considered the precursor of the fibrillated craze structure that ultimately leads to failure.

The environment accelerates the craze formation process by local plasticization (i.e., enhancement of the local relative movement of molecular chains by reduced intermolecular interaction between chains). However, the particular phase of craze precursor development during which acceleration by the environment occurs, as well as the susceptibility of individual polymer types, is less clear. The role of the environment has been proposed to determine when the voided precursors break down to form crazes. Also suggested is that the environment is important in void stabilization through surface energy reduction.

Stress concentration can be important not only for the development of local deformation zones (although this is not necessarily dependent on stress concentration), but also for concentrating absorbed molecules in response to the presence of dilatational stress.

The rapid growth of the craze precursor to a visible craze is believed to occur at a critical level of the inelastic strain, which is independent of the environment and temperature. This level has significant implications for assessing the durability of a polymer. For example, in polymer-fluid combinations that lead to plasticization-induced toughening, simultaneous exposure may delay the development of crazes.

However, exposure to the fluid after the sample has been stressed in air to attain the critical level of inelastic strain may lead to rapid crazing. This finding helps explain the very rapid development and growth of crazes in many cases when environment exposure times are relatively short, but the time under stress has been long.

2.1.4.2.5 Ionizing radiation. Ionizing radiation covers a wide range of different forms of radiation, including x-rays, gamma rays, neutrons, alpha particles, and beta

particles. When a polymer is irradiated, the ionizing radiation induces degradation by the formation of free radicals or ions in the polymer. These reactive intermediates are capable of initiating chemical reactions that occur by free radical or ionic mechanisms and that result in scission and in cross-linking reactions.

Free radicals with a long lifetime, which are present in the bulk of the material after irradiation, are responsible for changes in properties even a long time after exposure. The intensity of ionizing radiation on the earth's surface is not normally high enough to significantly affect most polymers; hence, radiation exposure tests are only required in connection with nuclear plants and where radiation is used for applications such as medical x-rays, sterilization, or cross-linking.

2.1.4.2.6 Biological degradation. Biological degradation is not a common form of degradation, as most commonly used thermoplastics are resistant to microbiological attack. The only cases were biological attack has influenced life expectancy has been with certain polyurethanes and some low molecular weight additives in PVC3. No predictive techniques for the life expectancy of conventional polymers due to biological degradation have been developed, although standards exist for testing resistance.

There is, however, growing interest in the development of deliberately short-lived polymers both for medical applications and for use as disposable packaging.

2.1.4.2.7 Fatigue. Polymers will suffer failure when they are exposed to cyclic loads at stresses well below those they can sustain under static load. This phenomenon is known as fatigue and is responsible for approximately 1 in 5 of all polymer failures. The general approach to fatigue is to develop curves of applied stress (S) against the number of cycles before failure (N). These are known as S-N curves and have a characteristic

sigmoidal shape, often flattening out when N is large, suggesting a fatigue limit. Unlike metals, the S-N curves for polymers are extremely frequency-dependent. This dependency is due to increases in the temperature of the polymer caused by mechanical hysteresis, resulting in thermal softening. Accordingly, failure under cyclic loading can be either ductile or brittle. Fatigue failures are particularly serious, as there is often little visual warning that failure is imminent.

     2.1.4.2.8 Creep. Creep is the gradual increase in strain that occurs in a material when it is subjected to a constant load over an extended period of time. Viscoelastic materials, such as polymers, can undergo creep at relatively low stress levels and often at temperatures below room temperature. Dimensional stability under stress is essential in many applications, so creep can be a significant problem. Creep will ultimately lead to rupture either by ductile or brittle failure. At low temperatures and high loads, creep rupture will be brittle; at intermediate loads and temperatures, failure will be ductile; and after long lifetimes, slow and low-energy brittle failures will occur. The slow, low-energy brittle failures are more problematic in predicting life expectancy.

2.2. RECENT RESEARCH STUDIES RELATED TO LONG-TERM DURABILITY OF FRP COMPOSITE SYSTEMS

     Since concrete structures strengthened with FRP composite materials behave as a system, assessment of the long-term performance of an FRP composite material itself, which was briefly discussed in the previous section, may not be directly applicable to FRP composite systems. Therefore, this section aims to address recent research studies on the long-term durability of FRP composite systems and to highlight key issues in this field.

Most research studies regarding long-term durability of concrete structures strengthened with FRP composites have focused on the following five environmental conditions: (1) freeze and freeze-thaw conditions, (2) wet-dry cycles and corrosion of steel reinforcement, (3) combined environmental conditions, (4) creep and fatigue, and (5) field study.

2.2.1. Freeze and Freeze-Thaw Conditions. FRP plating as a technique does have its problems; however, the most pressing issue is premature plate separation due to bond failure, which invariably leads to sudden and catastrophic failure of the reinforced concrete member. One major area of concern is that during freezing-and-thawing cycling, temperature-induced stresses in the adhesive layer (due to differential thermal expansion between the FRP and the substrate concrete) may lead to bond damage and contribute to or cause premature plate separation. Freezing and thawing damage to the FRP material itself, the adhesive, or the substrate concrete may also occur.

Bisby and Green, (2002) studied the effects of freezing and thawing cycling on the FRP-concrete bond by conducting flexural tests on a total of 39 small-scale, under-reinforced concrete beams of size 102 x 152 x 1220 mm (4 x 6 x 48 in.). Because the beams were fabricated in two groups, several months apart, the concrete strength for the beams designated CFRP-A and CFRP-B was 31 MPa (4.5 ksi), and that for the beams designated CFRP-C and GFRP was 43 MPa (6.25 ksi). These beams were plated on their tension faces with a single layer of one of four FRP materials. The FRP material was bonded only over a short length at each end of the beam to promote a debonding failure mode rather than tensile rupture of the FRP material (hence isolating the behavior of the bond). The bond length was chosen based on a review of previous work in the area.

Once plated, all beams were subjected to between 0 and 300 thermal cycles in a manner similar to ASTM C 310 (1961), consisting of freezing in air at –18° C (0° F) for 16 hours and thawing in water at 15° C (59° F) for 8 hours. However, they concluded freezing-and-thawing cycling for up to 200 or 300 cycles does not appear to significantly affect the overall load deflection behavior, the crack development, or the bond strain or stress distributions. The failure mode was affected slightly by freezing-and-thawing cycling, likely due to changes in the elastic properties of the adhesives. The overall performance of the carbon FRP-A plated beams, including bond behavior, appeared to be somewhat enhanced by freezing-and-thawing cycling. While both the load and deflection at failure seem to be decreased by freezing-and-thawing cycling for the carbon FRP-B plated beams, the bond does not seemed to be similarly affected and may even be improved by the cycling, as indicated by increased average bond stresses at failure. Similar results were found for both the carbon FRP-C and glass FRP sheets, although the bond may have experienced very minor deterioration due to freezing-and-thawing cycling, as evidenced by slight reductions in the average bond stresses at failure.

Soudki and Green, (1997) studied the change in response of the concrete confined by FRP composite sheets after exposure to 50 freeze-thaw cycles, which was a modified version of ASTM C 666 (standard test method for resistance of concrete to rapid freezing and thawing). They used standard cylinders of size 150 mm in diameter and 300 mm in height (6 x 12 in.) wrapped with carbon FRP sheets. During the freeze-thaw cycles, warm water at 18° C (65° F) was used to thaw the specimens. The results showed that the compressive strength of concrete cylinders wrapped with one layer of carbon FRP sheet decreased by approximately 15 percent from exposure to the freeze-thaw cycles.

Toutanji and Balaguru, (1999) reported similar results. They tested small-scale, unreinforced concrete columns of 75 mm in diameter and 300mm in height (3 x 12 in.) wrapped with different types of FRP sheets, in uniaxial compression, after exposure to 300 freeze-thaw cycles in accordance with ASTM C 666. During the freeze-thaw cycles, salt solution was used to thaw the specimens. After exposure to the freeze-thaw cycles, compressive strength decreased by 28 percent and 19 percent respectively, for glass FRP and carbon FRP wrapped columns. However, they concluded that the decrease in compressive strength was preliminary due to the effect of freeze-thaw cycles on the concrete itself in the end (top and bottom portion) of the column, which was directly exposed to the freeze-thaw cycles, rather than the degradation coming from FRP composite materials.

Green et al., (2000) also examined the effects of freeze-thaw cycling on the bond between the FRP and concrete. An experimental investigation was conducted using both single lap pull off and bond beam specimens. Only uniaxial CFRP strips were considered. The specimens were exposed to up to 300 freeze-thaw cycles consisting of 16 hours of freezing and 8 hours of thawing in a water bath. After exposure, the specimens were tested to failure. The development of strain along the bond length and the failure mode are presented for both types of specimens. The results indicated that the bond between carbon FRP strips and concrete was not significantly damaged by up to 300 freeze-thaw cycles.

Karbhari et al., (2000) also studied the behavior of the FRP wrapped column subjected to 200 freeze-thaw cycles. They used standard cylinders of size 150 mm in diameter and 300 mm in height (6 x 12 in.) to evaluate the change in ultimate strength.

The standard cylinders were wrapped with CFRP and GFRP sheets with different configurations. The freeze-thaw cycles in these tests were different from the ASTM C666-97 in that the temperature range was wider, and no thawing water was used. They reported that the freeze-thaw cycles in their study had no significant deteriorative effect on the strength of the FRP confined concrete regardless of the configurations and types of the FRP sheets. Rather, the cylinders wrapped with carbon FRP sheets exhibited a slight increase in compressive strength due to the freeze-thaw cycles exposure. In an earlier study performed by Karbhari and Eckel, (1994), similar results were observed. They placed the standard cylinders of size 150 x 300 mm (6 x 12 in.) wrapped with different FRP sheets under an extremely low temperature, -18° C (0° F), instead of freeze-thaw cycles to simulate the cold climate. The result showed that a slight increase in ultimate strength was observed regardless of the type of FRP sheet. They concluded that the increase was due to the matrix hardening effect.

Baumert et al., (1996) tested reinforced concrete (RC) beams strengthened with carbon FRP sheets to investigate the effect of cold region climate at -8° C (17° F). They concluded that the extremely low temperature did not affect the carbon FRP sheets in a negative way. Furthermore, the specimen exposed to the low temperature showed higher failure load when compared to specimens kept constantly at a low temperature.

2.2.2. Wet-Dry Cycles and Corrosion of Steel Reinforcement. Corrosion is a worldwide problem facing most bridges and structures. Recent surveys conducted on infrastructure in North America that needs strengthening and rehabilitation have reported that about 170,000 bridges in the United States (Klaiber et al., 1987) and 8,000 bridges in Canada (Bickley et al., 1993) are partially damaged by corrosion and need to be repaired,

33

requiring instant action. Corrosion of the steel reinforcement has a significant effect on the load carrying capacity of RC beams (Rodriguez et al., 1994; Mangat and Elgarf, 1999). A deterioration of the bond at the steel-to-concrete interface due to corrosion of the steel reinforcement has also been reported in numerous studies (Al- Sulaimani et al., 1990; Saifullah and Clark, 1994; Almusallam et al., 1996). Most studies reported that the bond strength at first increased with increasing corrosion levels, and then a continuous reduction in the bond strength took place. This reduction was especially marked by the absence of a confining reinforcement. Although FRP composites are considered to be an effective alternative to steel and solution for strengthening and/or rehabilitation of corrosion damaged RC structures, their effectiveness has not yet been fully studied. When an FRP composite material is used as external reinforcement, it can entrap the existing moisture chloride ions serving as a diffusion barrier of moisture ingress into the concrete. When being used as internal reinforcement, the FRP composite can be deteriorated by the high alkaline environment of concrete.

Maaddawy et al., (2005) developed a model for predicting the inelastic flexural response of corroded RC beams repaired with FRP laminates, which is presented here. The model accounts for the combined effects of corrosion, FRP strengthening, and FRP wrapping on the beam load-deflection response. The beam is modeled as a series of elements, each having a length equal to the mean stabilized crack spacing. Then, for a given value of load, the deflection of the beam is calculated by evaluating the elongation of the steel reinforcement within each element. The model was implemented into a computer program called *ACFRP* to examine its accuracy and reliability. A comparison of the model's predictions and the results of an experimental study carried out by the

writers showed that the model accurately predicted the load-deflection relationships of corroded FRP repaired beams.

Badawi and Soudki, (2004) conducted an experimental study to investigate the effect of CFRP confinement on the cracking damage induced by impressed current-accelerated corrosion of RC beams. The beams were 254 mm deep by 152 mm wide by 3,200 mm long (10 x 6 x 125 in.). Two different corrosion configurations, uniform corrosion and shear-span corrosion, were investigated in 8 specimens at 3 different degrees of corrosion (5, 10, and 15 percent theoretical mass loss). Uniform corrosion along the whole length of the beams (3,000 mm (10 ft)) and shear-span corrosion (900 mm (3 ft) from each beam end) were considered. The different degrees of corrosion were induced using an accelerated corrosion technique with an impressed current. Based on the results, they have made the following conclusions: Corrosion-induced crack width increases with time as corrosion activity progresses. Larger crack widths are obtained at higher levels of corrosion. The maximum permissible flexural crack width specified by North American codes was exceeded at around 3 percent mass loss. Comparable rates of corrosion activity were obtained for the shear-span and uniform corrosion beams; confining the corroded RC beams with carbon FRP U-wrap reduced the corrosion expansion by up to 70 percent for the shear-span corrosion beam and by up to 65 percent for the uniform corrosion beam. Carbon FRP U-wrap confinement reduced the corrosion mass loss in the post repaired beams by 35 and 33 percent for the shear-span and uniform corrosion beams, respectively, compared to the unwrapped corroded beams.

Maaddawy and Soudki, (2004) also conducted an experimental study designed to investigate the viability of using externally bonded CFRP laminates to extend the service

35

life of corroded RC beams. A total of 14 beams, 152 x 254 x 3,200 mm (6 x 10 x 125 in.)

each, were tested. Three beams were not corroded; two of them were strengthened by

carbon FRP laminates, while one specimen was kept as a virgin. The remaining 11

beams were subjected to different levels of corrosion damage up to a 31 percent steel

mass loss using an impressed current technique. Six of the corroded beams were repaired

with carbon FRP laminates, whereas the remaining five beams were not repaired.

Eventually, all specimens were tested to failure under four-point bending. The following

conclusions were made by the authors: Corrosion of the steel reinforcement has a

significant effect on the serviceability of RC beams. Average steel mass losses of about

9.6, 15.6, 23.3, and 30.5 percent resulted in maximum corrosion crack widths of about

1.1 mm (0.05 in.), 1.4 mm (0.055 in.), 2.5 mm (0.1 in.), and 3.1 mm (0.12 in.),

respectively. Corrosion of the steel reinforcement significantly reduces the yield and

ultimate loads of RC beams. The reduction in the yield load was almost proportional to

the reduction in the steel mass loss. For the beam ultimate strength, reductions of about

12, 14, 14.5, and 24 percent were recorded at steel mass losses due to corrosion of about

9.7, 15.4, 22.8, and 30 respectively. Carbon FRP repair that consists of one flexural

laminate along with U-shaped transverse strips is effective in increasing the strength of

corroded RC beams at all levels of corrosion damage (up to 31 percent steel mass loss) to

levels higher than the strength of the virgin uncorroded beam. For example, the ultimate

strength of a beam repaired with carbon FRP laminates at 31% steel mass loss was about

73 percent higher than that of a similar corroded and unrepaired beam and about 31

percent higher than that of the virgin beam that was neither corroded nor repaired. CFRP

repair significantly reduces the deflection capacity relative to that of the corroded and

unrepaired beams. The deflection capacity of the corroded and repaired beams was on average about 46 percent lower than that of the corroded and unrepaired beams. The beams repaired with Scheme I (flexural strengthening with a continuous wrapping) showed a higher stiffness but a lower deflection capacity than those of the beams repaired with Scheme II (flexural strengthening with an intermittent wrapping). This outcome is attributable to the greater confinement provided by the continuous wrapping compared with that provided by the intermittent wrapping, which accordingly improved the bond at the steel-to-concrete interface, and thus increasing the beam stiffness but reducing the deflection capacity.

Masoud et al., (2001) investigated the behavior of RC beams strengthened with carbon FRP sheets under corrosive environment. The specimens were subjected to an accelerated corrosion process consisting of impressed current and wet-dry cycles. Longitudinal cracks were observed after the accelerated corrosion process for both strengthened specimens and unstrengthened specimens; however, the cracked widths of the strengthened specimens were significantly smaller than those of the unstrengthened specimens. The results also revealed that the fatigue life of the specimens strengthened with carbon FRP sheets was greatly improved, even after the accelerated corrosion process, when compared to corrosion damaged unstrengthened specimens.

Toutanji and Gomez, (1997) studied the effect of wet-dry cycles using seawater on the behavior of unreinforced concrete beams strengthened with different types of FRP sheets. The specimens were conditioned by 300 wet-dry cycles and tested in four point bending. The ultimate failure load of the specimens exposed to the wet-dry cycle was lower than that of control specimens. The authors concluded that the reduction in the

ultimate failure load might be attributed to the degradation of epoxy resin used, which led to the weakening of the bond between concrete and FRP sheets. In addition, they stated that the extent of reduction was dependent on the type of epoxy resins used. Toutanji, (1999) also tested standard cylinders of size 150 mm in diameter and 300 mm in height (6 x 12 in.) wrapped with different types of FRP sheets and using two kinds of epoxy resins. Toutanji reported that the ultimate strength of GFRP wrapped specimens was reduced by 10 to 18 percent after exposure to the wet-dry cycles when using type A epoxy (modified amine/epoxy resin blend). In the case where type B epoxy (polyxylporpylenediamine hardener/epoxy resin) was used, insignificant loss (less than 3 percent) of ultimate strength was reported. For carbon FRP wrapped specimens, the decrease in ultimate strength was less than 5 percent regardless of which epoxy was used.

 2.2.3. Combined Environmental Conditions. During the entire life span of the structure, it passes through the different seasons. Thus, the need is arising to assess the durability of FRP composite systems under the combined environmental system, which includes freeze-thaw cycles, wet-dry cycles, high temperature cycles, UV radiation, and saline solution.

 Myers et al., (2001) conducted an experimental program to investigate the durability of the bond between concrete and various FRP sheets (carbon, glass aramid). The entire experimental program consisted of tests on forty-eight 152 x 152 x 610 mm (6 x 6 x 24 in.) pre-cracked beam specimens strengthened in flexure with carbon, glass, or aramid FRP sheets. The beams were pre-cracked under single point loading by applying the cracking load prior to strengthening with FRP sheets. After the beams were strengthened with the FRP sheets, they were subjected to combined environmental effects

including freeze-thaw, high moisture, high temperature cycling, and indirect ultraviolet radiation exposure under sustained load (0 percent, 25 percent, and 40 percent of ultimate load). After exposure, the longitudinal steel reinforcement in the beams was cut prior to testing to better assess the bond characteristics of the FRP laminates. The beams were tested under 2-point flexural load after the exposure period; crack growth, strain in FRP growth and strain in the FRP sheets were recorded. Based on their results, they concluded that combined environmental exposure has an adverse effect on the bond performance of FRP sheets to concrete. Members strengthened with three different FRP sheets indicated a reduction in flexural stiffness and a degradation of the FRP sheet's bond to the concrete. For a specimen conditioned under higher sustained loads (40 percent of ultimate load), comparatively more degradation in bond was observed, particularly when compared to unloaded specimens. One other thing researchers noted was that strain readings did not highlight a premature bond failure, meaning, if the surface preparation and sheet installation is done according to specifications, there should not be any danger of sudden peeling of FRP sheet from concrete.

Micelli et al., (2000) tested concrete cylinders wrapped with FRP sheets in uni-axial compression after exposure to the combined environmental cycles. They reported that specimens wrapped with glass FRP sheets, when compared to the unconditioned specimens, exhibited a 20 percent reduction of compressive strength after conducting an environmental cycle. CFRP wrapped specimens did not show this decrease in compressive strength. Also reported was that the use of saline solution during the environmental cycles aggravated the degradation of the compressive strength.

2.2.4. Creep and Fatigue. Infrastructure (e.g. bridges) is continuously subjected to repeated loads that may cause fatigue of the reinforcing bars. When corrosion is combined with repeated loads causing fatigue of reinforcement, the service life of the structure can be significantly reduced. Structural engineers are faced with the challenge of assessing the vulnerability of such deteriorated structures and deciding on appropriate retrofit techniques.

Masoud et al., (2005) conducted an experimental and analytical study of the fatigue performance of corroded RC beams repaired with FRP sheets. Ten RC beam specimens of size 102 x 152 x 1220 mm (4 x 6 x 48 in.) were constructed. One specimen was neither strengthened nor corroded to serve as a reference; 3 specimens were corroded and not repaired; another 3 specimens were corroded and repaired with U-shaped glass FRP sheets wrapping the cross section of the specimen; and the remaining 3 specimens were corroded and repaired with U-shaped glass FRP sheets for wrapping and CFRP sheets for flexural strengthening. The FRP sheets were applied after the main reinforcing bars were corroded to an average mass loss of 5.5 percent. Following FRP repair, some specimens were tested immediately to failure, while the other repaired specimens were subjected to further corrosion before being tested to failure to investigate their post repair (long-term) performance. The authors have made the following conclusions: Corrosion of the main reinforcing bars to a minor degree can result in a significant reduction in fatigue life if pits are formed. FRP repair scheme I (U-wrapping only) did not significantly improve the fatigue life at any degree of corrosion. The flexural strengthening utilized in FRP repair scheme II reduced the stress range in the main reinforcing bars, leading to a significantly longer fatigue life than that of the unrepaired

specimens. The fatigue life of the specimens repaired using scheme II was on average 2.5 times that of the unrepaired specimens. An equivalent fatigue notch factor was estimated for the specimens tested in fatigue. The factors obtained were 1.94 for the control specimen and 2.16 on average for the unrepaired and U-wrapped corroded specimens (scheme I). Pitting corrosion resulted in the increase in the fatigue notch factor compared to the control specimen. This increase resulted in a significant reduction in the fatigue life. For the U-wrapped specimens with a flexural sheet (scheme II), the fatigue notch factor was 2.33 on average. This increase in fatigue notch factor compared to the control specimen was due to pitting corrosion as well as a decrease in the stress level in the main reinforcement due to the presence of the flexural sheet.

Ekenel et al., (2006) strengthened seven RC beams with two FRP systems. Two beams were maintained as unstrengthened control samples. Three of the RC beams were strengthened with CFRP laminates; whereas, the remaining two were strengthened using FRP precured laminates. Glass fiber anchor spikes were applied in one of the carbon FRP laminate strengthened beams. One of the FRP precured laminate strengthened beams was bonded with epoxy adhesive, and the other one was attached by using mechanical fasteners (MF). Five of the beams were tested under fatigue loading for two million cycles. All of the beams survived fatigue testing. However, the authors drew the following conclusions: the FRP strengthening increased the fatigue life of RC beams by increasing stiffness and reducing crack propagation. The change in stiffness at 2 million cycles as compared to the initial cycle was approximately the same for all the beams (15 percent). This was due to the fasteners, which allowed greater crack formation and propagation until the strengthening engagement was complete. The fatigue loading

slightly reduced the member's ductility, but did not significantly affect the failure load for the carbon FRP laminate strengthened and unstrengthened specimens tested. Based on the flexural test results, it can be concluded that the analytical design using ACI Committee 440.2R-02 (ACI, 2002) was conservative in calculating the ultimate capacity of the beam, even after two million fatigue-cyclings at service load (except for the beam strengthened with MF-FRP).

FRP precured laminate showed a load at failure 14 percent lower than the expected value. This result can be partially attributed to the higher damage accumulation around the anchorage holes in the FRP precured laminate. Monitoring the damage accumulation in cyclic loading would be interesting for future investigation; the fatigue and static loading exhibited that the use of MF can be an alternative to the epoxy bonded systems. Moreover, the beam strengthened with MF-FRP showed a more desirable apparent ductile behavior as compared to the beam strengthened with an epoxy bonded FRP system. The use of anchor spikes resulted in a significant increase (39 percent) in the ultimate capacity of the beam as compared to a carbon FRP strengthened beam without anchor spikes. The increase in capacity is attributed to the presence of the anchor spikes, which improved the bond properties at the concrete-carbon FRP interface, as shown in the failure modes. The increase in labor costs using this anchorage technique could be offset by a reduction in the flexural reinforcement used.

Savoia et al., (2005) have done extensive research on long-term creep deformation of RC tensile elements strengthened by external FRP plates. Formation of discrete cracks in concrete under tension was taken into account. A kinematic model was used, where relative slips between concrete, steel bars, and FRP plates were considered,

governed by viscous interface shear stress-slip laws. Bazant's solidification theory and exponential algorithm were used to obtain incremental constitutive equations for concrete as well as for steel-concrete and FRP-concrete interface laws. Moreover, cohesive normal stresses across transverse cracks in concrete were considered. The incremental differential system of equations was transformed into a nonlinear algebraic system by a finite difference discretization with respect to axial coordinates. Several numerical examples were presented, concerning both short-term and long-term loadings. The research showed that reinforcing by means of FRP plates or sheets has significant beneficial effects on the behavior of RC elements under service loadings because it increases concrete tension stiffening effect, and it strongly reduces crack width.

Aidoo et al., (2004) examined the effects of one-dimensional FRP composite rehabilitation systems on the flexural fatigue performance of RC bridge girders. Eight 508 mm deep and 5600 mm long (20 x 220 in.) RC T-beams, with and without bonded FRP reinforcement on their tensile surfaces, were tested with a concentrated load at midspan under constant amplitude cyclic loading. The objective of this investigation was to establish the effect that these repair systems have on the fatigue behavior and remaining life of the girders. The investigation showed that the fatigue behavior of such retrofit beams is controlled by the fatigue behavior of the reinforcing steel. The fatigue life of a RC beam can be increased by the application of an FRP retrofit, which relieves some of the stress carried by the steel. Thus, it is important that the FRP retrofit be as stiff as possible. For this reason, carbon FRP, rather than glass, is preferred. Although, stiff retrofit measures also result in higher FRP-to-concrete bond stress. The observed increase in fatigue life is limited by the quality of the bond between the carbon FRP and

the concrete substrate. Debonding, initiating at midspan and progressing to a support, is common and is driven partially by the crack distribution and shear deformations of the beam. Once debonding has progressed, stresses are no longer transferred to the CFRP and the fatigue behavior of the beam reverts to that of an unretrofit beam.

Brena et al., (2002) tested eight RC beams externally strengthened with CFRP composites under the fatigue load. In their tests, load amplitudes generated stresses representative of service loads in a bridge. The carbon FRP composites used in the strengthening were of three types: pultruded plate, woven fabric, and unidirectional fiber. The test results showed that the bond between the composite laminates and the concrete surface was not degraded.

2.2.5. Field Study. The field applications of FRP composite materials in civil infrastructures date from the early 1990s. Therefore, field data on long-term durability performance of FRP strengthened reinforced concrete bridges is not abundant. However, the use of FRP composite materials for strengthening of RC structures has been successfully demonstrated to date.

3. ANALYTICAL METHOD

3.1. GENERAL

In order to investigate the life expectancy of FRP strengthened bridges or structures, three major aspects are to be considered: (1) bond degradation between FRP plates and existing concrete, (2) corrosion rate of the reinforcement before and after the strengthening of the structure, and (3) degradation of the FRP material alone. Amongst

these three variables, the first two are considered to be more important than the third one. This chapter covers the modeling aspect of each type of variable irrespective of the others.

3.2. BOND DEGRADATION BETWEEN FRP LAMINATES AND EXISTING CONCRETE

CFRP materials are increasingly being used for the repair and rehabilitation of flexural concrete elements in buildings and bridges. In this method, the carbon FRP material is bonded to the concrete surface using epoxy adhesives. As the load is transferred to the carbon FRP material by epoxy, the durability of its bond with the concrete is critically important for the integrity and safety of the repaired structure. Information on the long-term durability of a CFRP/epoxy/concrete bond is relatively scarce. Product literature sometimes contains data that purports to provide evidence of satisfactory performance, although evaluating techniques for long-term monitoring are seldom included.

3.2.1. Bond Behavior between FRP and Concrete. Bond behavior between FRP and concrete depends on many factors, including the properties of the FRP being terminated, the concrete strength, the bond width of the FRP, and the net width of the concrete portion of the horizontal fracture plane through the steel reinforcement. The beam design at the critical section, the shear and bending moment at the critical section, and the properties of the bond layer also all factor into bond behavior. This section will focus on bond related issues in the field of civil engineering.

3.2.2. Bond Behavior and Failure Modes. In regions where FRP sheets cross a crack, tensile stresses resulting from shear cracking must be transferred to the concrete.

Strength capacity is generally limited more by the bond between the FRP and the concrete than by the tensile capacity of the laminate. Bond may be developed by any of four mechanisms of adhesion: mechanical interlocking, diffusion, electronic, and absorption, with mechanical interlocking being by far the most prevalent mechanism of adhesion. Mechanical interlocking occurs with the linking of the uneven surfaces of concrete and epoxy wherein the epoxy occupies voids on the concrete surface. A roughened concrete surface, free from loose material, is essential in providing good mechanical interlocking. Karbhari, (1995) gives five possible modes of failure between the FRP and concrete substrate: peeling within the concrete substrate, interfacial failure between the concrete and adhesive surfaces, cohesive failure within the adhesive, failure between the adhesive and concrete surfaces, and finally, failure that alternates between the two surfaces. The most common failure modes in the literature for bonded specimens include shearing of concrete beneath the glue line and FRP failure after development of its full tensile capacity.

The typical assumption of perfect bond between the FRP and concrete surface was found to be initially justified in the linear elastic range of the concrete (Lee et al., 1999). After the concrete cracks, there is a load level at which the crack reaches a peak and begins to decrease abruptly (Bizindavyi and Neale, 1999). At the same time, the shear stress in the region adjacent to the crack begins to increase. The decrease in shear stress near the crack is attributed to distribute cracking in that region, resulting in shear stresses being increased to the adjacent region. This finding was similar to that of Maeda et al., (1997) who found that, in the initial stages of loading, strain is limited to a region within the effective bond length. Once delamination progresses in this area, the area of

46

active bonding is shifted further away from the crack. This phenomenon progresses until the entire sheet is debonded, often rapidly. This failure mechanism is reported by Taljsten, (1997) to be governed by tensile strain in the concrete (in tests of bonded steel and CFRP plates). The concrete begins to fracture at 0.8 to 1.0 mm (0.03 to 0.04 in.) as measured on the plate above the area of debonding.

3.2.3. Bond Strength. Use of average bond strength is limited to shorter length samples, since bond stress is developed over a relatively short distance (Dolan et al., 1998). This finding implies that average bond strength decreases as the bond length becomes longer, since at a certain bond length the ultimate strength cannot be increased any further. Samples with a longer bonded length will exhibit progressive debonding where bond stresses are shifted away from the crack as debonding progresses. The bond strength of FRP to concrete has been found to be limited by the strength of the adhesive bond to concrete—the concrete substrate shear strength (Dolan et al., 1999). The adhesive must have sufficient toughness to dissipate energy from cracking as well as sufficient strength and stiffness to transfer stress between the concrete and the composite (Xie and Karbhari, 1998).

Bond strength increases with increasing concrete strength (Horiguchi and Saeki, 1997; Izumo et al., 1997; and Khalifa, 1998). If shearing of the concrete beneath the bonded area governs failure, the value of bond strength will be proportional to the square root of the concrete strength (Chajes et al., 1996). However, the properties of the bulk concrete within the member may be different from the surface properties of the concrete since the surface is more prone to bleeding, segregation, and improper curing. Some researchers propose bond strength can be estimated by the concrete strength alone

because the dominant mode of failure, shear within the concrete substrate, is independent of the fiber type (Horiguchi and Saeki, 1997 and lzumo et al., 1998). Through the work of these researchers, the bond strength was found to be proportional to the 2/3 power of the concrete compressive strength.

Concrete surface properties affect the bond strength that can be developed. Surfaces should be mechanically abraded, sandblasted, or hydro blasted, and a primer should be applied to achieve the best bond. Chajes et al., (1996) compared different concrete surface preparations. Grinding improved bond strength by a small amount compared to using the surface as formed, but mechanical abrasion (with a wire wheel) gave a 10 percent increase in bond strength. This finish was claimed to be similar to what could be achieved with sand blasting. Above this level of roughness, Khalifa et al., (2001) found that no further improvement occurred from strengthening beams in shear using additional hydro-blasting or from drilling holes in the surface of the concrete at a grid spacing of about 25 mm (1 in.) to produce rougher surfaces. Bond tests completed by Sato et al., (1997) suggested that by using mechanical anchorage, the bond strength could be more than doubled. This anchorage consisted of bolts passing through the bond specimen, applying a clamping force to the bonded region. Full bond strength could not be determined because additional modes of specimen failure were caused by splitting the concrete.

Bond strength has also been found to vary according to the test set-up (Horiguchi and Saeki, 1997). Tensile tests result in the highest estimate of bond strength, followed by bending tests and shear tests. The peel tests used by Karbhari, (1995) are a mixture of

a direct tension test and a shear test, but is not intended as a structural efficacy test, only a means to evaluate the effects of environmental exposure on various materials.

3.2.4. Strain Distribution. Profiles of strain distribution were found to change depending on the level of loading (Bizindavyi and Neale, 1999). As the load is initially applied, strain exhibits an exponentially decreasing trend, from the maximum strain at the crack to no strain some distance away from the crack. The length over which the strain goes to zero is defined as the initial transfer length. The initial transfer length was found to be constant for all loads lower than those causing cracking (Bizindavyi and Neale, 1999). The second stage results in a bilinear decreasing strain profile with the change in slope occurring at the initial transfer length. The third stage was found to differ depending on the type of fiber. For GFRP, the third stage exhibited a linear decreasing trend, while for stiffer CFRP the trend was non-linear decreasing.

These findings were somewhat different from what had previously been found. Strain data from Izumo et al., (1998) shows an exponentially decreasing trend for all load stages with the maximum strain occurring just away from the crack and with a bond length of approximately 100 mm (4 in.) for all types and configurations of fibers studied. Maeda et al., (1997) found two stages in the strain distribution—a parabolic distribution at early stages of loading followed by a bilinear decreasing trend for the strain distribution at ultimate. Bizindavyi and Neale, (1999) found that the width of the bonded laminate had little influence on its strain distribution. However, the only widths considered were 25.4 mm (1 in.) and 50.8 mm (2 in.), considerably smaller than what would be necessary for shear strengthening of civil engineering structures. Furthermore,

the strain distribution was only considered with the crack running perpendicular to the fiber direction.

3.2.5. Effective Bond Length. No increase in bond strength occurs when the bond length exceeds the effective bond length (Izumo et al., 1998). A number of researchers have reported the bond length to be approximately 100 mm (4 in.) (Izumo et al., 1998; Volnyy and Pantelides, 1999). However, this length depends on the thickness of the sheets or plates being used, since Bizindavyi and Neale, (1999) reported effective bond lengths as low as 55 mm (2.16 in.) for carbon FRP sheets with a thicknesses of 0.111 mm (4.4×10^{-3} in.), while Taljsten, (1997) reported an effective bond length of approximately 300 mm (11.8 in.) for a thickness of CFRP plate thickness of 1.2 mm (0.047 in.). The effective bond length was also found to decrease as the stiffness of the fibers increased (Bizindavyi and Neale, 1999). Furthermore, effective bond length was found to be affected by geometry, test method, and plate width (Volnyy and Pantelides, 1999). Volnyy and Pantelides (1999) also predicted the effective bond length based on fracture mechanics theory. Stiffness of the FRP was used to predict the effective bond length in the Equation 3.1 by Maeda et al., (1997).

$$Le = e^{\left[6.134 - 0.580 \ln\left(I_{RRP}E_{FRP}\right)\right]} \tag{3.1}$$

This equation was determined from the least squares method using test results. The average bond stress could also be calculated based on observation that the strain gradient, or the slope of the strain distribution curve, was approximately constant at 110 x 10^{-6} per mm (2.8×10^{-3} per in.). This result was less than the average strain gradient found by Saco et al. (1997) of 168 x 10^{-6} per mm (4.27×10^{-3} per in.).

3.2.6. Modeling Approach. An analytical model for bond degradation of FRP and existing concrete is proposed in this section. The proposed model was developed based on correlating laboratory results conducted at Queen's University and published by Bisby and Green, (2002). Data provided by Bisby and Green indicates a slightly decreased ultimate load and mid span deflection, decreased maximum FRP strain prior to bond failure, and decreased average bond stress at failure with increasing numbers of freezing-and-thawing cycles. These trends would again indicate that the FRP-concrete bond might be damaged by exposure to freezing-and-thawing cycles over time, although the relative apparent damage after 50 cycles is greater than after 200 cycles, a result that is counterintuitive and suggests the bond deterioration rate slows over time as cycles increase..

Test results proposed by Bisby and Green observed an approximate reduction of 5 percent in load carrying capacity of externally carbon FRP laminated beams after 50 freeze-thaw cycles. After 200 freeze-thaw cycles, a reduction in the load carrying capacity was observed at around 10 percent. These losses were attributed to bond degradation. In laboratory tests, one freeze-thaw cycle was considered from -15 to 20°C (5 to 70°F). More than 30 years data collected at the case study bridge site and made available on the National Oceanic and Atmospheric Administration (NOAA) website was used to determine the average number of freeze-thaw cycles the bridge endures per year and to develop the bond degradation model. 200 freeze-thaw cycles were equivalent to 40 years of service exposure, based on analyzing site weather data. The authors have assumed the laboratory bond testing conditions may be representative of field conditions under similar freeze-thaw cycles even though many of the field freeze-thaw condition

51

gradients may occur over a less severe temperature-time cycle. This assumption was thought to be conservative, but much more work needs to be done to correlate lab durability studies to field conditions and to address some of the assumptions and limitations in this work

Figure 3.1 presents the sample data page collected from the NOAA website, which gives the detailed temperature record for the month of June, 1995 at Buffalo station in Dallas County, Missouri. This station was selected as the nearest possible location to the bridge P-0962.

Figure 3.1. Temperature data (sample of one month) at bridge site

Figure 3.2 is a map of United States illustrating the number of days on which the temperature falls below 28° F with 90 percent probability. Bridge locations where the ambient temperature is lower than -2°C (28° F) for around half a year (180 days) is also shown.
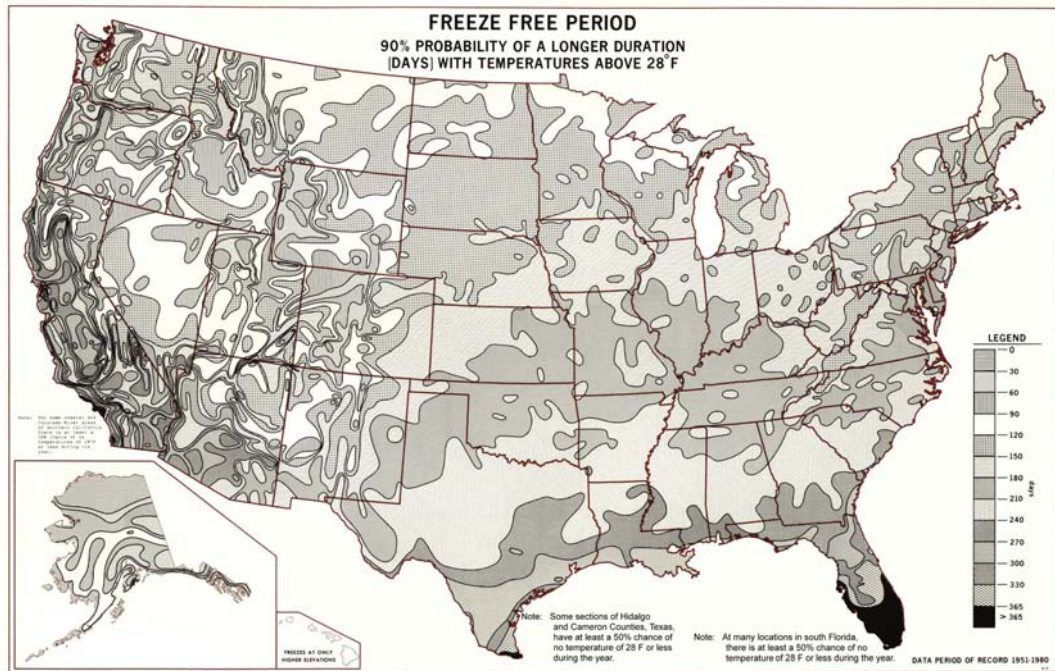
Figure 3.2. Map of USA's varying temperature conditions

Figure 3.3 illustrates a bond degradation model based on the above statistical data and considering Bisby and Green's laboratory results. As noted previously, this model assumes that the laboratory results obtained by Bisby and Green may be representative of field behavior. More work is required to validate this assumption and determine if some refinement in the presented model may be warranted. Lab testing results may in fact be more assertive than field behavior due to the more aggressive thermal cycles created in the laboratory. If this premise is true, the presented model will be conservative.
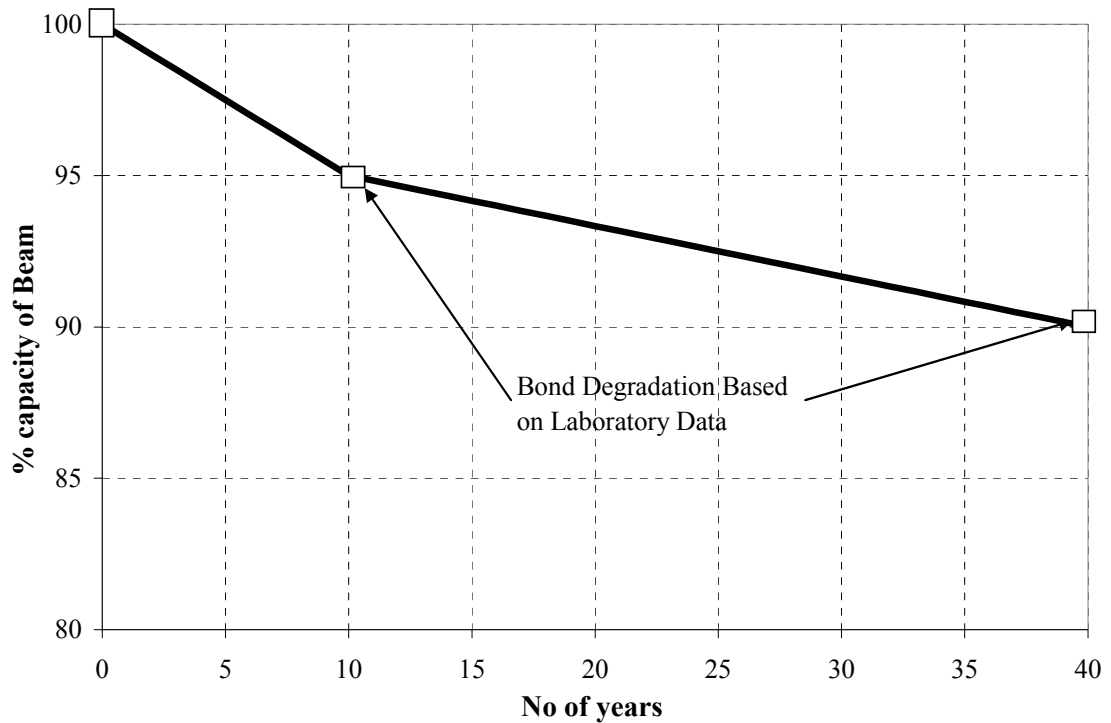
Figure 3.3. Bond degradation of between FRP and substrate concrete

3.3. CORROSION OF STEEL IN CONCRETE

Traditionally, the structural and non-structural factors affecting the serviceability of structures have been treated as separate issues by designers and have also been within separate circles of engineers. For an architect, the aesthetics of the structure stands as the focus during the design process, whereas the structural engineer sees his or her responsibility as delivering a structure that is safe and reliable under all loading conditions. However, it is not only mechanical loading that has to be considered. Every structure is exposed to environmental conditions, which may have an enormous influence on durability.

Usually the interaction between the material of the structure and the environment is called corrosion. Studying the history of steel reinforced concrete, we find very rare cases where the structure failed due to mechanical loadings that were not considered at the design stage. Technical standards provide sufficient information for and give guidance to civil engineers in designing a structure adequate to withstand all mechanical loading. The problem arises with a lack of sensitivity to and knowledge of corrosion issues by civil engineers. Therefore, corrosion of steel reinforcement in structures is now a feature that figures heavily into the maintenance of existing structures, such as bridges and buildings, and has contributed to a number of structural collapses.

3.3.1. Mechanism of Corrosion. Corrosion of steel in concrete is an electrochemical process. The corroding system consists of an anode in which steel is corroded, a cathode, an electrical conductor, and an electrolyte (concrete pore solution). The potential difference between the anode and cathode is the driving electrical force for steel corrosion. Usually, the process can be divided into primary electrochemical processes and secondary processes.

3.3.1.1 Primary electrochemical processes. For steel in concrete, as the passive film is degraded by chloride ions or the pH reduced by carbonation, the metallic Fe at the anode is oxidized to form ferrous ions F (e^{2+}) as illustrated in Equation 3.2.

$$Fe \rightarrow Fe^{2+} + 2e^- \qquad\qquad (3.2)$$
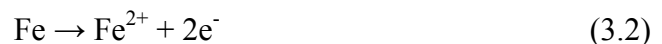
The electrons released at the anode flow through the steel to the cathodic areas, as illustrated in Figure 3.4. The above reaction is initially balanced by the cathodic reaction of dissolved oxygen (O_2) to hydroxyl ions (OH^-) illustrated in Equation 3.3.

$$O_2 + 2\,H_2O + 4e^- \rightarrow 4\,OH^- \tag{3.3}$$

The anodic product Fe^{2+} reacts with the cathodically formed hydroxyl ions to produce a ring of a white precipitate of ferrous hydroxide (Fe $(OH)_2$):

$$Fe^{2+} + 2OH^- \rightarrow Fe\,(OH)_2 \tag{3.4}$$

Ionic Current

$1/2O_2 + H_2O + 2e^- \rightarrow 2OH^-$

$4Fe\,(OH)_2 + O_2 + H_2O \rightarrow 4Fe(OH) \rightarrow \underline{2Fe_2O_3 H_2O} + 4H_2O$
$Fe^{2+} + 2OH^- \rightarrow Fe\,(OH)_2$
$Fe^- \rightarrow Fe^{2+} + 2e^-$

Electronic Current
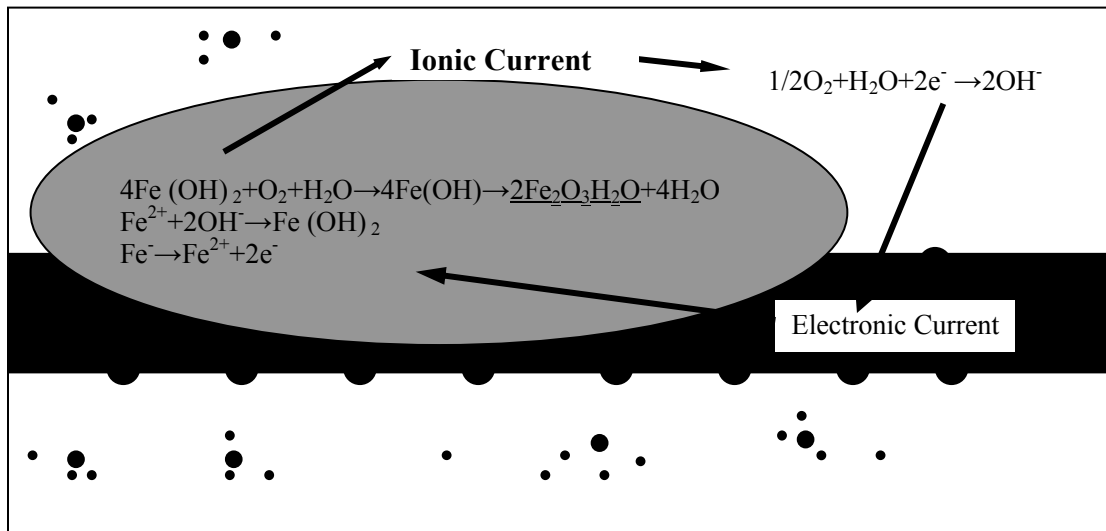
Figure 3.4. Mechanism of corrosion of steel in concrete

3.3.1.2 Secondary processes. The Fe $(OH)_2$ can be further converted to hydrated ferric oxide $F(e_2O_3 . H_2O)$, also known as ordinary red-brown rust, and black magnetite F (e_3O_4) preceded by the formation of green hydrated magnetite ($Fe_3O_4 . H_2O$):

$$4\,Fe\,(OH)_2 + O_2 \rightarrow Fe_2O_3 \times H_2O + 2H_2O \tag{3.5}$$

$$6\,Fe\,(OH)_2 + O_2 \rightarrow 2\,Fe_3O_4 \times H_2O + 4\,H_2O \tag{3.6}$$

$$Fe_3O_4 \times H_2O \rightarrow Fe_3O_4 + H_2O \qquad\qquad (3.7)$$
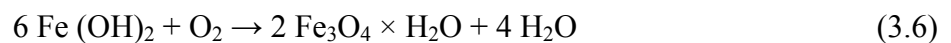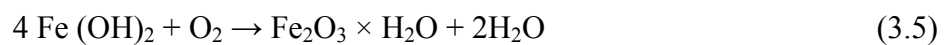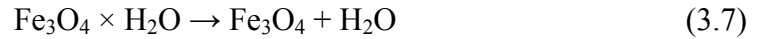
The composition of rust on iron may be expressed as a general formula given in Equation 3.8.

$$m \times Fe\,(OH)_2 + n \times Fe(OH)_3 + p \times H_2O \qquad\qquad (3.8)$$
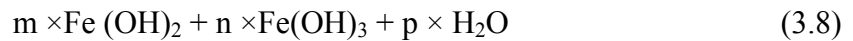
The values of m, n, and p vary considerably, depending on conditions such as pH of the solution, the oxygen supply, and moisture content.

Since the volume of rust products is much higher (about 4 to 6 times) than that of the iron, as shown in Figure 3.5, the formation of rust products will lead to cracking of the cover concrete when expansive stress exceeds the tensile strength of the concrete; the reduction of steel reinforcing cross section may lead to structure failure.

3.3.1.3 Initiation of steel corrosion in concrete. The high alkaline environment of good quality concrete forms a passive film on the surface of the embedded steel, which normally prevents the steel from further corroding. To maintain the passivity of steel in concrete requires a high pH and presence of both water and oxygen. Two major causes of steel corrosion in RC (and consequent initiation of active corrosion) are carbonation-induced corrosion and chloride-induced corrosion.

Fe

FeO

Fe3O4

Fe2O3

Fe(OH)2

Fe(OH)3

Fe(OH)3 3H2O

1 2 3 4 5 6 7

Volume, cm ^{3}
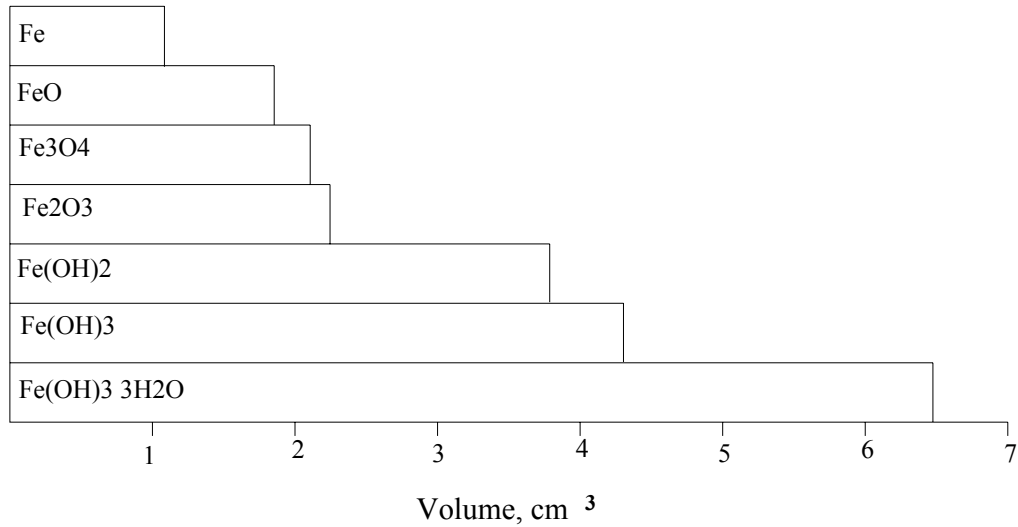
Conversion units: 1 cm^3 = 0.06 in.^{3}

Figure 3.5. The relative volumes of iron and its corrosion reaction products

3.3.1.3.1 <u>Carbonation-induced corrosion.</u> Concrete structures are constantly affected by CO_2 in the atmosphere. In the presence of CO_2, which in an aqueous solution is a weak acid, the different hydrates in cement paste, such as portlandite ($Ca(OH)_2$) and CSH, can react with CO_2 and become carbonated.

$$Ca(OH)_2 + CO_2 \rightarrow CaCO_3 + H_2O \qquad\qquad (3.9)$$

$$2NaOH + CO_2 \rightarrow Na_2CO_3 + H_2O \qquad\qquad (3.10)$$

The resulting carbonation lowers the pH value and dissolves the protective film which maintains a high pH environment for the steel; when steel surface is exposed corrosion results.

The carbonation rate is mainly determined by quality of concrete, which is a function of cement type, water/cement ratio, and proportion of cement. The degree of saturation of the concrete is also a decisive factor in determining the carbonation rate,

58

because the CO_2 permeates the concrete most rapidly in the gas phase, but the carbonation reaction takes place in the liquid phase. In a completely dry concrete or a completely saturated concrete, the carbonation reaction rate is very slow. When the pores have a layer of moisture on the walls but are not completely saturated (50 to 80 percent relative humidity), the CO_2 can rapidly reach the vicinity of the pore walls and have enough water to react.

3.3.1.3.2 <u>Chloride-induced corrosion</u>. The fact that the presence of chloride ions in RC can cause the steel to corrode if sufficient oxygen and moisture are present to sustain the reaction is well documented. Chloride-induced corrosion is the most prevalent and damaging cause of steel corrosion in concrete. Chloride ions may be introduced into concrete in two ways:

A) Internal source from concrete-making materials. Chloride ions may be introduced in the fresh concrete mix if the concrete-making materials (water, cement, and aggregate) are contaminated with chlorides. Some concrete admixtures, such as calcium chlorides, also contain chloride ions.

B) External source from deicing salts or seawater. Deicing salts are widely used in areas of the world where the pavement and bridge decks are kept clean and bare in the winter. Salts are the most common source of chloride ions. Chloride ions are also prevalent in seawater, so structures exposed to sea water are also contaminated. The penetration of chloride ions from external sources to the steel surface is mainly through capillary attraction and ionic diffusion.

3.3.1.3.3 <u>Mechanism of chloride attack</u>. The mechanism of chloride-induced corrosion of steel is not yet fully understood. The general belief is that the chloride ions

become incorporated in the passive film, replacing some of the oxygen, and increasing both its conductivity and its solubility.

It has been suggested that chloride ions can complex with the ferrous ions produced by corrosion to form soluble complexes of iron chloride. The resulting iron chloride complex ion then combines with hydroxyl ions to form Fe $(OH)_2$ in solution and releases the chloride ions back to solution to complex more iron, thus essentially acting as a catalyst in corrosion reactions.

3.3.1.3.4 <u>Threshold chloride concentrations</u>. To initiate corrosion, a threshold concentration of chloride (minimum concentration of chloride necessary to destroy the passive film) is required in excess of the amount immobilized by reaction with tri calcium aluminate in cement. The general belief is that only freely dissolved chloride ions in the concrete pore water can be involved in the corrosion reactions.

This threshold concentration of chloride ions to initiate corrosion is controversial because it is dependent on so many factors, including quality of concrete (w/c ratio, mixture proportions and type of cement), relative humidity and temperature of the concrete, and the pH of the pore solution, and sulfated content.

Figure 3.6 illustrates the relationship between some factors and the threshold chloride concentration given by Committee Euro-International d'Beton (CEB). The value of 0.4 percent of chloride ion by weight of the cement is considered by RILEM as an appropriate threshold. For the typical concrete mixtures normally used in practice, the threshold chloride content is reported to be in the range of 0.60 to 0.83 kg (1.32 to 1.83 lb) of chloride ions per cubic meter of concrete 0.58 to 0.82 kg/m^3 (1.0 to 1.4 lb/yd^3).

3.3.1.4 Corrosion activity of concrete. The fact that the corrosion rate of steel in concrete in different situations can vary widely, ranging from tens to even hundreds of times, is well known. The rate of corrosion of steel in concrete is mainly dependent on ionic conductivity of concrete electrolytes, its humidity and temperature, and the quality of cover concrete as related to the transport of the corrosive species from external environment to the steel surface.

3.3.1.4.1 <u>Conductivity of concrete</u>. Generally, the best measure of corrosivity of concrete is its conductivity, usually expressed as the reciprocal, the resistivity. A low concrete resistivity indicates a high corrosive activity. The resistivity of the concrete is mainly determined by the salt content in the pore water, degree of saturation, and temperature. The resistivity of the concrete can vary widely for different conditions.

There is an absence of complete correlation between electrical resistivity and concrete corrosivity. Because the corrosion process in concrete is a complex process, oxygen availability at a cathode area is also a controlling factor for the corrosion rate of steel in concrete. The relationship between moisture and oxygen in concrete is presented in Figure 3.6.

3.3.1.4.2 <u>Water-air relationship in concrete</u>. The concrete capillary-pore system filled with water and air acts as the corrosive electrolyte. Apart from the pore structure, porosity, and pore size distribution of the concrete, water content in the concrete is dependent on the local amount and time of rainfall and external relative humidity and temperature.

Certain water content in concrete is an essential requirement for corrosion to take place. As a rule, the presence of oxygen is also necessary for cathodic reaction process.

If a pore volume of the concrete is only partly filled with water, transfer of oxygen to the steel surface by means of diffusion in the gas phase will be easy. Whereas, when a pore volume of the concrete is completely filled with water, then oxygen can reach the steel surface only by diffusion through the pore water, and the diffusivity of oxygen in water is about four powers lower than that in air.
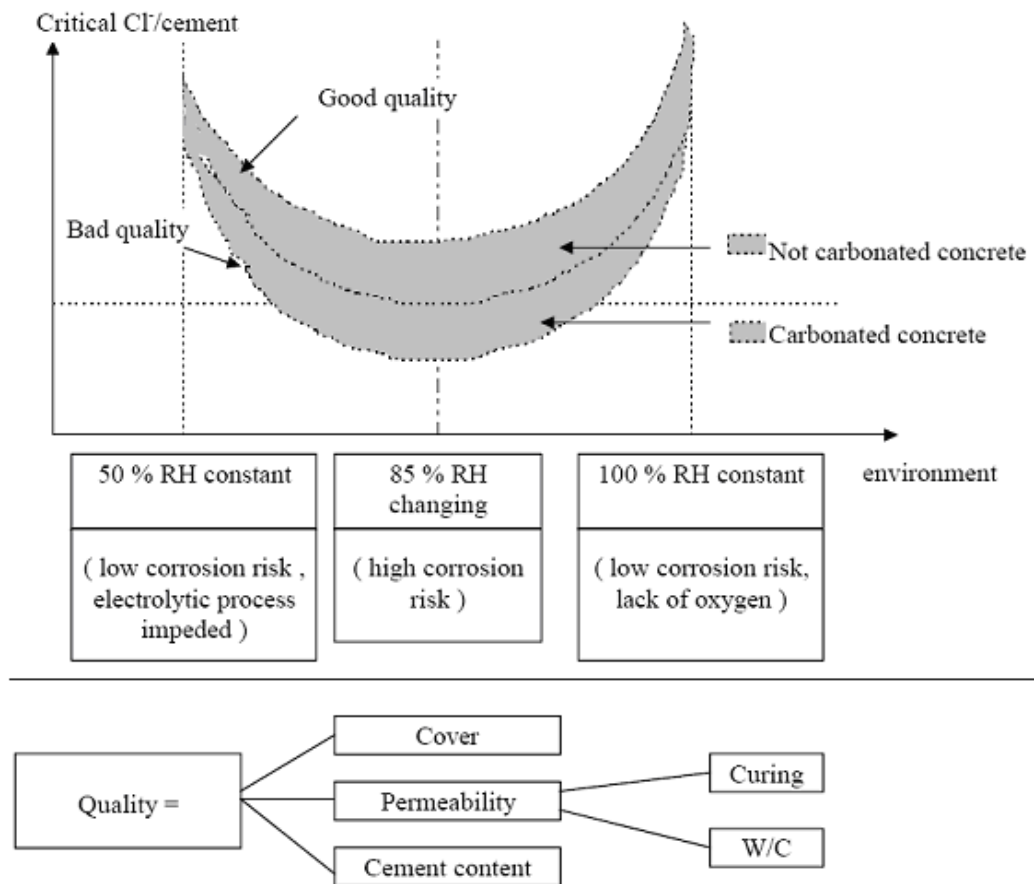

Figure 3.6. The critical chloride content according to CEB recommendations
(Draft CEB Guide to Durable Concrete Structures, 1985)

With an increase in the water content in concrete, the corrosion rate will first increase due to an improved conductivity. When the water content approaches the degree of a complete filling of the concrete pores, the corrosion rate rapidly decreases to a low value due to the strongly obstructed supply of oxygen. The importance of water content for oxygen transport explains why the corrosion rate is considerably higher in the structure located within the tidal and splash zone than below the tidal zone; corrosion is very rapid in the splash zone.

3.3.1.4.3 <u>Penetration of corrosion species in concrete</u>. Usually, penetration of a particular substance such as chloride ions into concrete can be in two forms, capillary attraction and ionic diffusion, depending on the degree of saturation in the concrete. The content of chloride ions (not total chloride content, only the soluble ones) at a steel surface has a great effect on the corrosivity of steel in concrete. The quality of cover concrete (permeability) and cover depth is the key to determine the ease of chloride ions reaching the steel surface.

Capillary movement is a fast method of transport; however, it is unlikely water will migrate this way. First, mature concrete has a discontinuous pore system, and second, concrete holds water in the capillaries, so the driving potential (capillary attraction) is ceased. Cracking provides an easy pathway for chloride ions to penetrate concrete cover and reach the reinforcing steel. Structural cracks, however, are aligned perpendicular to the main reinforcement and thus limiting access to the steel bars. Only subsidence cracking is dangerous with respect to chloride-induced corrosion. These cracks are positioned parallel and directly above the bars. Development of subsidence cracks depends on concrete cover, bar diameter, and the slump of concrete. Therefore,

the primary modes of transport of chloride ions into the concrete are through diffusion in uncracked concrete and through cracks and diffusion in cracked concrete.

Chloride ion migration into concrete is an ionic diffusion process following Fick's second law. Fick's second law of diffusion represents non-steady state diffusion and is expressed in a form of a partial differential equation:

$$\frac{\partial C}{\partial t} = D c \frac{\partial^2 C}{\partial x^2}$$ (3.11)

Where: C = Chloride ion concentration

Dc = diffusion coefficient

T = time

X = depth

Equation 3.11 has many solutions depending on the boundary conditions. The most common solutions used in the analysis of chloride distribution in concrete are the ones with a boundary condition of surface chloride concentration, C_0, being either constant (Equation 3.12) or dependent on the square root of time (Equation 3.13).

$$C(x,t) = CO \left(1 - erf \frac{x}{2\sqrt{DCt}} \right)$$ (3.12)

Where: $C_{(x,t)}$ = Chloride ion concentration at depth x after time t

Co = Chloride Surface Concentration

erf = Error function

Or

$$C\left(x,t\right) = k\sqrt{t}\left[e^{-x^2/4Dct} - \frac{x\sqrt{\Pi}}{2\sqrt{Dct}}\left(1 - erf\frac{x}{2\sqrt{DCt}}\right)\right]$$ (3.13)

Where: K   = material characteristics coefficient dependent on surface

concentration ($Co = k\sqrt{t}$)

3.3.1.4.4 <u>Reinforcing steel corrosion.</u> In RC structures, steel bars embedded in

concrete do not normally corrode initially. First, the concrete cover, if dense, intact, and

thick, forms a barrier greatly reducing the penetration rate of exterior degradation agents.

Second, concrete is highly alkaline in nature and causes embedded steel bars to be

covered with a passivation layer, a thin and dense impermeable film of iron oxide. This

film is strongly adhered to the surface and does not allow the anodic reaction to occur,

thus making steel passive to corrosion. As long as the passivation layer is intact, the

anodic reaction cannot take place. Due to the high concentration of alkalis in the pore

water and soluble calcium hydroxide in concrete, the pH is usually well above 12. The

passivation layer on the steel surface is thermodynamically stable as long as the pH of

concrete (pore water) remains above 11.5. The pH of concrete has a significant influence

on the behavior of steel in concrete. The general belief is that the lower the pH of

concrete, the higher the probability of corrosion. For different values of pH of concrete,

the rate of corrosion occurrence changes in the following manner:

- pH > 10   : no corrosion

- 4 < pH < 10   : corrosion rate is constant

- pH < 4   : corrosion rate is rapid

Another cause of passive film breakdown occurs when chloride ions are present at high concentrations on the bar surface. Chloride ion-induced corrosion of reinforcing steel in concrete elements is one of the main causes of concrete deterioration. Corrosion of steel in concrete structures is caused primarily by gradual intrusion of water and chloride ions from deicing salts, as well as from saltwater exposure in coastal regions, into the concrete. Cracks are not necessary for chloride penetration. Salts are capable of penetrating concrete together with the water in which they are dissolved. The resulting presence of chlorides and a loss of the alkaline environment cause the embedded steel to loose its surface passivity. Corrosion follows, as water and oxygen become available to the steel. Accumulated corrosion products, which occupy more volume than the reactants, cause cracking of the protective concrete cover. This cracking allows for intrusion of chlorides and oxygen at a much faster rate, thus accelerating the corrosion process. Depending on the bar size, bar spacing, and cover depth, cracking can be in the form of either delamination cracking or inclined cracking. Delamination cracking is characterized by horizontal cracks extending from one bar to another. Inclined cracking describes those cracks that propagate to the surface at an angle of about 45° and result in section loss and potholes, often seen in bridge decks. Figure 3.7 presents the two types of

cracking. Steel corrosion is also intensified when the protective concrete cover of the

embedded bars is inadequate or other design or construction inadequacies occur.
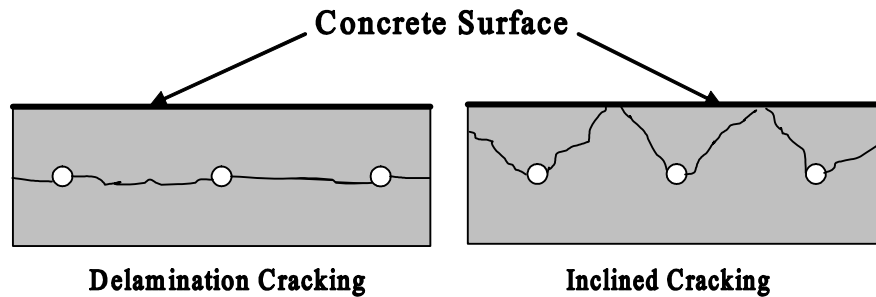
Figure 3.7. Corrosion related cracking in concrete

3.3.1.4.5 Corrosion types. Pitting and general corrosion are the two most

common types of corrosion of steel reinforcement in concrete. Pitting corrosion occurs

when only a small area of steel loses its passive layer, usually due to high concentrations

of Cl^- ions. Pitting corrosion is characterized by a large cathode area and a small anode

area, resulting in accelerated corrosion. General corrosion occurs when the pits grow

together, anode areas are large, and the cathode areas are small. The corrosion rate is

much slower when compared to pitting corrosion because of the lower cathode-to-anode

ratio.

Another classification is based on relative position of anodic and cathodic sites.

This relative position depends on a potential difference between the anodic and cathodic

sites. The larger the potential difference, the further apart the anode and the cathode can

be. If the two sites are in close proximity to each other, micro cell corrosion occurs.

When the anode and cathode sites are further apart and a large potential difference

between the anode and cathode exists, macro cell corrosion occurs. Slater, (1983) suggested that accelerated corrosion of bare steel reinforcement in the decks with bottom mats of coated steel is a result of macro cell corrosion. In most cases, however, since macro cell corrosion requires a larger potential difference than the micro cell corrosion does, it is more likely for the micro cell to be a dominant type.

3.3.2. Service Life Modeling. This section explains modeling of chloride-induced corrosion of steel in concrete and describes a diffusion model to be used for determining service life for bridge superstructure elements. The concentration is on modeling chloride-induced corrosion of steel rebar resulting from accumulation of chlorides in a bridge superstructure element exposed to chloride ions in the external environment (e.g., deicing salts). This section does not consider other corrosion mechanisms, such as carbonation or corrosion from chlorides cast into the concrete, or other deterioration mechanisms, such as alkali aggregate reactions, sulfate attack, or freeze-thaw damage. The model estimates accumulated damage as the function of age from construction completion of the bridge superstructure.

The process of chloride-induced corrosion of steel in concrete is described as follows:

1. Chlorides in the environment build up on the concrete surface.

2. Chlorides are transported through the concrete by a number of mechanisms, including diffusion and capillary action.

3. The chloride concentration builds up with time at the steel surface.

4. Once the chloride level achieves a critical threshold, the passive oxide layer on the steel breaks down, and corrosion starts.

68

5. Corrosion products have a higher volume than the steel consumed products exerting tensile stresses on the concrete.

6. Concrete is weak in tension, so the concrete cracks occur either vertically to the surface or horizontally to form a delamination between reinforcing bars.

7. Cracks form pot holes or spalls, which lead to a degradation in the structure's appearance, function, and safety, leading to end of service life or time to repair.

8. The repairs may be made, and the cycle continues either in the previously undamaged areas or as the repair system degrades with time.

The process of modeling, therefore, requires the following:

- Calculating the chloride ion content at the surface of the concrete. This activity is termed the surface chloride ion concentration (C_0).

- Calculating the rate of transport from the surface to the steel. This activity measures the rate of diffusion of the chloride ions into concrete and is designated by the use of a coefficient termed the diffusion coefficient (Dc).

- Determining the critical chloride concentration required to initiate corrosion. This measure is referred to as the corrosion threshold (Ccr).

- Estimating the time to corrosion initiation. This estimate is the age at which corrosion initiates on the reinforcing steel (Ti).

The chloride content in concrete for bridge P-0962 was determined through analysis of powdered concrete samples. Samples were collected on-site at different depths up to and beyond the depths and locations of the reinforcing steel using a masonry drill. The powdered samples were tested in the laboratory using non-destructive testing instrument CL-2000 chloride test system made by James Instruments confirms to

AASHTO-T-260. Figure 3.8 illustrates the collection of samples on site and Figure 3.9 illustrates the testing of the collected samples.

Figure 3.8. Collection of powdered sample on site

After calculating chloride content from the collected powdered samples, the time for initiation of corrosion of steel in concrete has been determined. Detailed calculations are attached in Appendix A. Also Appendix B details where samples were taken (in both high and low moment regions across the beam). Figure 3.10 presents a proposed model showing the loss of steel area with respect to the age of the structure.
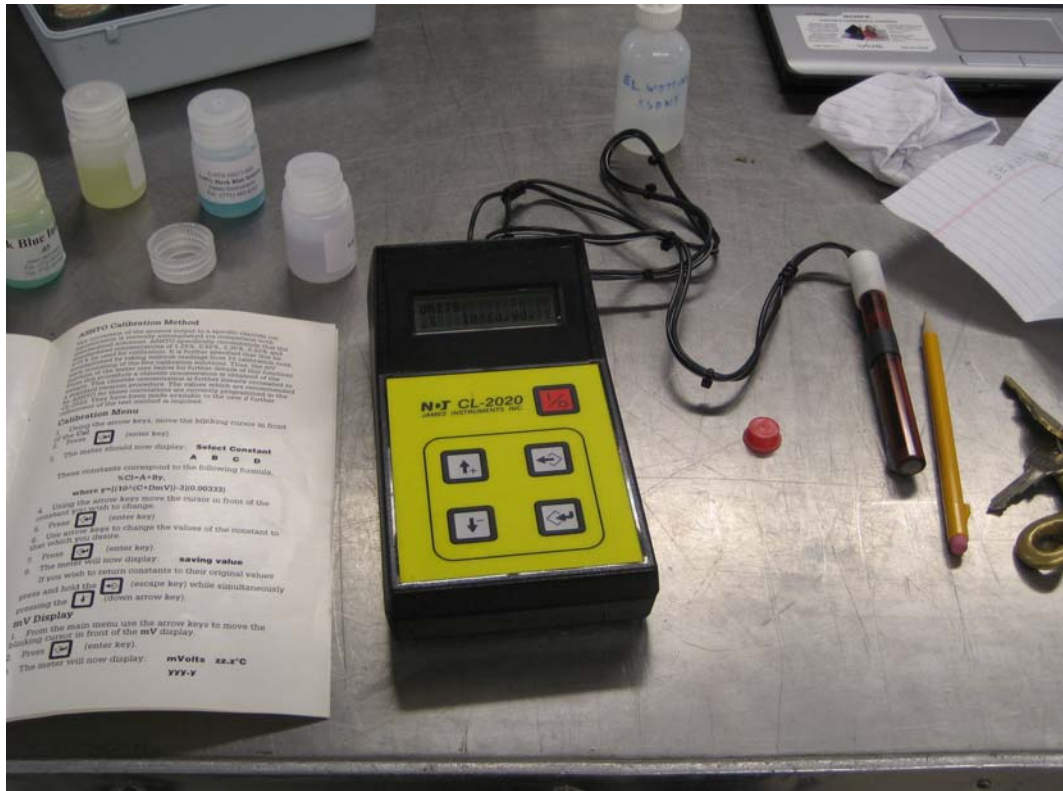
Figure 3.9. Laboratory test instrument for analyzing chloride content

Figure 3.11 shows the evidence of corrosion 50 years after construction of bridge. It should be noted that signs of longitudinal reinforcing bars corrosion was evident at the time the bridge was strengthened. This was an example of why the authors wanted to consider corrosion of steel within the life expectancy modeling.

In this fashion, the final life expectancy model is flexible and accommodates steel loss consideration if corrosion is applicable for a particular bridge. This approach also lends itself well to using advanced non destructive techniques, such as Half-cell potential, to identify an area of corrosion and estimate steel loss in critical high moment regions at the time of strengthening.
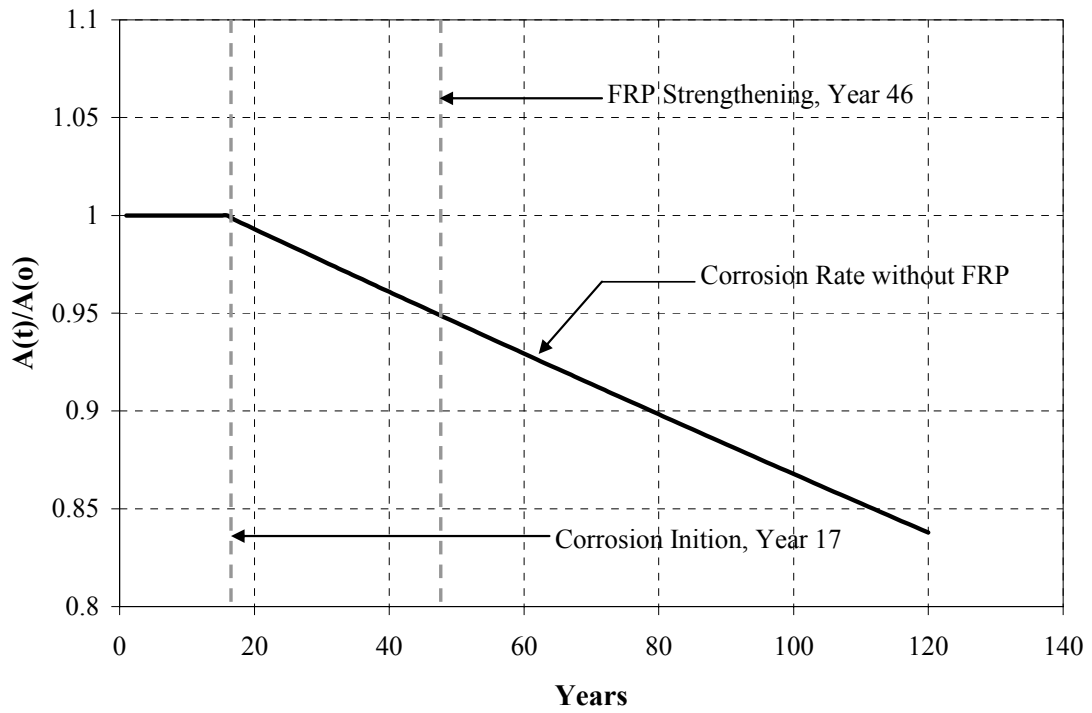
Figure 3.10. Reduction of reinforcement area (At) as a function of time

Figure 3.11. Evidence of corrosion 50 years after construction of bridge P-0962

3.4. LIFE PREDICTION OF FIBER REINFORCED POLYMER COMPOSITES

The extensive application of composites has seen the emergence of durability problems specific to these materials where durability relates to long-term performance under adverse conditions, often 20 or even 50 years of exposure. These problems are associated with in-service environmental conditions and handling procedures (including maintenance, repair, and modifications). Durability is a serious issue from both a health and safety aspect and in terms of economic costs. The repair or replacement of a deteriorated part is both labor and capital intensive. For large structural applications, such as aircraft, bridges and offshore construction, composite parts are very expensive and, due to "parts integration," are often very large.

The lack of resistance of composite structures to degradation agents often becomes apparent within a short period of time. In some circumstances, only a few hours of exposure may lead to catastrophic failure or seriously compromised structural integrity. Irreversible property changes in polymer matrix composites (PMCs) can be induced by any number of degradation agents (see list below) acting alone or collectively.

• Thermal-static heat aging, sub-zero exposure, or thermal cycling

• Humidity (including hot/wet) exposures

• Complete immersion in water at ambient and elevated temperatures

• Freeze-thaw and dry-wet cyclic conditions

• Continuous or intermittent saltwater immersion or spray

• Weathering (including rain and sand erosion)

• Combined load (i.e., stress) and environmental exposures

• Chemical (including water, fuel, acids, alkalis, solvents, and oxygen)

- Ultraviolet and high-energy radiation

- Electrical stress (e.g., lightning stress and galvanic reactions)

- Micro-organisms (e.g., fungi)

In many applications, composite structures will be exposed to a combination of two or more factors, often resulting in complex synergistic degradation of the material. Accelerated degradation may be caused by the combined action of two or more vectors (e.g., temperature and humidity). The relative importance of each agent will depend upon the agents present and at what levels. Degradation from one agent can also reduce resistance to other agents, similar to biological systems. The two predominant factors in climatic exposure are humidity and temperature. The severity of these two factors will depend on geographical location and need to be taken into account when designing with these materials.

Failure of polymer composites, insofar as it is no longer fit for use, may occur because of cumulative damage to the thermoset or thermoplastic matrix, interfacial separation with the fibers, chemical attack of the fibers, or a combination of two or more of these processes. The net effect is loss of stiffness and mechanical integrity. This section examines the degradation of composite materials and constituent components (i.e., fiber, matrix, fiber-matrix interface, and interphase) as a result of exposure to aggressive environments.

3.4.1. Effect of Moisture and Water on Composite Performance. Most PMCs will absorb small, but potentially damaging, amounts of moisture from the surrounding environments with the degree of degradation that occurs being linked directly to the amount of moisture absorbed. The absorbed water may adversely affect the material by:

dimensional changes (swelling), reduction in the glass transition temperature T_g of the resin, or reduction in mechanical and physical properties (i.e., stiffness, strength, and hardness).

In many instances, water reacts with the matrix and causes irreversible chemical changes and diminished performance. Capillary action along the fibers can account for a significant proportion of initial moisture uptake, although a chemically resistant matrix may encapsulate the fibers. Shrinkage of the resin away from the fibers during curing is a contributing factor to the capillary effect. The effect of moisture is to cause hydrolytic breakdown of the fiber-matrix interface resulting in a loss in the efficiency of load transfer between the matrix and the fiber reinforcement.

The moisture absorption kinetics of polymer systems differs widely between resin systems and also changes with chemical ageing. The glass transition temperature for a typical polyester resin decreases by approximately 15° to 20° C (59° to 68° F) for a 2 percent moisture weight gain. This reduction in T_g is induced by plasticization (softening) of the polymer matrix and in some cases by loss of organic additives through leaching to the surrounding media. It is advisable when using glass FRP products to ensure that the maximum operating temperature is at least 30° to 40° C (86° to 104° F) below the T_g of the material (taking into account moisture effects).

Although the process of moisture absorption and desorption within the surface layers occurs almost immediately on contact with the environment, moisture diffusion into the bulk material is usually a slow process. It may take weeks to months before a substantial amount of moisture has been absorbed by the composite, and considerably longer periods (i.e., 1–2 years) before the material is saturated. The rate of moisture

uptake by a composite laminate is dependent on the temperature, relative humidity, exposure time, and mechanical load. At elevated temperatures, the rate of moisture uptake and material property degradation is accelerated.

The presence of tensile loads accelerates moisture uptake by opening existing internal cavities or voids and by contributing to micro-crack formation. A laminate containing micro-cracks will absorb considerably more moisture than an undamaged laminate. Exposing the wet composite to sub-zero temperatures can further exacerbate this process. A commonly used test to assess the laminates crack resistance is to subject hot/wet conditioned laminates to thermal cycling in which the composite is exposed to temperatures as low as
–55º C (–67° F) for a given number of cycles..

All laminates when exposed to marine environments will allow water vapor to permeate the structure. As the water diffuses into the composite, it reacts with any hydrolysable components inside the laminate to form tiny cells of concentrated solution. Under this osmotic process, more water is drawn through the semi-permeable membrane of the laminate in an attempt to dilute the solution. The water can increase the fluid pressure of the cell by 50 atmospheres, which eventually distorts or bursts the laminate or gel coat and can lead to a blistering of the surface. Damage can be very extensive, requiring major repair or the replacement of the structure.

Osmosis blistering is a common problem occurring in glass FRP laminated structures that have been immersed in aqueous solutions for long periods and is often observed in glass FRP boats, water tanks, and swimming pools. A resin-rich layer (e.g., gel coat) is often applied to the composite surface where the material is to be exposed to

aqueous solutions for long periods of time. This protective layer acts as a barrier to moisture ingress, thereby protecting glass fibers from moisture degradation. Other protective measures against natural weathering include marine paint and polyurethane, which also shield the composite substrate from ultraviolet damage and weathering erosion.

Osmotic effects are amplified in the presence of hydrostatic pressure (e.g., submersibles). Entrapped air/gas/moisture vapor under pressure expands as the structure is raised from depths (as external pressure decreases), analogous to the effect of the bends experienced by divers. As a result, cracking and delaminations may occur, thus compromising structural integrity and the structure's life expectancy. Porous materials can be expected to be far more prone to this effect than well-compacted materials.

The effect of moisture on aramid (e.g., Kevlar) fiber-reinforced epoxy laminates is potentially greater than other composite systems. Aramid fibers tend to absorb moisture and degrade at room temperature with the rate of degradation accelerating as temperature is increased. Substantial hydrothermal strength losses have been observed with these materials, particularly under natural weathering conditions (i.e., combination of moisture and ultraviolet light).

3.4.2. Polymer Matrix Degradation. The polymer matrix provides a chemical barrier to the corrosive effects of moisture/water, alkalis, and mineral acids, thus extending the life of the structure when compared to loose fibers. Environmental stress cracking (ESC), weathering, and chemical attack are the principle mechanisms for failure of the polymer matrix, with the particular process being dependent on whether the matrix is a thermoplastic or thermoset and the nature of the exposure condition. ESC is an issue

for thermoplastic composites, and the mechanism and likelihood of attack are essentially those described for thermoplastics

The majority of thermoset resins are susceptible to oxidation by numerous oxidizing agents, from exposure to elevated temperatures (i.e., thermo-oxidation), hydrogen peroxide, and bleaches (e.g., hypochlorite). Often, it is other constituents, such as fillers, catalysts, hardeners, pigments, or fire retardants, rather than the resin or fiber reinforcement, that are more reactive to these chemicals. Formulators and users, although usually aware of the potential durability problems associated with these additives, often overlook minor constituents such as catalysts, hardeners, pigments, and processing aids.

Most of the commonly used resin systems employed by the composite industry are far more chemical resistant to strong acids, salt solutions, and oxidative agents than stainless steel or aluminum alloys. However, exposure to secondary solvents, such as paint strippers, can lead to irreversible material damage. Methylene chloride, a constituent of many paint strippers, is a known degradant of epoxy resins and other polymers.

3.4.3. Fiber Degradation. Fiber degradation is primarily an issue for glass fibers and aramid fibers; carbon fibers are stable in most environments. The tensile strength of freshly drawn E-glass fibers is typically 3.5 GPa (507 ksi). This strength can be fully realized, provided the fibers are carefully handled during fabrication to avoid surface damage and are stored in a dry environment. Exposure to humid air (including air-conditioned laboratories) will compromise the load bearing capacity of the fibers, resulting in a loss of strength and an increase in strength variability. Carbon fibers are

relatively insensitive to moisture; hence, the variability in the tensile breaking stress and strain for carbon fiber tows is noticeably less than for E-glass fiber tows.

The loss of tensile strength of E-glass fibers is dependent on exposure time, temperature, and degree of humidity. On initial exposure to a humid/water environment, the rate of fiber degradation is relatively rapid, even in benign environments, such as air-conditioned laboratories. The tensile strength is reduced to 3.0 GPa (435 ksi) after 3 weeks of exposure to standard laboratory conditions (23ºC (73^0F) and 50 percent relative humidity (RH)). Immersion in water at the same temperature for the same period results in a 20 percent reduction (2.5 GPa (363 ksi)). Further strength reduction occurs with increasing exposure time. After 100 days, in air and water, the strength is 2.6 GPa (377 ksi) and 2.1 GPa (305 ksi), respectively. Exposure to boiling water for 24 hours results in a 75 percent loss of strength. As a consequence of handling and moisture, an intrinsic tensile strength of 2.0 GPa (290 ksi) is often assumed for design purposes. Degradation of E-glass fibers in water can be mainly attributed to leaching of alkali oxides (sodium and potassium oxide) from the fiber surface, resulting in the formation of surface micro-cracks, which act as stress concentrators. The loss of strength can be expected to be permanent at all conditioning temperatures and exposure times. It is worth noting that deionized water is slightly more aggressive than either tap water or seawater.

3.4.4. Effects of Elevated Temperature. Prolonged, or even short-term, exposure to elevated temperatures will often produce irreversible chemical and physical changes within PMCs. As the temperature increases, the stiffness and strength decrease. All resin systems degrade at elevated temperatures.

Oxidation is the primary degradation process at elevated temperatures. The rate of degradation increases with the amount of oxygen present. PMCs are permeable to atmospheric gases.

The use of anti-oxidant additives in resin systems slows the degradation process by scavenging any free radicals. Elevated temperatures also depolymerize resins and degrade the fiber-matrix interface. Differences in thermal expansivity between fiber and matrix can induce residual stresses, thereby reducing fiber-matrix bond efficiency.

3.4.5. Effect of Other Agents. A number of other degradation agents relating to in-service environmental conditions, handling, and maintenance are known to have detrimental effects on the durability of composite laminates.

Solvents such as the paint stripper methylene chloride will soften and dissolve epoxy resins. Aircraft, boats, and bridges may need to be repainted repeatedly every 2–3 years during a service life, which can extend 20 to 50 years (or more). Hydraulic fluid has a similar effect to that of methylene chloride, but takes longer. Solvents such as methyl-ethyl-ketone (MEK) and acetone should not be left standing on either thermoset or thermoplastic composite surfaces.

A majority of matrix resins and carbon fibers (especially high strength fibers) are susceptible to oxidation by any one of numerous oxidizing agents (e.g., hydrogen peroxide and certain bleaches such as sodium hypochlorite, nitric, or sulphuric acid). Oxidation can result in loss of strength and discoloration. Atmospheric oxygen can induce degradation in matrix resins at elevated temperatures.

Intercalation affects high modulus carbon fibers and is an unusual process caused by chemical molecules (e.g., halogens and many inorganic salts such as ferric chloride)

inserting themselves between the graphite layer planes. The result is to induce large

changes in fiber dimensions.

3.4.6. Life Prediction from Fatigue Behavior. Fatigue behavior is usually

expressed in terms of the maximum applied fatigue stress S and fatigue life (number of

cycles to failure) Nf. This section examines a number of approaches to predicting fatigue

performance of composite laminates.

3.4.6.1 Empirical fatigue theories. There are many empirical fatigue theories

used to characterize S-N curves for polymer composites. A number of these are shown

below.

$$\sigma_{ULT} = \sigma_a N^{-m} \tag{3.14}$$

$$\sigma_a = \sigma_{ULT} - b \log N \tag{3.15}$$

$$\sigma_{range} = a + \frac{b}{N^x} \tag{3.16}$$

$$\sigma_{RANGE} = a + \frac{b}{N^x} + \frac{c}{A^y} \tag{3.17}$$

$$A = \frac{1-R}{1+R} = \frac{\sigma_{RANEGE}}{\sigma_{MEAN}} \tag{3.18}$$

$$R = \frac{\sigma_{MIN}}{\sigma_{MAX}} \qquad -1 < R \leq 1 \tag{3.19}$$

Where σ_{MIN} and σ_{MAX} and σ_{MEAN} are the minimum stresses, maximum stresses,

and mean stresses, respectively, for stress cycling, the relationships 3.14 to 3.19 lead to

the physically unreasonable situation of unbounded predictions when the number of

cycles tends to zero. A more sensible approach would be to replace N by N + 1 in these relationships, a change that leads to imperceptible differences when applied in a fatigue context.

Harris and co-workers developed a constant life-model (see Equation (3.20)), which according to the authors, agrees well with experimental data for tension-tension, compression-compression, and tension-compression fatigue. The model is based on a substantial experimental database including results for different R ratios (stress ratio R = $\sigma_{MIN}/\sigma_{MAX}$), constant and variable amplitude loading, materials (i.e., aramid, carbon, and glass fiber-reinforced systems), and lay-ups. The model claims to account for both undamaged and damaged composite materials.

The constant life model is given by Equation 3.20:

$$a = f (1\text{-}m)^{u} (c + m)^{v} \tag{3.20}$$

Where: $a = \dfrac{\Delta\sigma}{\sigma_{UTS}}$; $m = \dfrac{\sigma_{MEAN}}{\sigma_{UTS}}$; $c = \dfrac{\sigma_{UCS}}{\sigma_{UTS}}$

The parameter c is the normalized compression strength (i.e., ratio of compressive strength, σ_{UCS}, to tensile strength, σ_{UTS}), m is the normalized mean stress component ($\sigma_{MEAN}/\sigma_{UTS}$), and a is the normalized stress amplitude ($\Delta\sigma / \sigma_{UTS}$). The parameters f (stress function), u, and v in Equation (3.20) are linear functions of log Nf.

3.4.6.2 Normalized life prediction model. As previously mentioned, the general approach for assessing fatigue performance is to use S-N curves. These curves enable engineers and designers to determine the fatigue strength (i.e., maximum applied stress σ_{MAX} for given fatigue life Nf). Kawai developed a phenomenological model for determining the off-axis fatigue behavior of glass FRP and carbon FRP laminates. In the

model, the fatigue strength is normalized with respect to the ultimate (static) strength σ_{ULT} in the loading direction:

$$\sigma^*_{MAX} = \frac{\sigma_{MAX}}{\sigma_{ULT}} \qquad (3.21)$$

For tension-tension and compression-compression fatigue, respectively:

$$\sigma^*_{MAX} = \frac{\sigma_{MAX}}{\sigma_{UTS}} \qquad (3.22)$$

$$\sigma^*_{MAX} = \frac{\sigma_{MAX}}{\sigma_{UCS}} \qquad (3.23)$$

σ_{UTS} and σ_{UCS} are the ultimate tensile and compressive strengths.

The maximum normalized fatigue stress σ^*_{MAX} is related to the normalized alternating stress σ^*_A and normalized mean stress σ^*_{MEAN} as follows:

$$\sigma^*_{MAX} = \sigma^*_A + \sigma^*_{MEAN} \qquad (3.24)$$

The alternating and mean stress σ^*_A and σ^*_{MEAN} are defined as follows:

$$\sigma^*_A = \frac{(1\text{-}R)}{2}\sigma^*_{MAX} \qquad (3.25)$$

$$\sigma^*_{MEAN} = \frac{(1+R)}{2}\sigma^*_{MAX} \qquad (3.26)$$

The above relationships apply within the stress ratio range of $|R| \leq 1$.

A new term called the modified non-dimensional effective stress Σ^* is introduced, which is expressed as follows:

$$\Sigma^* = \frac{\sigma_A^*}{1-\sigma_{MEAN}^*} \tag{3.27}$$

This relationship can be written in the following form:

$$\Sigma^* = \frac{\frac{1}{2}(1-R)\sigma_{MAX}^*}{1-\frac{1}{2}(1+R)\sigma_{MAX}^*} \tag{3.28}$$

The evolution of fatigue damage with cycles can be represented by:

$$\frac{d\omega}{dN}=K(\Sigma^*)^{n^*}\left(\frac{1}{1-\omega}\right)^k \tag{3.29}$$

Where K, n*, and k are material constants.

The effective frequency on the growth of fatigue damage can be accounted for by considering the rate-dependence of the principal static strengths by which the modified non-dimensional effective stress is normalized. Essentially, the strength used for normalizing data has to be measured at the same effective rate as the fatigue test.

Assuming ultimate failure occurs when ω reaches unity, the fatigue life equation for constant amplitude loading is obtained:

$$N_f = \frac{1}{((k+1)/k)\left(\Sigma^*\right)^{n^*}} \tag{3.30}$$

Setting $N_f = 1/2$ when $\Sigma^* = 1$, then $(K+1)/K = 2$, which yields the following expression:

$$2N_f = \frac{1}{\left(\Sigma^*\right)^{n^*}} \tag{3.31}$$

The master S-N relationship obtained by plotting the modified non-dimensional effective stress Σ^* against the number of reversals $2N_f$ to failure on a log-log scale is straight line.

Equation 3.31 can be rewritten as follows:

$$\sigma_A^* = \left(\frac{1}{2N_f}\right)^{\frac{1}{n^*}}\left(1-\sigma_{MEAN}^*\right) \tag{3.32}$$

The normalized constant fatigue life diagram predicted using the above relationship equates to the linear relationship over the stress ratio range $|R| \leq 1$.

Alternatively:

$$\frac{(1-R)\sigma_{MAX}^*}{2-(1+R)\sigma_{MAX}^*} = \left(\frac{1}{2N_f}\right)^{\frac{1}{n^*}} \tag{3.33}$$

Kawai (2004) obtained values of n^*=14.1 for glass/epoxy and n^*=11.9 for carbon/epoxy. A normalized S-N curve can be approximated by the following log-linear relationship:

$$\sigma_{MAX}/\sigma_{ULT}=1-k\log N_f \qquad (3.34)$$

From the above equation the normalized S-N curve is obtained, which is indicated in Figure 3.12, whereas Figure 3.13 presents life expectancy of carbon FRP based on the fatigue analysis (S-N curve)
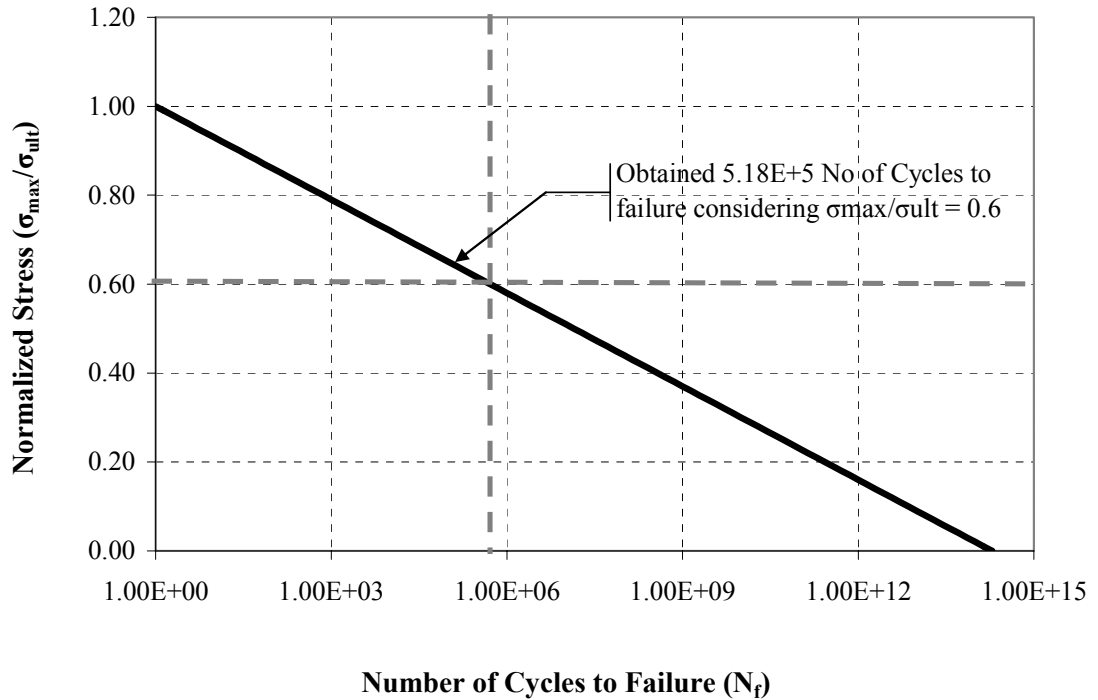
Figure 3.12. Normalized S-N curve
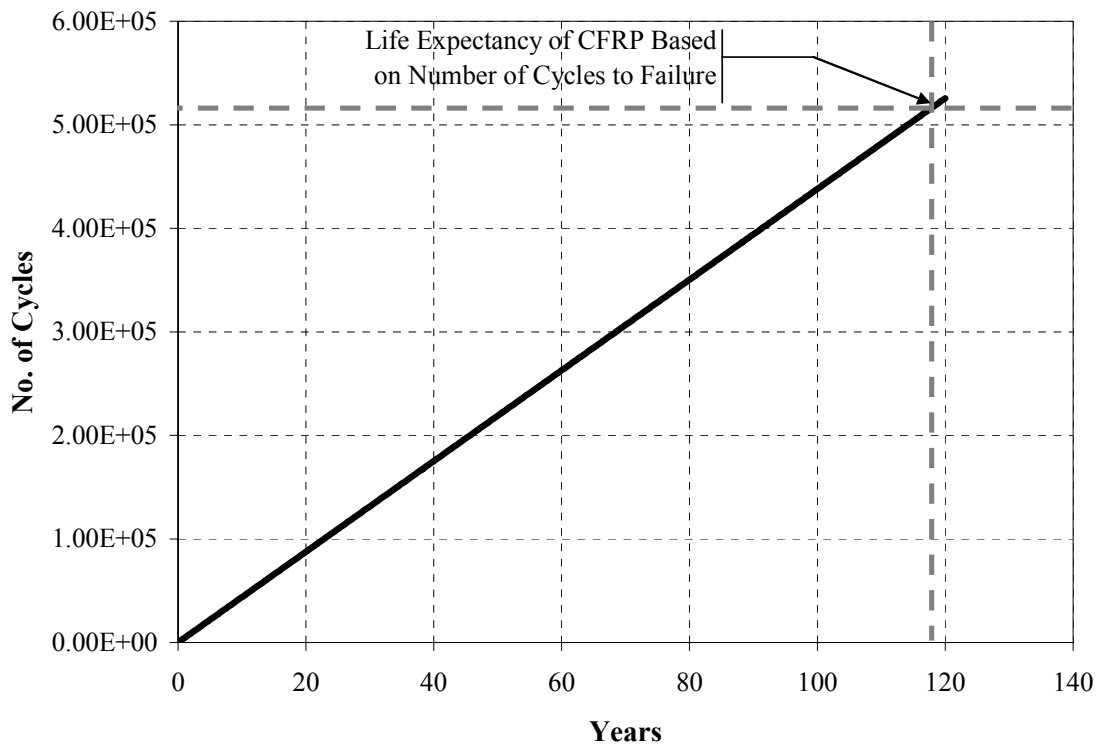
Figure 3.13. Life expectancy of carbon FRP based on number of cycles to failure

The above figure led the authors to focus more research effort on bond, the relationship between substrate concrete and FRP, and deterioration of concrete due to corrosion and other environmental factors, rather than focusing solely on FRP deterioration. Note here that material degradation for CFRP alone has already been reported by many researchers (Myers, 2006) and therefore material degradation of the CFRP for bridge P-0962 was not considered. For other fiber types, such as GFRP, material degradation would need to be included in the life expectancy model.

4. SERVICE LIFE MODELING AND INTRERACTION OF ANALYTICAL MODELS

4.1. INTRODUCTION

In this chapter separate, models were developed to evaluate service life of a CFRP strengthened bridge girder based on the corrosion of steel in the girder and bond degradation between the CFRP and substrate concrete. The models were validated against field structures and/or data on field structures available in literature. For the corrosion related considerations in this report, the model is based on chloride diffusion for chloride-induced corrosion.

4.2. MODEL FOR STEEL CORROSION

The proposed chloride diffusion model is based on functions of diffusion coefficient, surface chloride ion content, clear concrete cover from the structure, and chloride ion concentration. This model assumes that the past diffusion behavior and chloride accumulation will continue at the same rates in the future. However, it is clear that the diffusion process is affected by many factors, such as temperature, humidity, and concrete cure, and each of these factors varies with time and season, therefore limitations exist within the assumptions considered herein.

4.3. TIME TO INITIATION OF CORROSION

While determining the initiation time to reinforcement corrosion, the following assumptions are to be made based on the literature review:

- Chloride diffusion coefficient $(Dc) = 10^{-12} m^2/sec$ $(1.55 \times 10^{-9} in^2/sec)$

- Error function (erf) = 1

- Surface or equilibrium chloride concentration depends upon relative humidity

  (C_O) = 1.0, as a percent of cement weight

- Initial chloride concentration (Ci) = 0

From the collected samples and laboratory tests critical chloride ion concentration was attained around 0.031 to 0.035 as a percent cement weight. Figure 4.1 shows the location of collected samples.
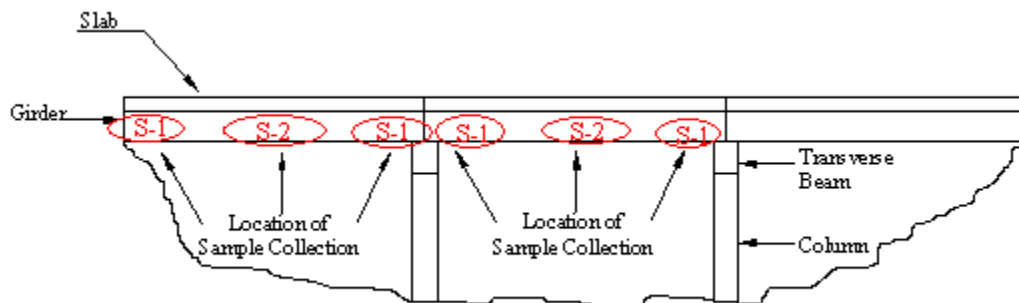
Figure 4.1 Collection of samples on bridge P-0962

Figure 4.2 illustrates the variation of chloride ion concentration along the length of the span. Both high and low moment regions were sampled to obtain an average chloride content. Appendix B shows additional information about sampling details.

Figure 4.3 illustrates rate of corrosion after CFRP strengthening of the bridge girder. Once the girder was strengthened with CFRP the rate of corrosion was decreased drastically and became negligible.
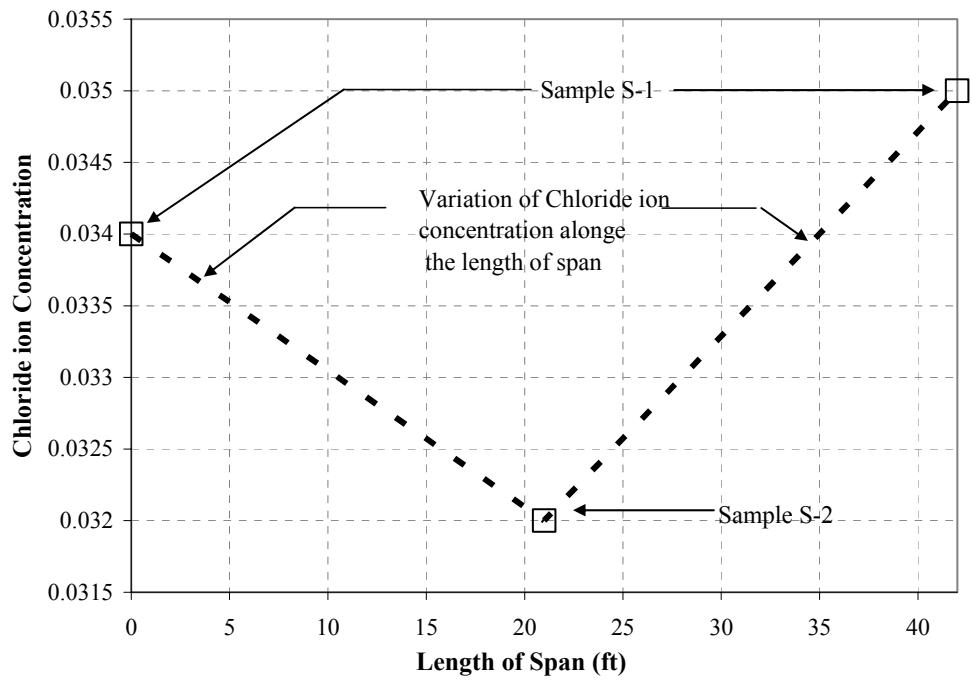
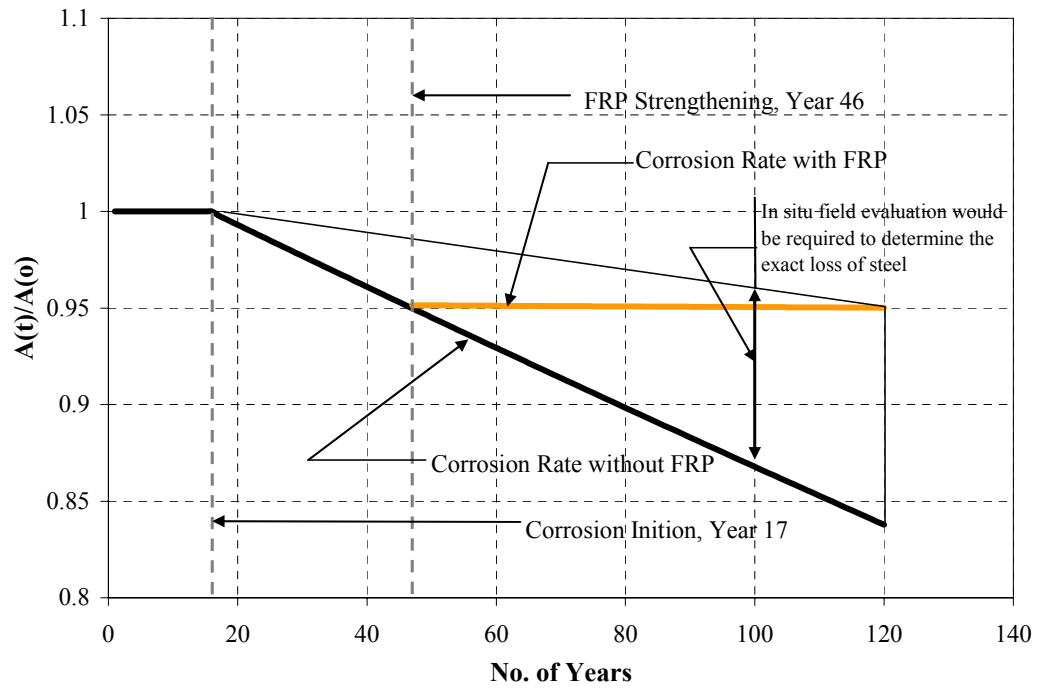Figure 4.2 Variation of chloride ion concentration along the length of the span

Figure 4.3. Rate of corrosion with FRP

4.4. BOND DEGRADATION

CFRP material is increasingly being used for the repair and rehabilitation of flexural concrete elements in buildings and bridges. In this method, the carbon FRP material is bonded to the concrete surface using epoxy adhesives. As the load is transferred to the carbon FRP material by epoxy, the durability of its bond with concrete is critically important for the integrity and safety of the repaired structure.

An essential requirement for successful performance of CFRP-strengthened structures is the physical and chemical compatibility between concrete and the adhesive material used for bonding. If incompatibilities exist, internal stresses develop that can lead to a weakening of the long-term carbon FRP/epoxy/concrete bond.

When epoxy is used to bond carbon FRP material to concrete, both physical and chemical incompatibilities are introduced. Physical incompatibility stems from a mismatch in the coefficient of thermal expansion between epoxy, CFRP, and concrete. For example, the coefficient of thermal expansion for epoxy, reported as 44 to 120 x 10^{-6} per degree Celsius (24 to 66 x 10^{-6} /^{0}F), is several times greater than concrete that varies between 6 to 13 x 10^{-6} per degree Celsius (3.5 to 7.2 x 10^{-6}/^{0}F) depending on aggregate. This finding suggests that if a carbon FRP-strengthened structure is subjected to large temperature variations, its performance may be impaired.

The authors' modeling for bond degradation presented in Figure 4.4 was based on correlating laboratory results conducted at Queen's University and published by Bisby and Green (2002) to historic ambient conditions in Dallas County, Missouri, USA. Bisby and Green observed an approximate reduction of around 5 percent in load carrying capacity of externally carbon FRP laminated beams after 50 freeze-thaw cycles. After

200 freeze-thaw cycles, a reduction in the load carrying capacity was observed at around

10 percent. These losses were attributed to bond degradation. In their laboratory test,

one freeze-thaw cycle was considered from -15 to 20ºC (5 to 70ºF). Data collected for

more than 30 years at the bridge site and made available on the NOAA website was used

to determine the average number of freeze-thaw cycles at the location of the case study

bridge and to develop the bond degradation model. Accordingly, 200 freeze-thaw cycles

were equivalent to 40 years of service exposure based on analyzing site weather data.

This model assumes that laboratory results would correlate to field performance. More

work is needed to confirm this behavior or refine the model presented in Figure 4.4. This

work, again, is intended to lay a foundation for future refinement as more field
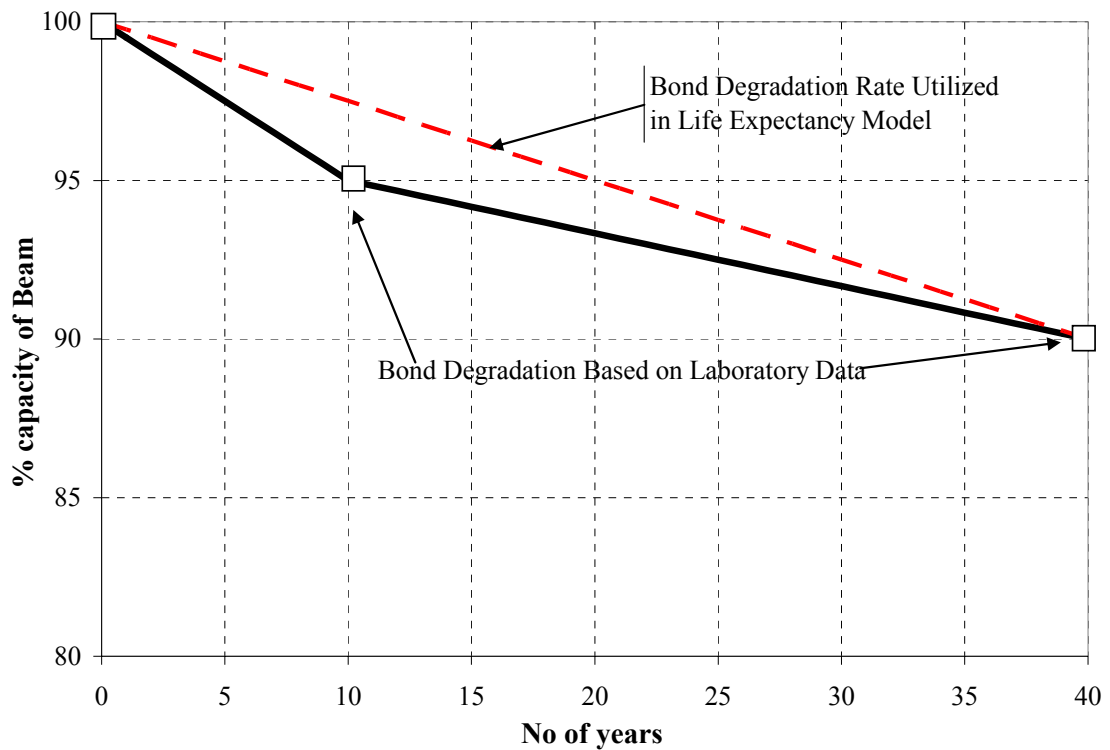
performance data becomes available.

Figure 4.4 Reductions in load carrying capacity due to freeze and thaw cycles

4.5. COMBINED EFFECT ON STRENGTH DEGRADATION

To obtain a combined effect, the following approach was used. First, the nominal moment capacity of the girder with existing reinforcement was calculated. Then, the corrosion model was applied to the girder. This corrosion model was applied before strengthening of the beam without external carbon FRP. Once the strengthening of the beam was completed, the capacity of the beam increased to satisfy the new design requirements. After, strengthening the combined effect of bond degradation and reinforcement corrosion with FRP wrap (i.e., strengthening) was taken into consideration. A number of studies have indicated that FRP strengthening significantly slows the corrosion process; therefore, the corrosion rate was adjusted accordingly after FRP strengthening (see Figure 4.5). Within this approach, carbon FRP material degradation was not considered by the authors, as most studies have indicated that degradation of the carbon material itself is minimal for the exposure conditions of the bridge. Should another FRP material be used, such as glass, the material degradation would be an important consideration to incorporate in the degradation modeling. In the following section, a case study for the Dallas County Bridge is detailed with the above approach.

4.6. CASE STUDY OF BRIDGE IN DALLAS COUNTY, MO (P-0962)

The following presents the characteristics of the case study bridge and the approach undertaken to determine the ultimate capacity of a typical exterior girder with the implementation of degradation considerations for corrosion and bond degradation.

To determine the ultimate strength of the girder prior to FRP strengthening, the ACI 318-05 generalized approach was used with one modification. A correction factor,

93

ψ_{cor}, was introduced to consider the loss of steel due to corrosion based upon the model presented in Figure 4.3. Equation 4.1. was used to determine the nominal moment capacity of the section.

$$M_n = \left[A_{st} f_y \left(d - \frac{a}{2} \right) \right] \tag{4.1}$$

where, $a = \dfrac{A_{st} f_y}{0.85 f'_c b_{eff}}$; $c = \dfrac{a}{\beta_1}$

After FRP strengthening, the ACI 440.2R-02 generalized approach was used with modifications to consider bond degradation and steel loss. For loss of steel due to corrosion after FRP strengthening, the authors assumed a steel loss rate of 0.65g/day (0.023 oz/day) based on a laboratory study conducted at University of Missouri-Rolla by Bae et al., (2005). The moment capacity expression that was used to determine the moment capacity of the section considering both corrosion and bond degradation is detailed below:

$$\phi M_n (X_i) = \left\{ \left[A_{st} f_y \left(d - \frac{\beta_1 c}{2} \right) + A_f f_{fe} \left(h - \frac{\beta_1 c}{2} \right) \right] \times \psi_b (X_i) \right\} - \left[\psi_{cor} (X_i) A_{st} f_y \left(d - \frac{a}{2} \right) \right] \tag{4.2}$$

Equation 4.1 and 4.2 Notations:

A_{st} = area of non-prestressed steel reinforcement., mm^2 ($in.^2$)

94

A_f = area of FRP reinforcement., mm^2($in.^2$)

$f_c^{'}$ = compressive strength of the concrete, MPa (ksi)

b_{eff} = effective width of compression block, mm (in.)

a = depth of compression block, mm (in.)

c = distance from extreme compressive fiber to neutral axis, mm (in.)

d = distance from extreme compressive fiber to cgs, mm (in.)

f_y = specified steel yield strength, MPa (ksi)

β_1 = ratio of depth of the equivalent rectangular stress block to the depth of the

neutral axis.

ψ_{cor} = steel loss factor based on Figure 4.3

ψ_b = bond reduction factor based on Figure 4.4

ψ_f = ACI FRP strength reduction factor

X_i = year at which strength needs to be calculate

X_s = year at which bridge strengthened

The loading and corresponding moments were figured using AASHTO LRFD (1998), which was determined to be 1640 kN-m (1210 kips-ft) including impact and load factors, See Figure 4.5.

This approach indicates that the life expectancy of the bridge would degrade to the required moment capacity in Year 79. If the safety factors are not considered within the AASHTO nominal required moment capacity, the life expectancy would be projected

based on this process to Year 182. This does not include the load factors, but does
include the impact factor, as shown in appendix D and E.
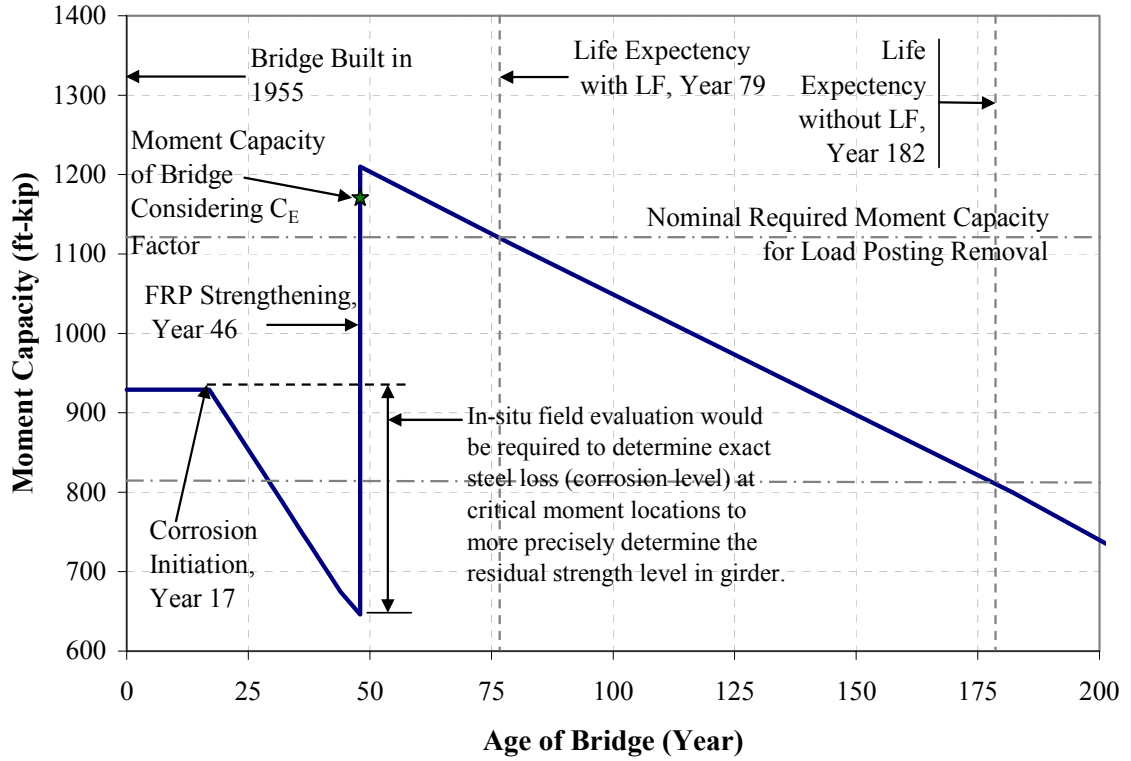
Conversion: 1 ft-kip. = 1.356 kN-m

Figure 4.5. Moment capacity model considering combined effects of steel corrosion
and bond strength reduction

5. CONCLUSIONS AND RECOMMENDATIONS

5.1. CONCLUSIONS

This report was presented to gain a better understanding of the degradation mechanism of FRP strengthened bridges and the durability performance of reinforcing steel, concrete, FRP materials, and bonding material between FRP and substrate concrete. This work involved an extensive literature review as well as experiments to investigate the effect of degradation on the selected material. The scope of this report included determining the life expectancy of FRP strengthened bridges for MoDOT with a MathCAD spreadsheet software, which can be used to vary bridge criterion.

For the case study example Bridge P-0962, located in Dallas County, Missouri, the time to initiate the reinforcement corrosion is predicted by an analytical method which predicted a 17 year initiation time to corrosion. This was shorter than the average value in the state of Missouri. The difference was primarily attributed to the variability of the apparent diffusion coefficient and a sensitivity of the time to first repair and rehabilitation to the apparent diffusion coefficient.

The work presented in this report examines the effects of freezing and thawing cycling, specifically on the FRP-concrete bond in external plating operations. Based on the extensive literature review and the weather and atmospheric conditions at the bridge location (obtained from NOAA website), freezing and thawing cycling up to 200 to 300 cycles does not appear to significantly affect the load carrying capacity and overall performance of the bridge.

A wide range of mechanisms for the potential degradation of CFRP composites are involved, including thermal degradation, weathering, chemical attack, ionizing

radiation, creep, and fatigue. In this report a model is presented based on fatigue

performance. Based on the literature review, the deterioration of CFRP material is not a

critical issue for the location of the bridge site. In addition, the wider impact of

degradation under synergistic mechanical, chemical, and thermal conditions appears to be

less well understood; in particular, the influence that more than one mechanism may have

on the overall degradation of the material needs further study. For example, specimens

weathered in the desert of Nevada often appear to suffer less degradation than specimens

artificially weathered in the laboratory. The reason for this apparent discrepancy is that

although all the specimens suffer similar ultraviolet damage, the abrasion of desert sand

in Nevada removes the degraded material from the surface of the samples. This type of

synergistic actions certainly requires investigations for more accurate life expectancy

predictions.

5.2. RECOMMENDATIONS

The life expectancy model presented in this report is one possible approach in

determining the life expectancy of a carbon FRP strengthened bridge structure. The work

discussed is based on an available corrosion model and bond degradation modeling based

on research done on bond degradation of carbon FRP and concrete.

The value of chloride initiation concentration can have a significant effect on the

prediction of life expectancy of FRP strengthened bridges. The prediction accuracy of

bridge life expectancy will be limited until the value, or distribution, of the chloride

initiation concentration or physical evidence of the steel loss level is better defined.

Research that investigates the chloride initiation concentration of field structures,

including those with electrochemical corrosion rate (ECR), linear polarization resistance (LPR), electrochemical noise (EN), and harmonic distortion analysis (HDA) techniques to determine both general and localized corrosion, would improve future prediction on life expectancy.

Working on this model in a future in-situ field evaluation would be required to determine exact loss of steel due to corrosion at critical moment locations, which would give a more precise determination of the residual strength level in girder. The authors have assumed the laboratory bond testing conditions may be representative of field conditions under similar freeze-thaw cycles, even though many of the field freeze-thaw condition gradients may occur over a less severe temperature-time cycle. This assumption is believed to be conservative, but much more work needs to be done to correlate lab durability studies to field conditions and to address some of the assumptions and limitations in this work. Additional modeling considerations on a variety of other factors are required to refine the initial work undertaken in this study. Finally, long-term monitoring is suggested to evaluate the FRP-substrate bond.

APPENDIX A.

REDUCTION IN REINFORCEMENT AREA DUE TO CORROSION

Table A.1 Reduction in reinforcement area due to corrosion.

Years	Reinforcement Area (mm^2)	Years	Reinforcement Area (mm^2)	Years	Reinforcement Area (mm^2)
1	368.15	17	367.37	33	357.88
2	368.15	18	366.77	34	357.29
3	368.15	19	366.18	35	356.70
4	368.15	20	365.58	36	356.11
5	368.15	21	364.99	37	355.53
6	368.15	22	364.39	38	354.94
7	368.15	23	363.80	39	354.35
8	368.15	24	363.20	40	353.77
9	368.15	25	362.61	41	353.18
10	368.15	26	362.02	42	352.60
11	368.15	27	361.42	43	352.01
12	368.15	28	360.83	44	351.43
13	368.15	29	360.24	45	350.84
14	368.15	30	359.65	46	350.26
15	368.15	31	359.06	47	349.68
16	368.15	32	358.47	48	349.09

Conversion units: $1mm^2 = 1.55 \times 10^{-3}$ in.^{2}, $1mm = 0.04$ in.

Table A.1 (Continued) Reduction in reinforcement area due to corrosion.

Years	Reinforcement Area (mm^2)	Years	Reinforcement Area (mm^2)	Years	Reinforcement Area (mm^2)
49	348.51	65	339.27	81	330.15
50	347.93	66	338.70	82	329.59
51	347.35	67	338.12	83	329.02
52	346.77	68	337.55	84	328.46
53	346.19	69	336.98	85	327.89
54	345.61	70	336.41	86	327.33
55	345.03	71	335.84	87	326.76
56	344.45	72	335.27	88	326.20
57	343.88	73	334.69	89	325.64
58	343.30	74	334.13	90	325.08
59	342.72	75	333.56	91	324.51
60	342.14	76	332.99	92	323.95
61	341.57	77	332.42	93	323.39
62	340.99	78	331.85	94	322.83
63	340.42	79	331.28	95	322.27
64	339.84	80	330.72	96	321.72

Conversion units: $1mm^2 = 1.55 \times 10^{-3}$ in.^{2}, $1mm = 0.04$ in.
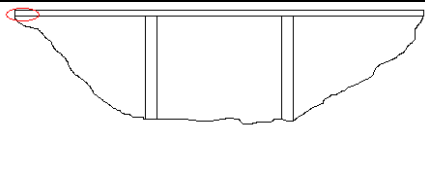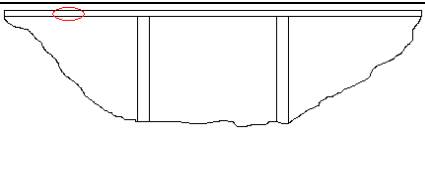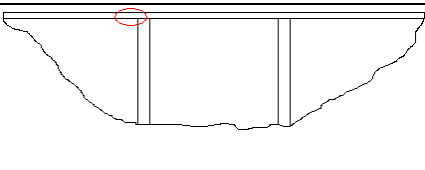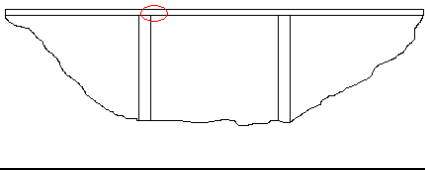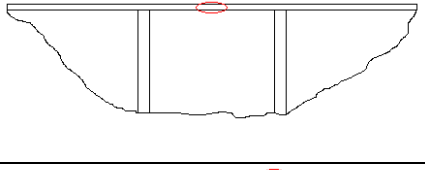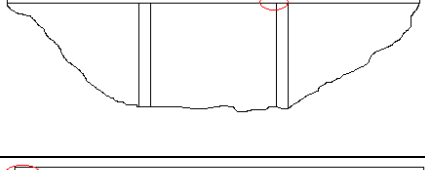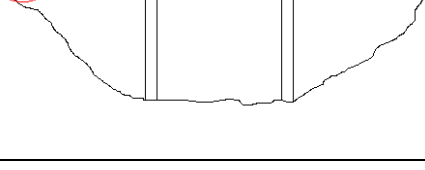
Table A.1 (Continued) Reduction in reinforcement area due to corrosion.

Years	Reinforcement Area (mm^2)	Years	Reinforcement Area (mm^2)	Years	Reinforcement Area (mm^2)
97	321.16	105	316.71	113	312.29
98	320.60	106	316.15	114	311.74
99	320.04	107	315.60	115	311.19
100	319.48	108	315.04	116	310.64
101	318.93	109	314.49	117	310.09
102	318.37	110	313.94	118	309.54
103	317.82	111	313.39	119	308.99
104	317.26	112	312.84	120	308.44

Conversion units: $1mm^2 = 1.55 \times 10^{-3}$ in.^{2}, $1mm = 0.04$ in.
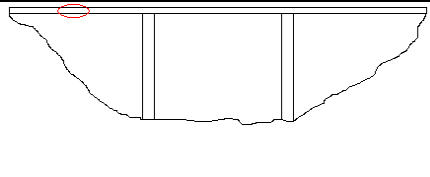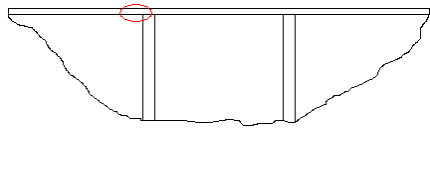
APPENDIX B.

CORROSION TEST RESULTS OF SAMPLES COLLECTED
FROM BRIDGE SITE P-0962

Table B.1 Critical chloride concentration in samples.

Sample No.	Critical Chloride Concentration (%)	Temperature (^{0}C)	Girder	Location
1	0.034	23.6	Exterior	
2	0.031	25.4	Exterior	
3	0.034	26.8	Exterior	
4	0.035	27.0	Exterior	
5	0.032	24.4	Exterior	
6	0.034	25.6	Exterior	
7	0.034	26.0	Interior	

Conversion units: °C = (°F-32) ÷ 1.8

Table B.1 (Continued) Critical chloride concentration in samples.

Sample No.	Critical Chloride Concentration (%)	Temperature (^{0}C)	Girder	Location
8	0.033	26.2	Interior	
9	0.032	23.4	Interior	
10	0.035	24.2	Interior	Near to the exposed reinforcement of transverse beam
11	0.035	25.6	Exterior	Near to the exposed reinforcement of transverse beam

Conversion units: °C = (°F-32) ÷ 1.8

APPENDIX C.

REDUCTION IN LOAD CARRYING CAPACITY DUE TO BOND
DEGRADATON BETWEEN FRP AND CONCRETE

Table C.1 Reduction in load carrying capacity due to F/T bond degradation.

No of Years	Cumulative No. of Cycles	Reduction in capacity (%)
5	25	2.5
10	50	5
15	75	5.83
20	100	6.67
25	125	7.5
30	150	8.33
35	175	9.17
40	200	10

APPENDIX D.

DETAILED CALCULATIONS OF LIFE EXPECTANCY ESTIMATION
(STANDARD AMERICAN ENGLISH UNITS)

Analysis of Girder

T-beam geometry:

h = 30 in.   (total depth of girder)

h_f = 6 in.   (height of flange)

b_{eff} = 53 in.   (effective width of flange

AASHTO section 8.10.1)

b_w = 17 in.   (width of web)

L = 42.5 ft   (simply supported beam)

Flexural reinforcement layout:

A_{st} = 12.48 in.^{2} (area of steel provided)

d = 25.625 in.   (distance of tensile steel from

topmost compression fiber)

f_y = 40 ksi   (yield strength of steel)

$$\rho_s = \frac{A_{st}}{b_{eff} \times d} \qquad \rho_s = 9.189 \times 10^{-3}$$ (percentage of steel)

E_s = 29000 ksi   (modulus of elasticity)

Concrete properties:

f'$_c$ = 6845 psi   (compressive strength of

concrete)

$$\beta_1 = \left[0.85 - 0.05 \times \frac{f'_c - 4000psi}{1000psi} \right] \qquad \beta_1 = 0.708$$ (strength reduction factor)

$$E_c = \left(57000\sqrt{6845} \right) \qquad E_c = 4.716 \times 10^3 ksi$$ (modulus of elasticity)

Computation of nominal moment capacity:

$$a = \frac{A_{st} \times f_y}{0.85 \times f_c \times b_{eff}}$$
$a = 1.619$ in. (depth of compression stress

block)

$$c = \frac{a}{\beta_1}$$
$c = 2.287$ in. (depth of neutral axis)

$$\frac{c}{d} = 0.089$$
$\emptyset = 0.9$ (tension controlled)

Design moment capacity of the beam:

$$\phi M_n = \phi \times \left[A_{st} \times f_y \times \left(d - \frac{a}{2} \right) \right]$$
$\phi M_n = 929.095$ kip.ft

Analysis of girder after strengthening:

Loading and corresponding moments

$$A = \left[(b_{eff} \times h_f) + (h - h_f) \times b_w \right]$$
$A = 5.042$ ft^2 (cross sectional area of beam)

$$DL = \left(A \times 1 ft \times 150 \times \frac{lb}{ft^3} \right)$$
$DL = 756.25$ lb (dead load computation)

$DL = 0.8$ kip / ft $LL = 0.64$ kip / ft   (loads)

$I = 1.29$ kip / ft   (impact factor)

$\beta_d = 1$ (dead load coefficient as per

AASHTO)

$$w_u = 1.3 \left[\beta_d \times DL + 1.67 (LL + I) \right]$$ $w_u = 5.23$ klf   (factored load as per

AASHTO)

$$M_{DL} = DL \times \frac{L^2}{8}$$
$M_{DL} = 180.625$ kip.ft

111

$$M_{LL} = LL \times \frac{L^2}{8}$$ $M_{LL} = 144.5 \text{ kip.ft}$

$$M_u = w_u \times \frac{L^2}{8}$$ $M_u = 1180.84 \text{ kip.ft}$ (factored moment)

External FRP strengthening configuration:

$t_f = 0.00065$ in.   (thickness of single ply)

$w_f = 16$ in.   (width of single ply)

$n = 3$ (number of plies)

$A_f = n \times t_f \times w_f$ $A_f = 0.312 \text{ in.}^2$ (area of FRP)

$$\rho_f = \frac{A_f}{b_w \times d}$$ $\rho_f = 7.162 \times 10^{-4}$ (percentage of FRP)

FRP guaranteed tensile properties:

$f_{fum} = 550 \text{ksi}$ (ultimate strength)

$\varepsilon_{fum} = 0.017$ (ultimate strain)

$E_f = 33000$ ksi   (modulus of elasticity)

FRP final properties:

$f_{fu} = f_{fum}$ $f_{fum} = 550$ ksi   (design strength)

$\varepsilon_{fu} = \varepsilon_{fum}$ $\varepsilon_{fu} = 0.017$ (design ultimate strain)

Determine existing strain on sofit under dead load only (cracked moment of T-beam, I_{cr})

$$n_e = \frac{E_s}{E_c}$$ $n_e = 6.149$ (ratio of elastic modulus of

steel to that of concrete)

$$k = \sqrt{2 \times \rho_s \times n_e + \left(\rho_s \times n_e\right)^2} - \rho_s \times n_e \quad k = 0.284$$ (depth of neutral axis of

cracked transformed section)

$$I_{cr} = \left[\frac{b_{eff}}{3} \times (k \times d)^3 \right] + \left[n_e \times A_{st} \times (d - k \times d)^2 \right]$$ (cracked moment of inertia)

$$I_{cr} = 3.264 \times 10^4 \, in^4$$

$$\varepsilon_{bi} = \frac{\dfrac{M_{DL}}{12} \times [h - (k \times d)]}{I_{cr} \times E_c}$$ $\varepsilon_{bi} = 2.665 \times 10^{-5}$ (strain at sofit of beam)

Compute design tensile strain and strength:

$K_m = 0.9$ (bond dependent coefficient)

$C = 4.05$ in.   (depth of neutral axis)

$$\varepsilon_{fe} = \min\left[\varepsilon_{fu} \times \left(\frac{h - C}{C} \right) - \varepsilon_{bi}, k_m \times \varepsilon_{fu} \right]$$ $\varepsilon_{fe} = 0.015$ (effective FRP strain)

$$\varepsilon_s = (\varepsilon_{fe} + \varepsilon_{bi}) \times \left(\frac{d - C}{h - C} \right)$$ $\varepsilon_s = 0.011$ (effective strain in steel)

$F_s = \min\left(E_s \times \varepsilon_s, f_y \right)$ $F_s = 40$ ksi   (effective stress in steel)

$F_{Fe} = E_f \times \varepsilon_{fe}$ $F_{Fe} = 504.9$ ksi   (effective stress in FRP)

$\gamma = 0.85$ (multiplier on $f`_c$ – ACI 440.2R-02)

$$C = \frac{A_s \times F_s + A_f \times F_{Fe}}{\gamma \times f`_c \times \beta_1 \times b_{eff}}$$ $C = 3.009$ in.   (equilibrium check with convergence of assumed C)

$\phi = 0.9$ (tension controlled)

$\Psi = 0.85$ (additional FRP strength factor)

$$M_n = A_s \times F_s \times \left(d - \frac{\beta_1 \times C}{2} \right) + \Psi \times A_f \times F_{Fe} \times \left(h - \frac{\beta_1 \times C}{2} \right)$$

$M_n = 1345$ kip.ft

$\phi M_n = 1210$ kip.ft

Reduction in moment capacity after strengthening:

$$\phi M_n(X_i) = \phi M_n . \psi_b(X_i) - \phi.A_{st}\psi_c(X_i).f_y\left(d - \frac{a}{2}\right)$$ (moment for a particular year

capacity after strengthening)

Where as,

$$\psi_b(X_i) = 1 - \left[(X_i - X_s) \times 2.5 \times 10^{-3}\right]$$ (bond strength reduction

factor for a particular year)

$$\psi_c(X_i) = \left[(X_i - X_s) \times 9.91 \times 10^{-6} in^2\right]$$ (strength reduction factor for

corrosion)

X_i = year at which moment capacity is to be determined

X_s = year of bridge strengthening.

Table D.1 Reduction in moment capacity after strengthening

Year	Moment capacity (kip.ft)	Year	Moment capacity (kip.ft)	Year	Moment capacity (kip.ft)
48	1210.00	65	1156.00	82	1104.00
49	1204.00	66	1153.00	83	1101.00
50	1201.00	67	1150.00	84	1098.00
51	1198.00	68	1147.00	85	1095.00
52	1195.00	69	1144.00	86	1092.00
53	1192.00	70	1141.00	87	1089.00
54	1189.00	71	1138.00	88	1086.00
55	1186.00	72	1134.00	89	1083.00
56	1183.00	73	1131.00	90	1080.00
57	1180.00	74	1128.00	91	1077.00
58	1177.00	75	1125.00	92	1074.00
59	1174.00	76	1122.00	93	1071.00
60	1171.00	77	1119.00	94	1068.00
61	1168.00	78	1116.00	95	1065.00
62	1165.00	79	1113.00	96	1062.00
63	1162.00	80	1110.00	97	1059.00
64	1159.00	81	1107.00	98	1056.00

Conversion units: 1 kip.ft = 1.356 KN.m, 1 kip = 0.448 KN, 1 ft. = 0.305 m

Table D.2 (Continued) Reduction in moment capacity after strengthening.

Year	Moment capacity (kip.ft)	Year	Moment capacity (kip.ft)	Year	Moment capacity (kip.ft)
99	1053.00	116	1001.00	133	949.93
100	1050.00	117	998.34	134	946.91
101	1047.00	118	995.31	135	943.88
102	1044.00	119	992.29	136	940.86
103	1041.00	120	989.26	137	937.83
104	1038.00	121	986.24	138	934.81
105	1035.00	122	983.21	139	931.78
106	1032.00	123	980.19	140	928.75
107	1029.00	124	977.16	141	925.73
108	1026.00	125	974.13	142	922.70
109	1023.00	126	971.11	143	919.68
110	1020.00	127	968.08	144	916.65
111	1016.00	128	965.06	145	913.63
112	1013.00	129	962.03	146	910.60
113	1010.00	130	959.01	147	907.58
114	1007.00	131	955.98	148	904.55
115	1004.00	132	952.96	149	901.53

Conversion units: 1 kip.ft = 1.356 KN.m, 1 kip = 0.448 KN, 1 ft. = 0.305 m

Table D.2 (Continued) Reduction in moment capacity after strengthening.

Year	Moment capacity (kip.ft)	Year	Moment capacity (kip.ft)	Year	Moment capacity (kip.ft)
150	898.50	159	871.27	168	844.04
151	895.48	160	868.25	169	841.02
152	892.45	161	865.22	170	837.99
153	889.42	162	862.20	171	834.97
154	886.40	163	859.17	172	831.94
155	883.37	164	856.15	173	828.92
156	880.35	165	853.12	174	825.89
157	877.32	166	850.09	175	822.87
158	874.30	167	847.07	176	819.84

Conversion units: 1 kip.ft = 1.356 KN.m, 1 kip = 0.448 KN, 1 ft. = 0.305 m

APPENDIX E.

DETAILED CALCULATIONS OF LIFE EXPECTANCY ESTIMATION
(STANDARD S.I. METRIC UNITS)

Analysis of Girder

T-beam geometry:

h = 762 mm   (total depth of girder)

h_f = 152.4 mm   (height of flange)

b_{eff} = 1346.2 mm   (effective width of flange

                                                   AASHTO section 8.10.1)

b_w = 431.8 mm   (width of web)

L = 12.954 m.   (simply supported beam)

Flexural reinforcement layout:

A_s = 8051.6 mm^2 (area of steel provided)

d = 650.88 mm   (distance of tensile steel from

                                                   topmost compression fiber)

f_y = 275.8 MPa   (yield strength of steel)

$$\rho_s = \frac{A_s}{b_{eff} \times d} \qquad \rho_s = 9.189 \times 10^{-3}$$ (percentage of steel)

E_s = 199.95 GPa   (modulus of elasticity)

Concrete properties:

f'_c = 47.2 MPa   (compressive strength of

                                                   concrete)

$$\beta_1 = \left[0.85 - 0.05 \times \frac{f'_c - 27.58\text{MPa}}{6.9\text{MPa}} \right] \qquad \beta_1 = 0.708$$ (strength reduction factor)

$$E_c = \left(149700\sqrt{47195} \right) \text{kPa} \qquad E_c = 32.52 \text{ GPa}$$ (modulus of elasticity)

Computation of nominal moment capacity:

$$a = \frac{A_s \times f_y}{0.85 \times f_c \times b_{eff}}$$

a = 41.12 mm   (depth of compression stress

block)

$$c = \frac{a}{\beta_1}$$

c = 58.09 mm   (depth of neutral axis)

$$\frac{c}{d} = 0.089$$

Ø = 0.9   (tension controlled)

Design moment capacity of the beam:

$$\varphi M_n = \varphi \times \left[A_{st} \times f_y \times \left(d - \frac{a}{2} \right) \right]$$

φM_n = 1260 kN.m

Analysis of girder after strengthening:

Loading and corresponding moments

$$A = \left[(b_{eff} \times h_f) + (h - h_f) \times b_w \right]$$

A = 0.468 m²   (cross sectional area of beam)

$$DL = \left(A \times 1 \text{ m.} \times 2250 \times \frac{kg}{m^3} \times 9.81 \frac{N}{kg} \right) DL = 10.338 \text{ kN}$$ (dead load computation)

DL = 10.5 kN / m   LL = 9.35 kN / m   (loads)

I = 18.845 kN / m   (impact factor)

β_d = 1   (dead load coefficient as per

AASHTO)

$$w_u = 1.3 \left[\beta_d \times DL + 1.67 (LL + I) \right]$$ w_u = 76.38 kN / m   (factored load as per

AASHTO)

$$M_{DL} = DL \times \frac{L^2}{8}$$

M_{DL} = 220.25 kN.m

120

$$M_{LL} = LL \times \frac{L^2}{8} \qquad\qquad M_{LL} = 196.10 \text{ kN.m}$$

$$M_u = w_u \times \frac{L^2}{8} \qquad\qquad M_u = 1570.27 \text{ kN.m} \qquad \text{(factored moment)}$$

External FRP strengthening configuration:

$t_f = 0.1651$ mm (thickness of single ply)

$w_f = 406$ mm (width of single ply)

$n = 3$ (number of plies)

$A_f = n \times t_f \times w_f \qquad\qquad A_f = 201.1 \text{ mm}^2 \qquad$ (area of FRP)

$$\rho_f = \frac{A_f}{b_w \times d} \qquad\qquad \rho_f = 7.162 \times 10^{-4} \qquad \text{(percentage of FRP)}$$

FRP guaranteed tensile properties:

$f_{fum} = 3.8 \text{GPa}$ (ultimate strength)

$\varepsilon_{fum} = 0.017$ (ultimate strain)

$E_f = 227.53$ GPa (modulus of elasticity)

FRP final properties:

$f_{fu} = f_{fum} \qquad\qquad f_{fu} = 3.8 \text{ GPa} \qquad$ (design strength)

$\varepsilon_{fu} = \varepsilon_{fum} \qquad\qquad \varepsilon_{fu} = 0.017 \qquad$ (design ultimate strain)

Determine existing strain on sofit under dead load only (cracked moment of T-beam, I_{cr})

$$n_e = \frac{E_s}{E_c} \qquad\qquad n_e = 6.149 \qquad \text{(ratio of elastic modulus of}$$

steel to that of concrete)

$$k = \sqrt{2 \times \rho_s \times n_e + (\rho_s \times n_e)^2} - \rho_s \times n_e \quad k = 0.284 \qquad \text{(depth of neutral axis of}$$

cracked transformed section)

$$I_{cr} = \left[\frac{b_{eff}}{3} \times (k \times d)^3\right] + \left[n_e \times A_{st} \times (d - k \times d)^2\right]$$ (cracked moment of inertia)

$$I_{cr} = 0.014\text{m}^4$$

$$\varepsilon_{bi} = \frac{\dfrac{M_{DL}}{12} \times \left[h - (k \times d)\right]}{I_{cr} \times E_c}$$ $\varepsilon_{bi} = 2.397 \times 10^{-5}$ (strain at sofit of beam)

Compute design tensile strain and strength:

$K_m = 0.9$ (bond dependent coefficient)

$C = 102.87$ mm (depth of neutral axis)

$$\varepsilon_{fe} = \min\left[\varepsilon_{fu} \times \left(\frac{h - C}{C}\right) - \varepsilon_{bi}, k_m \times \varepsilon_{fu}\right]$$ $\varepsilon_{fe} = 0.015$ (effective FRP strain)

$$\varepsilon_s = (\varepsilon_{fe} + \varepsilon_{bi}) \times \left(\frac{d - C}{h - C}\right)$$ $\varepsilon_s = 0.015$ (effective strain in steel)

$Fs = \min\left(E_s \times \varepsilon_s, f_y\right)$ $F_s = 275.8$ MPa (effective stress in steel)

$F_{Fe} = E_f \times \varepsilon_{fe}$ $F_{Fe} = 3.481$ GPa (effective stress in FRP)

$\gamma = 0.85$ (multiplier on f'_c – ACI

440.2R-02)

$$C = \frac{A_s \times F_s + A_f \times F_{Fe}}{\gamma \times f'_c \times \beta_1 \times b_{eff}}$$ $C = 76.403$ mm (equilibrium check with

convergence of assumed C)

$\phi = 0.9$ (tension controlled)

$\Psi = 0.85$ (additional FRP strength

factor)

$$M_n = A_s \times F_s \times \left(d - \frac{\beta_1 \times C}{2}\right) + \Psi \times A_f \times F_{Fe} \times \left(h - \frac{\beta_1 \times C}{2}\right)$$

M_n = 1823 kN.m

$\phi M_n = 1640 \text{kN.m}$

Reduction in moment capacity after strengthening:

$$\phi M_n\left(X_i\right) = \phi M_n \cdot \psi_b\left(X_i\right) - \phi \cdot A_{st} \psi_c\left(X_i\right) \cdot f_y\left(d - \frac{a}{2}\right)$$

(moment for a particular year capacity after strengthening)

Where as,

$$\psi_b\left(X_i\right) = 1 - \left[\left(X_i - X_s\right) \times 2.5 \times 10^{-3}\right]$$

(bond strength reduction factor for a particular year)

$$\psi_c\left(X_i\right) = \left[\left(X_i - X_s\right) \times 6.39 \times 10^{-6} \text{mm}^2\right]$$

(strength reduction factor for corrosion)

X_i = year at which moment capacity is to be determined

X_s = year of bridge strengthening.

APPENDIX F.

PROGRAMMING FOR ESTIMATION OF LIFE EXPECTANCY OF
FRP STRENGHTENED RC BRIDGES USING MATH-CAD

1. INTRODUCTION

Included with this report is a CD-ROM, which contains the two sheets of Math-CAD. The first Math-CAD sheet has been programmed for calculating life expectancy of FRP strengthened RC bridges in Standard American English Units (S.A.E.). Second Math-CAD sheet has a programmed for calculating life expectancy of FRP strengthened RC bridges in S.I. Metric Units (S.I.)

2. STANDARD AMERICAN ENGLISH UNITS (S.A.E.)

3. S.I. METRIC UNITS (S.I.)

BIBLIOGRAPHY

American Association of State Highway and Transportation Officials. (1998). *LRFD bridge design specifications* (2nd ed.). (2002). *Standard specifications for highway bridges* (17th ed.). Washington D.C.: AASHTO.

ACI Guide for the Design and Construction of Concrete Reinforced with FRP Bars, ACI 440.1R-03 (2003), American Concrete Institute Committee 440, Farmington Hills, MI.

ACI Guide for the Design and Construction of Externally Bonded FRP Systems for Strengthening Concrete Structure, ACI 440.2R-02 (2002), American Concrete Institute Committee 440, Farmington Hills, MI.

Aidoo, J., Harries, K., A., and Petrou, M., F.(2004), "Fatigue Behavior of Carbon Fiber Reinforced Polymer- Strengthened Reinforced Concrete Bridge Girders," Journal of Composites for Construction, Vol. 8, No. 6, December 1, 2004. ASCE, 501-509

Alagusundaramoorthy, P., Harik, I., E., and Choo, C., C. (2003), "Flexural Behavior of Reinforced Concrete Beams Strengthened with Carbon Fiber Reinforced Polymer Sheets or Fabric," Journal of Composites for Construction, Vol. 7, No.292-301, November 1, 2003.ASCE

Almusallam, T., H., Al-Salloum, Y., A., Al-Sayed, S., H., Amjad, M., A., (1996), "Evaluation of service load deflection for beams reinforced by GFRP bars," Proc. 2nd Int. Conf. Advance Composite Material in Bridges and Structure, El-Badry, ed., Can. Soc. for Civ. Engrg., Montreal, Canada, 165-172

Al-Sulaimani, G., J., Kaleemullah, M., Basunbul, I., A., and Rasheeduzzafar, (1990), "Influence of corrosion and cracking on bond behavior and strength of reinforced concrete members," ACI Structural Journal, 87 (2), 220-231.

American Association of State Highway and Transportation Officials (AASHTO) (1998). LRFD Bridge Design Specifications: Second Edition. Washington, D.C.

American Association of State Highway and Transportation Officials (AASHTO) (2001). AASHTO Journal Weekly Transportation Report. Vol.101, No.8, Feb. 23, 2001.

Arduini, M., and Nanni, A., (1997). "Performance of decommissioned RC girders strengthened with FRP laminates," Publication: Structural Journal. Volume: 94. Issue: 4. Date: July 1, 1997

Badawi and Soudki K., A., (2004), "Control of corrosion-induced damage in RC beams using CFRP laminates," ASCE Journal of Materials in Civil Engineering, (21 pp., March 2004).

Bae, S., W., (2004), "Evaluation Effects of Various Environmental Conditions on Reinforced Concrete Columns Wrapped with FRP Sheets," (2004), Dissertation in Civil, Architectural, and Environmental Engineering, University of Missouri-Rolla.

Bakis, C.E., Bank, L.C., Brown, V.L., Cosenza, E., Davalos, A.M., Lesko, J.J., Machida, A., Rizkalla, S.H., Triantafillou, T.C. (2002). "Fiber-Reinforced Polymer Composites for Construction – State-of-the-Art Review," Journal of Composites for Construction, 2002, Vol.6, No. 2, pp. 73-87.

Baumert, M., E., Green, M., F., and Erki, M.A. (1996), "Low temperature behaviour of concrete beams strengthened with FRP sheets," CSCE Annual Conference, Edmonton, Alberta, 29 May – 1 June, IIa, 179–190.

Benmokrane, B. and El-Salakawy, E., (2004), "Serviceability of Concrete Bridge Deck Slabs Reinforced with Fiber-Reinforced Polymer Composite Bars," ACI Structural Journal, Vol 101, No. 5, 2004, pp. 727-736.

Berenberg, B., www.composites.about.com, 02/14/2007.

Bickley, L., A., Neale, K., W., and Fabbnizzo, G., (1993), "Market potentiai and identification of suppliers of advanced industrial materials for construction of bridges and other structures," Industry Science and Technology, Canada.

Bizindavyi, L., Neale, K., W., (1999), "Transfer lengths and bond strengths for composites bonded to concrete," Journal of Composites for Construction, ASCE, 3(4), 153-160

Broomfield, J. P. (1997), "Corrosion of Steel in Concrete," E. and F.N. Spon, London, UK.

Bisby, L.A. and Mark F. Green, (2002), "Resistance to Freezing and Thawing of Fiber-Reinforced Polymer-Concrete Bond," ACI Structural Journal, Vol. 99, No. 2, April 2002, pp. 215-223.

Berke, N., S., Hicks, M., C., (1994), "Predicting Chloride Profiles in Concrete," Corrosion (Houston), v. 50, n. 3, March 1994, pp. 234-239.

Benmokrane, B., and Rahman, H., (1998), "Improvement of the durability performance of FRP reinforcement for concrete structures," Proceedings of the First International Conference, Sherbrooke, Quebec, Canada, (1998) p.571-578.

127

Bertolini, L., Elsener, B., Pedeferri, P., Polder, R., (2003), "Corrosion of Steel in Concrete," (2003) WILEY-VCH Verlag GmbH &Co. KGaA, Germany

Brena, S., F., Wood, S., L. and Kreger M., L., (2002), "Fatigue tests of reinforced concrete beams strengthened using CFRP Composites", Proceedings of the Second International Conference on Durability of Fibre Reinforced Polymer (FRP) Composites for Construction, Sherbrooke, Canada, 575-586.

Chaallal, O., and Benmokrane, B., (1996), "Fiber-Reinforced Plastic Rebars for Concrete Applications," Composites: Part B, 27B, pp. 245-252.

Chajes, M., J., Ted, F., J., Mertz, D., R., Theodore, T., A., Jr., and Finch, W., W., Jr., (1995), "Shear Strengthening of Reinforce Concrete Beam using Externally Applied Composite Fibers," (1995) ACI Structural Journal, V. 93, no. 3, pp 295-303.

Chajes, M., J., Ted, F., J., Mertz, D., R., Theodore, T., A., Jr., and Finch, W., W., Jr., (1996), "Bond and Force Transfer of Composite Material Plates Bonded to Concrete," (1996) ACI Structural Journal, V. 93, no. 2, pp 208-217.

Chajes, Michael J., Shenton, Harry W., and Finch, William W. (2001), "Performance of a GFRP Deck on Steel Girder Bridge," Proceedings of the 80th Annual Meeting of the Transportation Research Board, Transportation Research Board, Washington, D.C., U.S.

Chong, K., (1998), "Durability of Composite Materials and Structures," Durability of Fiber Reinforced Polymer (FRP) Composites for Construction – Proceedings of the first International Conference (CDCC), 1998, pp. 1-12.

Clark, L., A., Saifullah, M., (1993), "Effect of corrosion on reinforcement bond strength", Int. Conf. Structural faults and repair, Edinburgh, U.K., pp.113-119.

Clark, C. R. and Johnston, D. W., (1983), "Early Loading Effects on Bond Strength," ACI Journal, Nov-Dec., pp. 532-539.

Cosenza, E., Manfredi, G., Nanni, A. (2002), "Composite in Construction – A Reality," (2002), American Society of Civil Engineers, U.S.A.

Dolan, C.,W., Rizkalla, S., H., and Nanni, A., (1999), Fourth International Symposium on Fiber Reinforced Polymer Reinforcement for Reinforced Concrete Structures, SP-188, American Concrete Institute.

"Evaluation and Performance Monnitoring of Corrosion Protection by Fiber-Reinforced Composite Wrapping," Center for Transportation Research Bureau of Engineering Research, University of Texas at Austin, (2001).

Ekenel, M., Rizzo A., Myers, J., J., and Nanni, A., (2006), "Flexural Fatigue Behavior of Reinforced Concrete Beams Strengthened with FRP Fabric and Precured Laminate Systems," Journal of Composites for Construction, Vol. 10, No. 5, October 1, 2006. ASCE, 433-442.

El Maadawy and Soudki, K., A., (2004), "CFRP repair to extend the service life of corroded reinforced concrete beams," ASCE Journal of Composites for Construction, (38 pp., April 2004).

El-Tawil, S., Ogunc, C., Okeil, A., and Shahawy, M., (2001), "Static and Fatigue Analysis of RC Beams Strengthened With CFRP Laminates," Journal of Composites for Construction, Vol. 5, No.4, November, 2001.ASCE,258-267.

Green, M.F., L.A. Bisby, Y. Beaudoin and P. Labossiere, (2000), "Effect of Freeze-Thaw cycles on the Bond Durability Between Fibre Reinforced Polymer Plate Reinforcement and Concrete," Canadian Journal of Civil Engineering, Vol. 27, 2000, pp. 949-959.

"Guide for the Design and Construction of Concrete Reinforced with FRP Bars," (2001), American Concrete Institute Committee 440, Farmington Hills, MI.

Hallaway, L., (1994), "Handbook of Polymer Composites for Engineers," Woodhead Publishing Limited, England, (1994).

Horiguchi, T., and Saeki, N., (1997), "Effect of test methods and quality of concrete on bond strength of CFRP sheet," Non-Metallic (FRP) Reinforcement for Concrete Structures, Vol. 1, Japan Concrete Institute, Japan, pp. 265-270.

Izumo, K., M., Saeki, N., Asamizu, T., Shimura, K., (1997), "Strengthening reinforced concrete beams by using prestressed fiber sheets," Proceedings of the Third International Symposium on Non-Metallic (FRP) Reinforcement for Concrete Structures (FRPRCS-3), I: 379-386.

James Instruments Inc. The Corrosion rate Meter for Steel in Concrete, James Instruments Inc., Chicago, IL.

James Instruments Inc., www.ndtjames.com, 11/09/2006.

Jones, D., A., (1992), "Principles and Prevention of Corrosion," Macmillan Publishing Company, New York, NY, 1992.

Jang, B., Z., (2000), "Advanced Polymer Composites: Principle and Applications," ASM International, U. S. A. (1994).

Karbhari, V. M. and Seible, F., (2000), "Fiber Reinforced Composites – Advanced Materials for the Renewal of Civil Infrastructure," Applied Composite Materials, Vol. 7, Nos. 2-3, 94-124.

Karbhari, V. M., Seible, F., Burgueno, R., Davol, A., Wernli, M., and Zhao, L. (2000), "Structural Characterization of Fiber-Reinforced Composite Short- and Medium-Span Bridge Systems," Applied Composite Materials, Vol. 7, No. 2-3, 155-182.

Karbhari, V. M., Chin, J. W., Hunston, D., Benmokrane, B., Juska, T., Morgan, R., Lesko, J. J., Sorathia, U., and Reynaud, D. (2003), "Durability Gap Analysis for Fiber Reinforced Polymer Composites in Civil Infrastructure," Journal of Composites for Construction, Vol. 7, No. 3, 238- 247.

Karbhari, V.M. (1998), "Use of Composite Materials in Civil Infrastructure in Japan," International Technology Research Institute, World Technology (WTEC) Division, October-1998- http://www.wtec.org/loyola/compce.

Karbhari, V. M. (2000), "Chapter.2 - Advancing the design and construction through innovation," Gap Analysis for the durability of Fiber Reinforced Polymer Composites in Civil Infrastructure.

Karbhari, V. M., Morgan, R., and Williams, C. (2000). "Effect of Moisture/Aqueous Solutions," Gap Analysis for the durability of Fiber Reinforced Polymer Composites in Civil Infrastructure-Advancing the design and construction through innovation, CERF.

Karbhari, V. M., (2006), "Characteristics of adhesion between composites and concrete as related to structure rehabilitation," International Society for the Advancement of Material and Process Engineering, Proceedings of the 27th International SAMPE Technical Conference, v. 27, Albuquerque, New Mexico, October g, pp. 1083- 1094.

Kawai, M., (2004), "A phenomenological model for off-axis fatigue behavior of unidirectional polymer matrix composites under different stress ratios," composites: part A, 35: 955–963.

Khalifa, A. and A. Nanni, (2002), "Rehabilitation of rectangular simply supported RC bearns with shear deficiencies using CFRP composites," Construction and Building Materials, Aprilrggg, Vol. 16, No. 3, 2002, pp. 135-146.

Klaiber, F., W., Dunker, K., F., Wip, T., J., and Sanders, W., W., Jr., "Methods of strengthening existing highway bridges," NCHRP research report No. 293, Transportation research board, Sep. 1987:11.

Kumar, A., Gupta, R., (1998), "Fundamentals of Polymers," McGraw-Hill, (1998), New York, U.S.A.

Kumar P. (2000), "Evaluation of an Innovative FRP Bridge Deck System," Master's Thesis, University of Missouri-Rolla.

Lenwari, A., Thepchatri, T., and Albrecht, P., (2006), "Debonding Strength of Steel Beams Strengthened with CFRP Plates," Journal of Composites for Construction, Vol. 10, No. 1, February 1, 2006. ASCE, 69-78

Lee, Y., J., Boothby, T., E., Bakis, C., E., Nanni, A., (1999), "Slip modulus of FRP sheets bonded to concrete," Journal of Composites for Construction, ASCE, 3(4), 161-167.

Liu, Y., and Weyers R. E. (1997), "Predicting the Corrosion Rate of Steel in Chloride Contaminated Concrete," Paper for Fourth Canmet/ACI International Conference on Durability of Concrete, Sydney, Australia.

Maeda, T.; Asano, Y.; Sato, Y.; Ueda, T.; and Kakuta, Y. (1997), "A Study on Bond Mechanism of Carbon Fiber Sheet," Non-Metallic (FRP) Reinforcement for Concrete Structures, Vol. 1, Japan Concrete Institute, Japan, pp. 279-286

Mangat, P., S., and Elgarf, M., S., (1999), "Flexural strength of concrete beams with corroding reinforcement." ACI Structural Journal, 96 (1), 149-158.

Masoud, S., Soudki, K., A., and Topper, T., (2001), "Corroded RC beams strengthened with CFRP sheets under monotonic and fatigue loading, " ASCE Journal of Composites in Construction Vol. 5, No. 4, pp. 228-236

Mehta, P., K., (1993), "Concrete Structure, Properties and Materials," Prentice-Hall, Inc., Englewood Cliffs, New Jersey, 1993.

Meier, U., and Kaiser, H., (1991), "Strengthening of structures with CFRP laminates". Advanced composite materials in civil engineering structures. Proceedings of the Speciality Conference, Las Vegas, Nev., 31 January – 1 February, pp. 288–301.

Micelli, F., Myers, J., J., and Murthy, S., (2002), "Performance of FRP confined concrete subjected to accelerated environmental conditioning." Proceedings of the 2nd International Conference on Durability of Fiber Reinforced Polymer (FRP) Composites for Construction, B. Benmokrane and E. El-Salakawy (Eds.), Montreal, Canada, pp. 87–98.

Molander, M., (2001), "Instrumentation of a Smart Composite Bridge," Master's Thesis, University of Missouri-Rolla.

Myers, J., J., Jeffries, J., and Shen, X., (2007), "Effect of varied surface roughness and concrete strength on the bond performance of FRP fabrics," Proceedings of ACIC, Advance Composite in Construction , April 2007.

Myers, J., J., Shen, X., and Maerz, N., (2007), "Effect of varied surface roughness, putty thicknesses and concrete strength on interfacial bond strength of FRP to concrete," Transportation Research Board, 86th Annual Meeting Washington, D. C. January 2007.

Myers, J.J., Murthy, S. Micelli, F., "Effect of Combined Environmental Cycles on the Bond of FRP Sheets to Concrete," Proceedings of the International Conference on Composites in Construction (CCC-2001), Porto, Portugal, October 10-12, 2001, pp. 339-344.

Norris, T. and Saadatmanesh., (1997), "Shear And Flexural-Strengthening Of R/C Beams With Carbon Fiber Sheets." Journal of Structural Engineering, 123(7), 903-911.

Ritchie, P., Thomas, D., Lu, W.L., and Connelly, G., (1991), "External Reinforcement of Concrete Beams Using Fiber Reinforced Plastics." ACI Structural Journal, ACI, Vol.88, pp. 490-500.

Rodriguez, J.,Ortega, L., Garcia, A., (1994), "Corrosion of reinforcing bars and service life of R/C structures: corrosion and bond deterioration", Int. Conf. Concrete across borders, Odense, Denmark, Vol.II, pp.315-326.

NPL Report, DEPC MPR 016, "Review of Accelerating ageing Methods and Lifetime Prediction Techniques for Polymeric Materials," (2005).

Saetta, A., V., (2005), "Deterioration of Reinforced Concrete Structures due to Chemical–Physical Phenomena: Model-Based Simulation," Journal of Materials in Civil Engineering, Vol. 17, No. 3, June 1, 2005., ASCE, 313-319.

Savoia, M., Ferracuti, B., and Mazzotti, C., (2005), "Creep Deformation of Fiber Reinforced Plastics-Plated Reinforced Concrete Tensile Members," Journal of Composites for Construction, Vol. 9, No. 1, February 1, 2005.63-72.

Sawant, A., and Myers, J., (2007), "Strength degradation modeling approach to life expectancy of FRP strengthened bridges," International Conference on Durability of Fiber Reinforced Polymer (FRP) Composites for Construction, Quebec, Canada, (Accepted May 2007).

Shahawy, M., and Beitelman, E., T., (1999), "Static and Fatigue Performance of RC Beams Strengthened with CFRP Laminates", ASCE Journal of Structural Engineering, 125(6), 613-621.

Sohanghpurwala, A., A., (2006), NCHRP, Report 558, "Manual on Service Life of Corrosion-Damaged Reinforced Concrete Bridge Superstructure Elements," Transportation Research Board, (2006).

Sohanghpurwala, A., A., (2006), NCHRP, Web only Document 88, "Service Life of Corrosion-Damaged Reinforced Concrete Bridge Superstructure Elements," Transportation Research Board, (2006).

Soudki, K.A. and T.G. Sherwood, (2000), "Behaviour of Reinforced Concrete Beams Strengthened with Carbon Fibre Reinforced Polymer Laminates Subjected to Corrosion Damage," Canadian Journal of Civil Engineering, Vol. 27, 2000, pp. 1005-1010.

Soudki, K., A., and Green, M., F., (1997), "Freeze Thaw Durability of Compression Members Strengthened by Carbon Fibre Wrapping," Concrete International, Vol. 19, No. 8, August, pp. 64-67.

Stone, D., Nanni, A., and Myers, J., (2001), "Field and Laboratory Performance of FRP Bridge Panels," Proceedings, Council of Composites in Construction, Porto, Portugal, Oct. 10-12, 2001, pp. 701-706.

Taljsten, B., (1997), "Defining anchor lengths of steel and CFRP plates bonded to concrete," International Journal of adhesion and adhesives, Vol. 17, No. 4, 319-327.

Toutanji, H., and Balaguru, P,. (1998), "Durability characteristics of concrete columns wrapped with FRP tow sheets." Journal of Materials in Civil Engineering, ASCE, 10, 52–57.

Toutanji, H., Gomez, W., (1997), "Durability of concrete beams externally bonded with FRP sheets in aggressive environments," Cement and Concrete Composites Journal, Vol. 19, No. 4, August 1997.

Triantafillou, T., and Plevris, N., (1991), "Post Strengthening of R/C Beams with Epoxy Bonded Fiber Composite Materials."" Proceedings of a Conference on Advanced Composite Materials in civil Engineering Structures, Las Vegas, NV, ASCE, pp. 245- 256.

University of Missouri- Rolla, C.I.E.S., "Preservation of Missouri Transportation Infrastructure," Research Plan, A Proposal to Missouri Department of Transportation, Report R98 (2002).

University of Missouri- Rolla, C.I.E.S., "Preservation of Missouri Transportation Infrastructure," R03M04-1, Volume 1, Bridge Design and Load Rating, Bridge P-0962, (2004).

U.S. Department of Transportation, Federal Highway Administration, National Bridge Inventory: Deficient Bridges by State and Highway System, Washington, DC: 2001, www.fhwa.dot.gov/bridge/britab.htm as of Jan. 31, 2002.

Volnyy, V., A., and Pantelides, C., P., (1999), "Bond Length of CFRP Composites Attached to Precast Concrete Walls," Journal of Composites for Construction, Volume 3, Issue 4, pp. 168-176 (November 1999).

Zureich, A., H., Nettles, A., T., (2002), "Composite Materials-Testing, Design, and Acceptance Criteria," ASTM International, U.S.A., (2002).

Zemajtis, J. (1998), "Modeling the Time to Corrosion Initiation for Concretes with Mineral Admixtures and/or Corrosion Inhibitors in Chloride-Laden Environments," Dissertation in Civil and Environmental Engineering, Virginia Polytechnic Institute and State University.